

**STUDY OF DYNAMIC PARAMETERS OF THE JAMUNA
MULTIPURPOSE BRIDGE**



BY

A.Z.M. MUSTAFIZUR RAHMAN

MASTER OF SCIENCE IN CIVIL ENGINEERING (STRUCTURAL)



Department of Civil Engineering

BANGLADESH UNIVERSITY OF ENGINEERING AND TECHNOLOGY

July, 2008

**STUDY OF DYNAMIC PARAMETERS OF THE JAMUNA MULTIPURPOSE
BRIDGE**

A Thesis

By

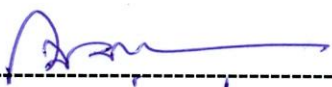
A.Z.M Mustafizur Rahman

Approved as to style and contents by



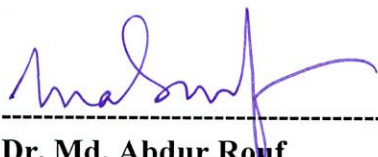
Dr. Raquib Ahsan
Associate Professor
Department of Civil Engineering
BUET, Dhaka-1000

Chairman



Dr. Muhammad Zakaria
Professor and Head
Department of Civil Engineering
BUET, Dhaka-1000

Member (Ex-Officio)



Dr. Md. Abdur Rouf
Professor
Department of Civil Engineering
BUET, Dhaka-1000

Member



Dr. Mohammad Nazmul Islam
Head, Department of Civil Engineering
Presidency University, Gulshan, Dhaka-1212

Member (External)

DECLARATION

It is hereby declared that except for the contents where specific reference have been made to the work of others, the studies contained in this thesis is the result of investigation carried out by the author. No part of this thesis has been submitted to any other University or other educational establishment for a Degree, Diploma or other qualification (except for publication)

Signature of the Candidate



A.Z.M. Mustafizur Rahman

CONTENTS

Declaration	iii
Contents	iv
List of Tables	viii
List of Figures	ix
List of Notations	xiii
List of Abbreviations	xv
Acknowledgment	xvi
Abstract	xvii
Chapter 1 INTRODUCTION	
1.1 GENERAL	1
1.2 OBJECTIVE OF THE STUDY	3
1.3 SCOPE OF THE STUDY	3
Chapter 2 LITERATURE REVIEW	
2.1 GENERAL	4
2.2 CONCEPT OF SYSTEM IDENTIFICATION	5
2.3 ACTIVITIES BASED ON SYSTEM IDENTIFICATION	5
2.4 THE PROCESS OF SYSTEM IDENTIFICATION	6
2.5 VARIOUS STUDIES ON SYSTEM IDENTIFICATION	7
2.5.1 Paultre <i>et al.</i> (1992)	7
2.5.2 Street <i>et al.</i> (1994)	7
2.5.3 Wangans and Haldar (1995)	8
2.5.4 Nelson <i>et al.</i> (1998)	8
2.5.5 Tang and Huang (1999)	8
2.5.6 Koh <i>et al.</i> (1999)	9
2.5.7 Chang <i>et al.</i> (1999)	9
2.5.8 Chaudhary <i>et al.</i> (1999)	10
2.5.9 Shi <i>et al.</i> (2000)	10
2.5.10 Schulz <i>et al.</i> (2000)	11

2.5.11	Lus <i>et al.</i> (2001)	11
2.5.12	Maeck <i>et al.</i> (2001)	11
2.5.13	Shen <i>et al.</i> (2001)	12
2.5.14	Calvert and Mooney (2002)	12
2.5.15	Feng <i>et al.</i> (2001)	13
2.5.16	Peterson <i>et al.</i> (2003)	13
2.5.17	He <i>et al.</i> (2004)	14
Chapter 3	BRIDGE PARAMETERS AND SEISMIC INSTRUMENTATION	
3.1	GENERAL	16
3.2	BRIDGE DESCRIPTION	16
3.3	PILE CONFIGURATION	18
3.4	PIER STEM	18
3.5	DECK CONFIGURATION	23
3.6	ISOLATION SYSTEM	24
3.7	SEISMICITY OF BRIDGE SITE	25
3.8	FREE-FIELD STATIONS	27
3.9	SENSORS ON THE BRIDGE	28
Chapter 4	SYSTEM IDENTIFICATION OF THE BRIDGE	
4.1	GENERAL	34
4.2	MATHEMATICAL MODELING OF THE BRIDGE	34
4.3	SYSTEM IDENTIFICATION BY AMBIENT VIBRATION	34
4.3.1	Ambient Vibration of The Pier-Deck System	34
4.3.2	Single Degree of Freedom Model (SDOF)	37
4.3.3	Two Degrees of Freedom Model (TDOF)	38
4.4	SYSTEM IDENTIFICATION BY TRANSFER RATIO	40
4.4.1	Formulation of Three Degree of Freedom System	40
4.4.2	Calculation of Transfer Ratio	43
4.5	APPLICATION OF THE TRANSFER RATIO	48
4.6	VERIFICATION OF THE TRANSFER RATIO	49
4.7	RESPONSE OF BRIDGE UNDER TRANSFER RATIO	51

	4.7.1 Application TR under Local Earthquake	51
	4.7.2 Application of TR under the El Centro Earthquake, Imperial Valley, California, USA, 1940	55
	4.7.3 Application of the Mexico City Earthquake, September 19, 1995	58
Chapter 5	FINITE ELEMENT MODELING OF THE SYSTEM	
	5.1 GENERAL	61
	5.2 FINITE ELEMENT MODELING OF THE BRIDGE	61
	5.2.1 Salient features for modeling of the bridge	61
	5.2.2 Bridge Layout Line	61
	5.2.3 Deck Section	64
	5.2.4 Pier, Diaphragm, Exterior Rail Girder	66
	5.2.5 Bearing and Restraint	67
	5.2.6 Applying Lateral Prestressing to the Deck	69
Chapter 6	MODAL ANALYSIS	
	6.1 GENERAL	73
	6.2 INTERPRETATION OF VARIOUS MODELS	73
	6.3 MODAL ANALYSIS OF THE SYSTEM	74
	6.4 GRAPHICAL DESCRIPTION OF VARIOUS TRANSVERSE MODELS	76
Chapter 7	BRIDGE BEHAVIOR UNDER VARIOUS DYNAMIC LOADS	
	7.1 GENERAL	89
	7.2 EARTHQUAKE PARAMETERS	89
	7.3 TIME HISTORY OF EARTHQUAKE DATA	89
	7.4 EARTHQUAKE RESPONSE OF THE BRIDGE	93
	7.5 RESPONSE UNDER VARIOUS DYNAMIC LOADING	94

Chapter 8	CONCLUSIONS AND RECOMMENDATIONS	
	8.1 GENERAL	101
	8.2 FINDINGS IN BRIEF	102
	8.3 FUTURE RECOMMENDATIONS	104
	REFERENCES	105
	APPENDIX	109

LIST OF TABLES

Table 3.1	Salient features of the bridge	17
Table 3.2	Cross Sectional Properties of Pier Stem	18
Table 3.3	Maximum Earthquake Magnitude in different Tectonic Blocks	25
Table 3.4	Free-field Instruments	27
Table 3.5	List of sensors and recorders installed on the bridge and bore-hole	29
Table 7.1	Summary of ground motion in FF stations, June 16, 2004 earthquake	93
Table 7.2	Summary of Earthquake Data in Bridge, June 16, 2004 Earthquake	94
Table 7.3	Comparison of Earthquake data and various dynamic loads on Bridge for Various traffic conditions	95

LIST OF FIGURES

Fig. 1.1	Location of the Jamuna Multipurpose Bridge	2
Fig. 3.1	A Typical Seven-Span Module	17
Fig. 3.2(a)	General Arrangement of 2 Piles Pier	19
Fig. 3.2(b)	General Arrangement of 3 Piles Pier	20
Fig. 3.2(c)	General Arrangement of Piles	21
Fig. 3.3(a)	Cross-section of Pier Stem	22
Fig. 3.3(b)	Elevation of Pier Stem	22
Fig. 3.4	A Typical Deck cross-section	23
Fig. 3.5(a)	Schematic of Pin-Dissipating Device	26
Fig. 3.5(b)	Plan of the Energy-Dissipating Device	26
Fig. 3.6	Free-field Instrument Setup	28
Fig. 3.7	Data Recorders and the Communication Enclosure within the Deck	30
Fig. 3.8(a)	Triaxial Accelerometer on the Pile Cap	30
Fig. 3.8(b)	Uniaxial Accelerometer on the Pile Cap	31
Fig. 3.9	Location of various Accelerometer and Displacement Sensor in the Jamuna Bridge at the pile caps and pier	32
Fig. 3.10	Location of Various Accelerometers at Deck of Jamuna Bridge	33
Fig. 4.1	Amplitude vs. Time (without traffic BR-1X)	35
Fig. 4.2	Amplitude vs. Time (without traffic BR-5X)	35
Fig. 4.3	FFT of BR-1X (without traffic)	36
Fig. 4.4	FFT of BR-5X (without traffic)	36
Fig. 4.5	Simplified deck profile	37
Fig. 4.6	Simplified deck cross section	37
Fig. 4.7	TDOF model.	38
Fig. 4.8	Ideal multiple degree of freedom system.	40
Fig. 4.9	(a) Free body diagram of masses (b) Free body diagram of mass m_2 (c) Free body diagram of mass m_3 .	41
Fig. 4.10	Displacement of the bridge at BR-5X due the earthquake, June 17, 2004	45

Fig. 4.11	FFT of the displacement of the bridge due the earthquake, June 17, 2004	45
Fig. 4.12	Ground motion of the earthquake, June 17, 2004	46
Fig. 4.13	FFT of the ground motion of the earthquake, June 17, 2004	46
Fig. 4.14	TR vs. frequency plot	47
Fig. 4.15	Theta vs. frequency plot	47
Fig. 4.16	IFFT of the response of the bridge due to the earthquake, June 17, 2004	50
Fig. 4.17	Displacement of the bridge due to the earthquake, June 17, 2004	50
Fig. 4.18	Ground motion of the earthquake, February 14, 2006	51
Fig. 4.19	FFT of ground motion of the earthquake, February 14, 2006	52
Fig. 4.20	IFFT of the response of the bridge due to the earthquake, February 14, 2006	53
Fig. 4.21	Displacement of the bridge the due to the earthquake, February 14, 2006	53
Fig. 4.22	Ground motion of the earthquake, August 05, 2006	54
Fig. 4.23	FFT of ground motion of the earthquake, August 05, 2006	54
Fig. 4.24	Displacement of the bridge due to the earthquake, August 05, 2006	55
Fig. 4.25	Ground motion of the El Centro Earthquake, Imperial Valley, California, USA, 1940	56
Fig 4.26.	FFT of ground motion of the El Centro Earthquake, Imperial Valley, California, USA, 1940	56
Fig. 4.27.	IFFT of the response of the bridge due to the El Centro Earthquake, Imperial Valley, California, USA, 1940	57
Fig 4.28	Predicted displacement of the bridge due to the El Centro Earthquake, Imperial Valley, California, USA, 1940	57
Fig. 4.29.	Ground motion of the Mexico City Earthquake, September 19, 1995	58
Fig. 4.30.	FFT of ground motion of the Mexico City earthquake, September 19, 1995	59
Fig. 4.31.	IFFT of the response of the bridge due to the Mexico City earthquake, September 19, 1995	59
Fig. 4.32.	Predicted displacement of the bridge due to the Mexico City earthquake, September 19, 1995	60
Fig.5.1	3D view of the Finite Element Bridge Model	62

Fig.5.2	Sap window for horizontal layout line	63
Fig.5.3	Sap window for vertical layout line	63
Fig.5.4	Typical Deck section at pier and at mid span respectively	64
Fig.5.5	Sap window shows parametric variation for the thickness of bottom slab of the 64.6875 m. hinge segment	65
Fig.5.6	Sap window shows parametric variation for the thickness of the bottom slab of the 99.375 m. span	65
Fig. 5.7	Sap window shows parametric variation for the thickness of the bottom slab of the 26.325 hinge segment	66
Fig. 5.8	3D View of only pier, diaphragm and exterior girder	67
Fig.5.9	Bearing and restraint layout	68
Fig.5.10	Bearing and shock transmission device of Jamuna Bridge (fixed and mobile type)	68
Fig.5.11	Sap window shows link or support conditions	69
Fig. 5.12	Typical lateral prestressing layout for deck section	70
Fig.5.13	Sap window shows tendon is modeled as element	70
Fig 5.14	Sap window shows prestressing is done for odd number of tendon and the jacking end is J-end	71
Fig.5.15	Sap window shows prestressing are done for odd number of tendon and the jacking end is I-end	71
Fig. 5.16	3D View of the lateral prestressing tendon.	72
Fig. 6.1	Time period vs. mode no. of different model	75
Fig. 6.2	Deformed shape of the mode 1	77
Fig. 6.3	Deformed shape of the mode 2	78
Fig. 6.4	Deformed shape of the mode 3	79
Fig. 6.5	Deformed shape of the mode 4	80
Fig. 6.6	Deformed shape of the mode 5	81
Fig. 6.7	Deformed shape of the mode 6	82
Fig. 6.8	Deformed shape of the mode 7	83
Fig. 6.9	Deformed shape of the mode 8	84
Fig. 6.10	Deformed shape of the mode 9	85

Fig. 6.11	Deformed shape of the mode 10	86
Fig. 6.12	Deformed shape of the mode 11	87
Fig. 6.13	Deformed shape of the mode 12	88
Fig. 7.1	Time History of West –End Source (E-W Direction)	90
Fig. 7.2	Time History of West –End Source (N-S Direction)	90
Fig. 7.3	Time History of West –End Source (U-D Direction)	91
Fig. 7.4	Time History of East –End Source (E-W Direction)	91
Fig. 7.5	Time History of East-End Source (N-S Direction)	92
Fig. 7.6	Time History of East-End Source (U-D Direction)	92
Fig. 7.7-a	FFT of BR-1X	96
Fig. 7.7-b	FFT of BR-3Z	96
Fig. 7.7-c	FFT of BR-4Z	97
Fig. 7.7-d	FFT of BR-5X	97
Fig. 7.7-e	FFT of BR-7Z	98
Fig. 7.7-f	FFT of BR-8Z	98
Fig. 7.7-g	FFT of BR-9Z	99
Fig. 7.7-h	FFT of BR-10X	99
Fig. 7.7-i	FFT of BR-12X	100
Fig. 7.7-j	FFT of BR-13X	100

NOTATION

A_1	Absolute value of the FFT of the displacement of the bridge at the deck at pier P10 in the NS direction.
A_2	Absolute value of the FFT of the ground acceleration recorded at the west-end free-field station in the north-south direction.
BR	Name of sensor channel
G	Absolute value of the FFT of the ground acceleration of the applied earthquake
Hz	Unit for frequency
R	Absolute value of the FFT of the response of the bridge to the applied earthquake
R_I	Imaginary value of the response of the bridge to the applied earthquake
R_R	Real value of the response of the bridge to the applied earthquake
T	Absolute value of TR
T_I	Imaginary value of TR
T_R	Real value of TR
a	Real value of the FFT of the ground acceleration recorded at the west-end free-field station in the north-south direction
b	Imaginary value of the FFT of the ground acceleration recorded at the west-end free-field station in the north-south direction
c	Real value of the FFT of the displacement of the bridge at the deck at pier P10 in the NS direction; i.e. at BR5X
c_n	damper of the m_n mass
d	Imaginary value of the FFT of the displacement of the bridge at the deck at pier P10 in the NS direction; i.e. at BR5X

k_n	stiffness of the m_n mass
m_n	concentrated mass of nth part of the system
u_n	displacements of the m_n mass
\hat{u}	FFT of the displacement of the bridge at the deck at pier P10 in the NS direction; i.e. at BR5X
\ddot{u}_g	ground acceleration due to external source of excitation
\hat{u}_n	FFT of the displacement of m_n mass
$\hat{\ddot{u}}_g$	FFT of the ground acceleration
$\hat{\ddot{u}}_{gf}$	FFT of the ground acceleration recorded at the west-end free-field station in the north-south direction
ω	Angular frequency
ν	Oscillating frequency
θ_1	Phase angle of the FFT of the displacement of the bridge at the deck at pier P10 in the NS direction
θ_2	Phase angle of the FFT of the ground acceleration recorded at the west-end free-field station in the north-south direction
θ_g	Phase angle of the FFT of the ground acceleration of the applied earthquake
θ_R	Phase angle of the FFT of the response of the bridge to the applied earthquake
θ_t	Phase angle of TR

ABBREVIATIONS

ERA	Eigensystem Realization Algorithn
FEM	Finite Element Model
FFT	Fast Fourier Transformation
GA	Genetic Algorithm
IFFT	Inverse Fast Fourier Transformation
JMB	Jamuna Multipurpose Bridge
NExT	Natural Excitation Technique
PWD	Public Works Datum
SI	System Identification
SDOF	Single Degree of Freedom
TDOF	Two Degree of Freedom
TR	Transfer Ratio
UTC	Universal Time Coordinate

ACKNOWLEDGEMENT

The author wishes to convey his profound gratitude to Almighty Allah for His graciousness, unlimited kindness and blessings and for allowing him to complete the thesis.

The author wishes to express his sincere appreciation and gratitude to his supervisor; Dr. Raquib Ahsan, Associate Professor, Department of Civil Engineering, BUET, Dhaka, for his continuous guidance, invaluable suggestions and continued encouragement throughout the progress of the research work.

The author wishes to express his sincere gratitude to Md. Mehedi Hasan, Shahedreen Ameen and Shahrin Anwar, graduates from this institution for providing necessary cooperation and assistance.

The author expresses profound gratitude to his family members for their support, help and inspiration.

ABSTRACT

The Jamuna Multipurpose Bridge over the mighty Jamuna River has established the long cherished road link between the East and West of Bangladesh. The bridge is expected to promote better inter-regional trade, economic and social development and play a very significant role in the socio-economic development of the country. However, the bridge is located in a seismically active region. The bridge has seismic pintles for protection against a design ground acceleration of 0.2 g. However it is important to study the dynamic properties of the bridge. For this purpose, the bridge was instrumented with sensors in order to monitor the dynamic behavior. In the present study the earthquake data recoded by the sensors are used to analyze the response of the bridge.

The amplitudes of bridge response due to the application of earthquakes of different magnitudes are evaluated in this study. For this purpose, at first dynamic parameters are identified by ambient vibration assuming simplified geometry and deflection parameters of the bridge. Finally, a multi degree of freedom system is formulated to determine a Transfer Ratio function of the system. The concept of Transfer Ratio (TR) allows one to use the actual recorded data to determine the system behavior without any simplified assumption regarding the geometry of the bridge. Using the earthquake data recorded by the sensors a Transfer Ratio function is derived and used to predict possible response of the Jamuna Bridge. This Transfer Ratio is verified and also applied for the earthquakes of February 14 and August 5, 2006 recorded near the Jamuna Bridge. For case study, the earthquake of El Centro earthquake, Imperial Valley, California, USA in 1940 and Mexico City Earthquake, September 19, 1995 have been applied on the Transfer Ratio function to investigate the response of the bridge to predict any seismic event.

One of the prime objectives of the present study is to develop a detailed finite element model of the bridge considering all features of the bridge geometry such as horizontal and vertical curvature of the bridge, variable deck thickness etc. For this study eight different types of models are developed. Modal analyses of the generated models are carried out. It is observed that prestressing has no significant effect on modal periods. To make the model simple hollow section at the top of the piers can be ignored as it has a very little effect on modal frequencies.

The piers can also be modeled using shell elements instead of solid elements as both the models give similar results. It is observed from the study that the model with solid elements shows slight increase in modal frequency. To model the exterior rail girder and diaphragm frame elements can also be used. It will increase the modal value insignificantly. From modal analysis it is observed that the transverse vibration occurred at the modal frequency of 1.00174 Hz in its 3rd mode which almost matches with the frequency of 1.00098 Hz of the Transfer Ratio.

The goal of this study is to determine bridge behavior under various dynamic loads. A comparative study of bridge response has been carried out at various locations under various dynamic loads such as ambient vibration, traffic vibration, combined train and traffic vibration, only train vibration and earthquake. From the responses of bridge under various dynamic loading, it is observed that there is a common peak frequency at around 1.013Hz which almost mach with the predominant frequency in transverse vibration as obtained from the Finite Element Model (1.00174Hz) and the Transfer Ratio (1.00098Hz).

CHAPTER 1

INTRODUCTION



1.1 GENERAL

Bangladesh is one of the most disaster-prone countries in the world. Although it is vulnerable to a wide variety of natural hazards, viz. flood, cyclone and storm surge, drought, riverbank erosion and earthquake, most of the recent disasters have been caused by floods and cyclones. The low incidence of severe earthquakes during this century has led to a situation where people do not perceive seismic risks to be important. However, due to increasing number of bridges, buildings and industrial structures being built during the last two decades, assessment of seismicity of different regions in the country received considerable attention of engineers and scientists. There is lack of awareness about the earthquake hazard in the country. A review of the available data shows that considerable seismic hazard exists for major parts of the country.

The Jamuna Multipurpose Bridge, opened in June 1998, is the longest bridge in Bangladesh as well as in South Asia, and the 12th longest bridge in the world according to available information. It was constructed over the Jamuna River, the fifth largest river in the world in terms of volumetric discharge. The Bridge connects the eastern and northwestern parts of Bangladesh. The location of the bridge is shown on the map in Figure 1.1. It crosses the Jamuna River, the main channel of the Brahmaputra River in Bangladesh, from Bhupur on the East Bank to Sirajganj on the West Bank.

The bridge generates multifarious benefits for the people and especially, promotes inter-regional trade in the country. Apart from quick movement of goods and passenger traffic by road and rail, it facilitated transmission of electricity and natural gas, and integration of telecommunication links. The bridge, stretching from Tangail to Sirajganj is located on the Asian Highway and the Trans-Asian Railway which, when fully developed, will provide uninterrupted international road and railway links from Southeast Asia to Northwest Europe.

The bridge has been instrumented with sensors to record and collect noise, traffic and earthquake data. The objectives of such installation are to observe and predict the dynamic behavior of the bridge structure.

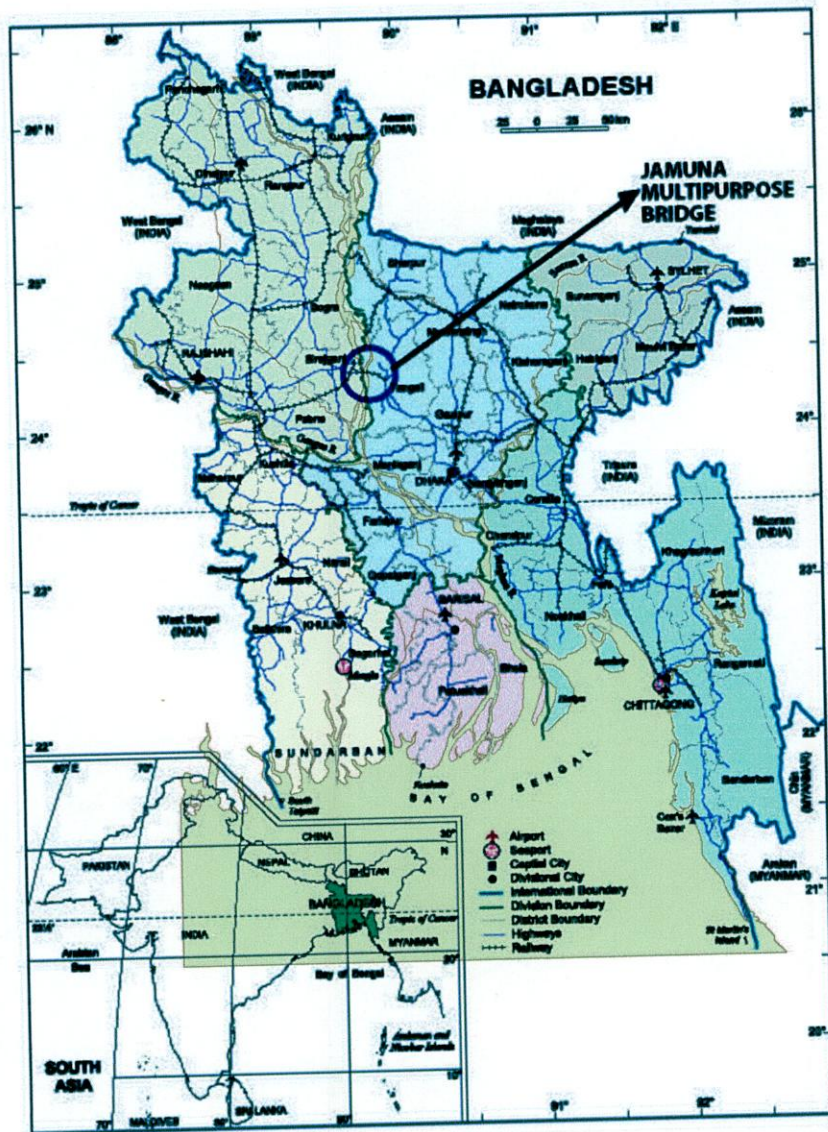


Fig. 1.1 Location of the Jamuna Multipurpose Bridge.

The objectives of the present study are to develop a mathematical model and a detailed finite element model of the bridge and to compare the dynamic behavior of the models with the actual response of the structure. This study of dynamic behavior is specially

confined into the determining the predominant frequency in transverse direction of the models by using the recorded data.

1.2 OBJECTIVES OF THE STUDY

Behavior of bridges under the influence of seismic load has been a major point of interest for engineers over a long period of time. The 1971 San Fernando earthquake was a major turning point in the development of seismic design criteria for bridges. Although significant advances have been achieved since that time in the design and construction of an earthquake resistant bridge, numerous gaps still remain in the understanding of the seismic behavior of bridges. The principal objectives of the present study are:

1. To establish a transfer ratio for the transverse vibration of the Jamuna Multipurpose Bridge based on recorded data of bridge and free-field.
2. To perform dynamic analysis on appropriate finite element model of the Jamuna Multipurpose Bridge.
3. To compare bridge response under various dynamic loads such as earthquake, combination of train and various traffic loads, only train load and ambient vibration from recorded data.

1.2 SCOPE OF THE STUDY

The research work involves the seismic response of the Jamuna Bridge. The study concentrated mainly on evaluating the amplitude of the bridge for the prediction of any seismic events. The followings are limitations, assumptions and considerations of the study.

- The structural behavior of the bridge is assumed to be linear ignoring material and other non-linearity.
- In the mathematical modeling of the bridge a three degree of freedom system has been formulated to study the response of the bridge.
- The isolation device is not considered in the mathematical modeling of the bridge.

- The isolation device is considered in the finite element modeling of the bridge.
- The horizontal and vertical curvatures of the bridge have been considered.
- The variation in the depth of the deck along its length is considered parabolic as per the actual condition.
- The variation in the width of the deck along its length is considered parabolic as per the actual condition.
- Only modal analysis is carried out. No time-history analysis is performed.

CHAPTER 2

LITERATURE REVIEW

2.1 GENERAL

It is not feasible to experimentally test the dynamic behavior of civil structures due to their huge inertia. Strong motion data acquired from such structures during seismic events can play a vital role in gaining insight into the behavior of these systems if a systematic procedure is adopted in analyzing the acquired data. This process, known as system identification (SI), is an inverse problem in structural dynamics that involves the determination of mathematical models and the estimation of structural parameters on the basis of measured responses under known excitations. Several techniques, from the simple transfer function method to the more sophisticated output error method have been devised.

2.2 CONCEPT OF SYSTEM IDENTIFICATION

System identification (SI) is the process of constructing or updating the mathematical model of a dynamical system based on input and output observations. Among other applications, SI can be applied to structural health monitoring and damage assessment, e.g., by determining the structural stiffness values and comparing them with previously determined values or originally intended values. Research interest in this subject area has increased steadily over the years.

2.3 ACTIVITIES BASED ON SYSTEM IDENTIFICATION

Vibration monitoring of civil engineering structures (e.g. bridges, buildings, dams) has gained a lot of interest over the past few years, due to the relative ease of instrumentation and the development of new powerful system identification techniques. Sometimes it is doubted whether the measured deviations of dynamic properties (eigen frequencies, modeshapes) are significant enough to be a good indicator of damage or deterioration. The comparison of original and new dynamic properties can also be hampered by natural changes caused by environmental influences (e.g. temperature changes). Another issue of continuing research is the localisation of damage starting from any observed difference in

dynamic properties. To convince the engineering community that vibration monitoring is a valuable technique for structural assessment a proof of feasibility is essential.

In the context of civil engineering structures, Caravani *et al.* (1977) were among the first to carry out SI study by means of a recursive least-square algorithm. Carmichael (1979) presented two case studies of state estimate to illustrate the use of the Kalman filter and the extended Kalman filter (EKF). Yun and Shinozuka (1980) applied two SI algorithms, namely, the EKF and the iterated linear filter-smoother, to identify the hydrodynamic coefficient matrices for an offshore structure problem. Hoshiya and Satio (1984) proposed a weighted global iteration algorithm to improve the convergence characteristics of the EKF process. This method was subsequently applied in the study of a running load on a beam by Hoshiya and Maruyama (1987). Yun *et al.* (1988) identified the structural parameters of a damaged bridge structure by the EKF. Sato and Qi (1998) developed another bridge structure by the EKF. In the same year Sato and Qi developed another filter based SI approach by incorporating a memory fading function. Other recent research works include Wang and Haldar (1994), Ghanem and Shinozuka (1995), Shinozuka and Ghanem (1995), Chen and Lee (1997), Cobb and Liebst (1997), Herrmann and Pradlwarter (1998), and Quek *et al.* (1999).

2.4 THE PROCESS OF SYSTEM IDENTIFICATION

The engineering profession has recently paid increasing attention to the use of SI techniques as a nondestructive evaluation procedure to locate defects in existing structures. In most SI techniques, the information on output excitation and output responses must be measured. However, in many cases, it is extremely difficult to accurately measure the input excitation under actual operating conditions or during actual vibrations of practical importance, e.g. earthquakes, winds, microseismic tremors, flow induced vibration and mechanical vibration. The measured input data could be highly contaminated by noise. The output measurements would also contain some noise.

System Identification is an Integrated Process of the following six steps:

1. A Model Development
2. Experimental Design
3. Full-scale Testing

4. Data Processing tools
5. Model Calibration and Parameter Estimation
6. Utilization

The quality of each step is improved by integrating experimental and analytical components. Any step may be repeated to ensure that the geometric model converges to a mathematically optimal and a physically realistic solution.

2.5 VARIOUS STUDIES ON SYSTEM IDENTIFICATION

2.5.1 Paultre *et al.* (1992)

Dynamic bridge testing techniques were used by Paultre *et al.* (1992) at the University of Sherbrooke on a series of highway bridges in Quebec, Canada. These procedures were developed to obtain a reliable evaluation of the dynamic amplification factor for bridges, as part of an ongoing rehabilitation program of the province's road network. Vertical acceleration responses were obtained under normal or controlled traffic using different test vehicles and loading patterns. The vibration frequencies and mode shapes were calculated from a frequency analysis of the measured data and used to calibrate finite element models for each structure.

2.5.2 Street *et al.* (1994)

Street *et al.* (1994) assessed the structural integrity of the double deck through-truss Brent-Spence Bridge when subjected to a seismic event from the New Madrid, Wabash Valley, or Anna seismic zones. To achieve this, the scope of work was divided into several tasks as follows: field testing of the main bridge, analytical modeling, and determination of site-specific ground motion, and seismic response analysis. The ambient vibration properties of the main bridge were determined through field testing under traffic induced excitation. The purpose of measuring the ambient vibration properties was to determine the mode shapes and the associated natural frequencies. These vibration properties were subsequently used as the basis for calibrating the finite element model for seismic response analysis. A three dimensional finite element model of the main bridge was developed for the three vibration analysis.

2.5.3 Wangans and Haldar (1995)

A time domain system identification technique was proposed by Wangans and Haldar (1995) to estimate the stiffness and damping parameters, at the element level, of a structure excited by unknown or unmeasured input forces. The unknown input forces could be of any type, including seismic loading. The unique feature of this technique is that it does not require response measurements at all dynamic degrees of freedom of the structure. This new procedure is a combination of an iterative least-squares procedure with unknown input excitations proposed earlier by these workers, and the extended Kalman filter method with a weighed global iteration. The uncertainty in the output responses was considered and its effect on the accuracy on the identified parameters was analyzed. The accuracy of the proposed procedure required a longer response measurement. However, the efficiency of the new algorithm could be improved by considering a shorter duration of response measurements.

2.5.4 Nelson *et al.* (1998)

Estimating observability matrices or state sequences is the central component of existing subspace identification methods. Nelson *et al.* (1998) proposed a different approach, in which Markov parameters were first estimated under general input excitation, was proposed. The prominent difference of this approach is that a three-block arrangement of data matrices is used. It is shown that one advantage of this approach over other subspace algorithms is that several unbiased estimating procedures can be carried out. One immediate application is to obtain balanced or nearly balanced models directly from the estimated Markov parameters. Another application is that with the estimated Markov parameters, consistently initialized Kalman filter state sequences can be obtained, from which the system matrices can be easily determined without bias. Performance of the proposed algorithms is investigated in two case studies which are based on real data taken from two industrial systems.

2.5.5 Tang and Huang (1999)

Tang and Huang (1999) developed an identification algorithm to investigate the dynamic properties of a base-isolated highway bridge equipped with lead-rubber bearings, which was conducted in 1998 in Taiwan. A linear model was used for the substructure while a

bilinear hysteretic model was chosen for the bearing system. The nonlinear hysteretic in the latter was characterized through a backbone curve. Application of Masing criterion enabled the multivalued restoring force to be transformed into a single-valued function. Consequently, the identification scheme, which was effective for a linear system, could be applied. A numerical example illustrated the proposed identification procedure and its applicability.

2.5.6 Koh *et al.* (1999)

Though many methods of system identification are currently available for parameter estimation of structural systems, the challenge lies in the numerical difficulty in convergence when the number of unknowns is large. To overcome this difficulty Koh *et al.* (1999) adopted the genetic algorithm (GA) approach, which has several advantages over classical system identification techniques. Nevertheless, if applied directly, this approach requires tremendous computational time when dealing with structural systems large in both unknowns and degrees of freedom. A method has therefore been proposed to alleviate this problem by conducting a GA search in modal domains of a much smaller dimension than the physical domain. The objective function was defined based on the estimated modal response in time domain and the corresponding modal response transformed from the measured response. With some modification, this method also works well even with incomplete response measurement. Numerical examples of structural systems of up to 50 degrees of freedom are presented. Effects of measurement noise are considered.

2.5.7 Chang *et al.* (1999)

The investigation of dynamic response for long-span cable-stayed bridges largely depends on detailed understanding of their dynamic characteristics, such as the natural frequencies, mode shapes, and damping ratios. Chang *et al.* (1999) studied the dynamic characteristics of a fairly long cable-stayed bridge in Hong Kong using finite-element analysis and ambient vibration measurements. A three-dimensional finite-element model was first established for the bridge based on design drawings. The dynamic characteristics were then analyzed from the statically deformed configuration. Ambient vibration measurements were also conducted to obtain dynamic characteristics of the

bridge. Comparison between these two results shows that, for the most total of 31 modes can be correlated with a reasonable agreement. However, the frequency differences higher modes can range between 15 and 30%. This implies that, if the measurement is more reliable, a finite element model updating is necessary in order to achieve better correlation between these two results.

2.5.8 Chaudhary *et al.* (1999)

Identification of system parameters from seismic accelerations recorded on a base-isolated bridge provides an excellent opportunity to examine the performance of various components of such bridge systems. Such a study, made by Chaudhary *et al.* (1999), proposed a two-step system identification method for identifying structural parameters from strong motion records. The first step of the study entails identification of complex modal parameters of a nonclassically damped base-isolated bridge-pier-pile-foundation system for which necessary theoretical formulations are first derived. In the second step a global search scheme was introduced to identify the structural parameters of the system corresponding to the identified modal parameters. The proposed system identification method was applied to two base-isolated bridges such that recorded responses at pier cap and girder were successfully recreated for one main shock and four aftershocks of the 1995 Kobe earthquake and modal and structural parameters were identified. Performance of the base-isolation system was evaluated by comparing the physical properties of the bearings, determined from experimental data, with the identified values and was found to be satisfactory in both bridges.

2.5.9 Shi *et al.* (2000)

System identification of very large structures is of necessity accomplished by analyzing output measurements, as in the case of ambient vibration surveys. Conventional techniques typically identify system parameters by assuming (arguably) that the input is locally Gaussian white, and in so doing, effectively reduce the number of degrees of freedom of the estimation problem to a more tractable number. Shi *et al.* (2000) described a new approach that has several novel attributes, among them, elimination of the need for the Gaussian white input assumption. The approach involves a filter applied to an

identification problem formulated in the frequency domain. The filter simultaneously estimates both system parameters and input excitation characteristics.

2.5.10 Schulz *et al.* (2000)

Fiber optic Bragg gratings packaged in long gage configurations are being used to measure static and dynamic strain in structures and structural models to monitor structural health and predict damage incurred from a seismic event. These long gage sensors were used by Schulz *et al.* (2000) to experimentally verify analytical models of post-earthquake evaluation based on system identification analysis. This fibre optic deformation measurement system could play a significant role in monitoring/recording with a higher level of completeness the actual seismic response of structure and in non-destructive seismic damage assessment techniques based on dynamic signature analysis. This new sensor technology will enable field measurements of the response of real structures to real earthquakes with the same or higher level of detail/resolution as currently in structural testing under controlled laboratory conditions.

2.5.11 Lus *et al.* (2001)

Lus *et al.* (2001) presented the theory for a system identification and damage detection algorithm for linear systems. The proposed approach has two well-defined phases: (1) identification of a state space model using the Observer/Kalman filter identification algorithm, the eigensystem realization algorithm, and a nonlinear optimization approach based on sequential quadratic programming techniques, and (2) identification of the second-order dynamic model parameters from the realized state space model.

2.5.12 Maeck *et al.* (2001)

In the framework of developing a non-destructive damage identification technique, vibration monitoring is a useful evaluation tool that relies on the fact that the occurrence of damage in a structural system leads to changes in its dynamic properties. The damage identification techniques are based on the observed shifts in eigenfrequencies and modeshapes and relate the dynamic characteristics to a damage pattern of the structure. The presented technique makes use of the calculation of modal bending moments and curvatures to derive the bending stiffness at each location. Damage identification results

were compared with results from a classical sensitivity based updating technique by Maeck *et al.* in 2001. The basic assumption in both techniques was that damage could be directly related to a decrease of stiffness in the structure. Damage assessment techniques were validated on the progressively damaged prestressed concrete bridge Z24 in Switzerland, tested in the framework of the BRITE-EURAM project SIMCES. A series of full modal surveys were carried out on the bridge before and after applying a number of damage scenarios.

2.5.13 Shen *et al.* (2001)

A bridge with lead-rubber seismic isolation bearings was field-tested by Shen *et al.* (2001) to evaluate the assumptions and uncertainties in the design and construction. A numerical model was established based on satisfactory predictions of the dynamic characteristics under ambient vibration, free vibration tests, and the seismic performance under the 1022 Gia-Yi earthquake. Parametric studies of this model, under simulated near-fault ground motions, were carried out to investigate the near-fault effect. Two types of velocity pulse that characterize the near-fault effect were investigated. Results revealed amplified seismic response when the pulse period was close to the effective period. The response amplification by a longer period pulse was not consistent for the two pulse types. Additional observations included the ratio of dissipated energy by the lead-rubber bearings to the total input energy, which could be influenced by the near-fault effect. Variation of the near-fault effect due to a change of structural parameters was studied to provide information on possible mitigation strategy.

2.5.14 Calvert and Mooney (2002)

Blue Road Research and the University of California at San Diego have been collaborating over the past many years to develop a system employing fibre Bragg grating strain sensors and model analysis to provide real time, quantitative information on a bridge's response to a dynamic input (such as a seismic event), and a fast prediction of the structure's integrity. The research being funded by the National Science Foundation has several publications showing its strong progress. In the latter part of 2004, this system was installed on the Broadway Bridge in downtown Portland, Oregon, USA. In the preparation for this deployment, the system underwent testing from the sensors through

the readout unit and bridge modeling to ensure its performance once installed. The steps of the preparation and procedures were discussed by Calvert and Mooney in 2002.

2.5.15 Feng *et al.* (2002)

A baseline model is essential for long-term structural performance monitoring and evaluation. Feng *et al.* (2002) pioneered a study by applying a neural network-based system identification technique to establish and update a baseline finite element model of an instrumented highway bridge based on the measurement of its traffic-induced vibrations. The neural network approach is particularly effective in dealing with measurement of a large-scale structure by a limited number of sensors. In this study, sensor systems were installed on two highway bridges and extensive vibration data were collected based on which modal parameters including natural frequencies and mode shapes of the bridges were extracted using the frequency domain decomposition method as well as the conventional peak picking method. Then an innovative neural network was designed with the input being the modal parameters and the output being the structural parameters of a three-dimensional finite element model of the bridge such as the mass and stiffness elements. After extensive training and testing through finite element analysis, the neural network became capable to identify, with a high level of accuracy, the structural parameter values based on the measured modal parameters, and thus the finite element model of the bridge was successfully updated to a baseline. The neural network developed in this study can be used for future baseline updates as the bridge being monitored periodically over its lifetime.

2.5.16 Peterson *et al.* 2003

A method of global nondestructive evaluation for identifying local damage and decay in timber beams was developed in previous analytical studies and verified experimentally using simply supported beams in the laboratory by Peterson *et al.* in 2003. The method employs experimental modal analysis and an algorithm that monitors changes in modal strain energy between the mode shapes of a damaged structure with respect to the undamaged structure. A simple three-girder bridge was built and tested in a laboratory to investigate the capability and limitations of the method for detecting damage in a multimember timber structure. The laboratory tests showed that the method can correctly

detect and locate a simulated pocket of decay inflicted at the end of a girder as well as detect a notch removed from the midspan of a girder. The tests showed that the method can correctly detect damage simultaneously at two locations within the bridge, but also that large magnitudes of damage at one location can mask smaller magnitudes of damage at another location. When a calibrated baseline model is used to represent the undamaged state of the bridge, the results show that the method of nondestructive evaluation is able to detect each case of inflicted damage, but with some increase in localization error.

2.5.17 He *et al.* (2004)

The simulation of reliable ambient vibration data is essential to overcome the scarcity of actual ambient vibration test data in order to study the effects of various damage scenarios on system identification results for large and complex bridge structures. The time histories of wind-induced vibration response of the Vincent Thomas Bridge, a suspension bridge located in San Pedro near Los Angeles, California, were simulated by He *et al.* (2004) by using a detailed three-dimensional finite element model of the bridge and a state-of-the-art stochastic wind excitation model. The horizontal and vertical wind velocity fields along the bridge axis were simulated as two independent stochastic vector processes using the spectral representation method. Based on the simulated wind-induced ambient vibration data, the dynamic characteristics of the bridge were identified using the Natural Excitation Technique (NExT) combined with the Eigensystem Realization Algorithm (ERA). The identified modal properties were verified by the computed eigenproperties of the bridge finite element model and compared with the results of previous system identification studies based on actual ambient vibration data. The approach presented by He and his co-researchers provides a framework to investigate the effects of various realistic damage scenarios on system identification results in order to develop robust and reliable vibration-based structural health monitoring methods for long span bridge structures.

The literature review reveals that identification of structural systems (SI) has been a major tool in the last two decades to verify and determine vibration characteristics. It is, in fact, a unique tool to monitor the health of a structure. With the advent of more sophisticated computing software and hardware, the practicality of effectively

implementing an ambient vibration based global structural health monitoring system has been greatly enhanced. SI also helps to assess the damage and thus not only minimizes the economic cost of maintenance but also saves 'out of use' time. It is a non-destructive and user-friendly evaluation procedure.

CHAPTER 3

BRIDGE PARAMETERS AND SEISMIC INSTRUMENTATION

3.1 GENERAL

The 4.8 km long Jamuna Multipurpose Bridge (JMB) over the mighty Jamuna River has established the long cherished road link between the East and West of Bangladesh. This bridge connects Bhuapur in Tangail (East Bank) with Sirajganj (West Bank). The bridge site location map is shown in Figure 1.1. The bridge is located in a seismically active region and has been designed to resist dynamic forces due to earthquakes with peak ground acceleration as high as 0.2g. JMB is the first bridge in the country where seismic pintles have been used. The pintles act as an isolation device for protection against earthquakes.

3.2 BRIDGE DESCRIPTION

The Jamuna Multipurpose Bridge consists of four lane roads with a single track dual gauge railway, a footpath, a 230 KV electrical power line, a high pressure natural gas pipeline and telecommunication cables. The bridge is slightly curved in plan and runs through large sand islands (known as chars) in the middle of the river. The main bridge is about 4.8 km long, prestressed concrete box-girder type, and consists of 47 nearly equal spans of 99.375 m. plus 2 smaller end spans of 64.6875 m. The main bridge is supported by twenty one 3-pile piers and twenty nine 2-pile piers. There are 128 m long road approach viaducts at both ends of the main bridge. There are six hinges (expansion joints) that separate the main bridge structure into seven modules (two end modules, four 7-span module and a 6-span module in the middle) Figure 3.1. For seismic protection of the Jamuna bridge, seismic protection devices (type MEP and MEPOT, manufactured by FIP Industrial, Italy) consisting of steel pin dissipating elements and shock transmitter units have been placed in between the girders and the piers. The difference between MEP and MEPOT is due to the presence of shock transmission units (OT devices) in the latter. During earthquakes, the behaviors of MEP and MEPOT devices are identical. The seismic protection of the bridge is based upon the reduction of dynamic forces transmitted between the superstructure and the piers. This system of reduction of

dynamic forces can be termed as the base- isolation system of the bridge. Salient features of the bridge are shown in Table3.1.

Table: 3.1 Salient features of the bridge

Length of bridge	4.8 km
Length of viaduct of each side	128.0 m
Width of bridge	18.5 m
Number of spans	47+2
Length of each span	99.375 m
Length of end span	64.6875 m
Number of lanes	4
Number of rail-lines	1
3 Pile Pier (2500 mm OD)	21
2 Pile Pier(3150 mm OD)	29
Number of Total Piers	50
Number of Total Piles	121
Tubular steel Pile Thickness	40 mm to 60 mm
Average Length of Pile	83.0 m (72 m below river bed level)
Box girder segment length	4.0 m
Absolute rake of Pile (Batter Pile)	1: 6
Pier Stem height	2.72 m to 12.04 m

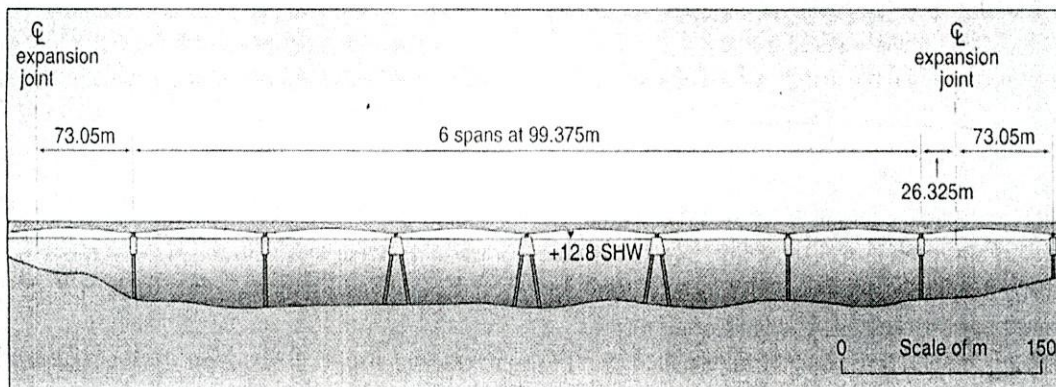


Fig. 3.1 Typical seven-span module.

3.3 PILE CONFIGURATION

The substructure of each module consists of three 3-pile piers and three or four 2-pile piers for the six and seven span modules respectively. The foundations consist of driven tubular steel piles, filled with concrete. Pile diameters are 3.15m for the 2-pile piers and 2.50m for the 3-pile piers, and toe levels vary from -70.0 m PWD (Public Works Datum) to -82.0 m PWD, with a head level of ± 11 m PWD. The thickness of the steel tube varies along the length of the pile. For 2-pile system the thickness varies as 60mm (from pile cut-off upto -6.0 m PWD), 55mm (from -6.0 m PWD to -26.0 m PWD) and 50mm. (From -26.0 PWD up to pile toe). And for 3-pile system the thickness varies as 50mm (from pile cut-off up to -6.0 m PWD), 45mm (from -6.0 m PWD up to -26.0 m PWD) and 40mm (from -26.0 PWD up to pile toe). Pile caps are of precast reinforced concrete shell with in-situ reinforced concrete infill construction. They have a base level of $+11.0$ m PWD, and so the piles are embedded some 7m within the caps. The pile caps carry pier stems which in turn support the bearings. Figure 3.2 (a), Figure 3.2 (b) and Figure 3.2(c) shows the general arrangement of piles.

3.4 PIER STEM

The height of pier stem varies from 2.72m to 13.05m and is constructed of reinforced concrete. Figure 3.3 (a) and Figure 3.3 (b) show the cross-section and elevation of the pier stem respectively. The hollow section of pier stem is filled with concrete up to 3m of its height. The cross-sectional properties of hollow and solid sections are given in Table 3.2.

Table 3.2 Cross Sectional Properties of Pier Stem

Section type	Area (m ²)	Moment of inertia (longitudinal) (m ⁴)	Moment of inertia (longitudinal) (m ⁴)
Hollow	6.84	5.85	38.42
Solid	15.0	7.81	45.0

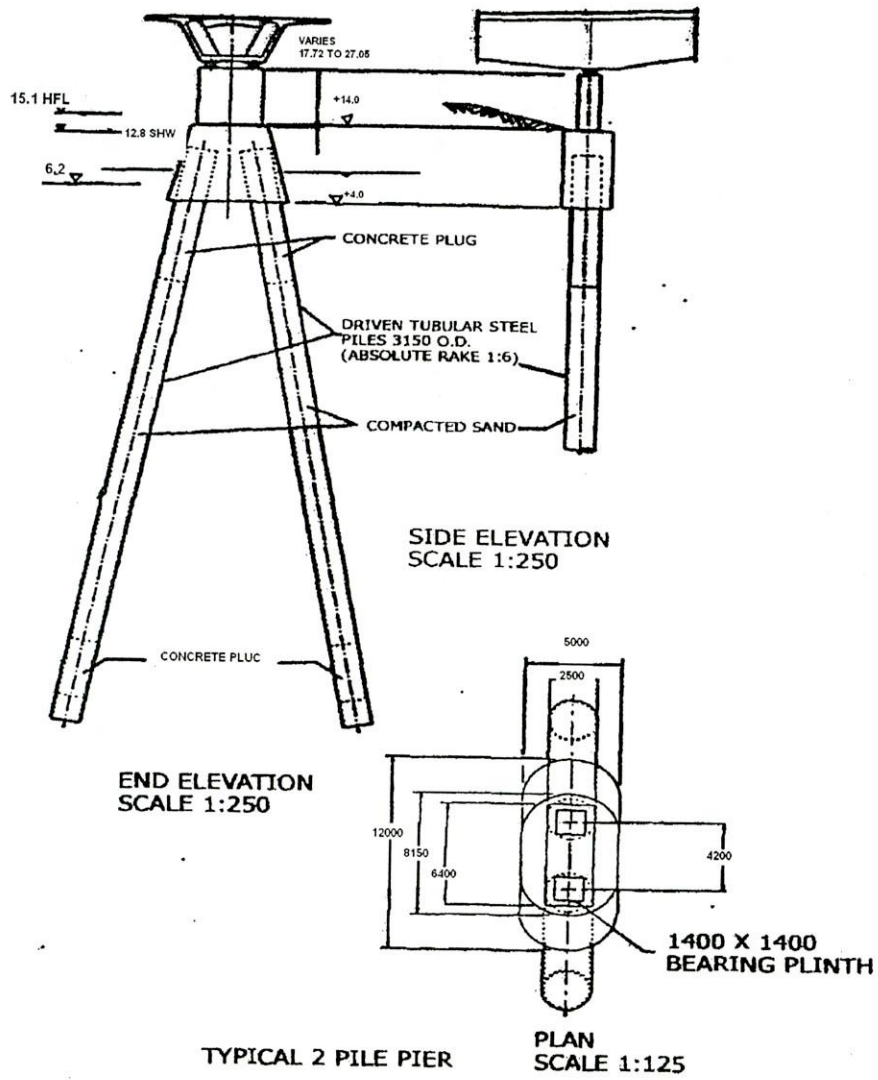


Fig. 3.2(a) General Arrangement of 2 Piles Pier

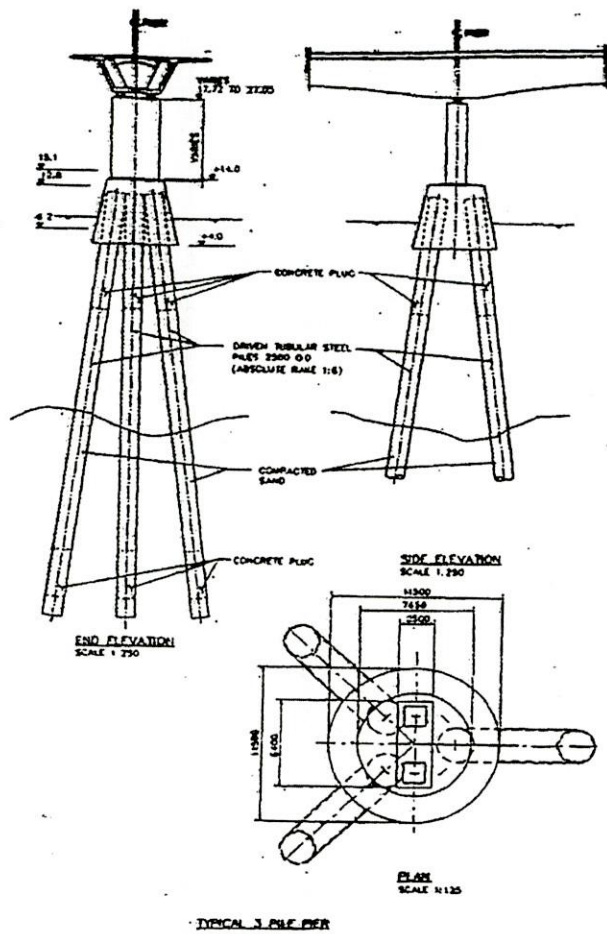


Fig. 3.2(b) General Arrangement of 3 Piles Pier

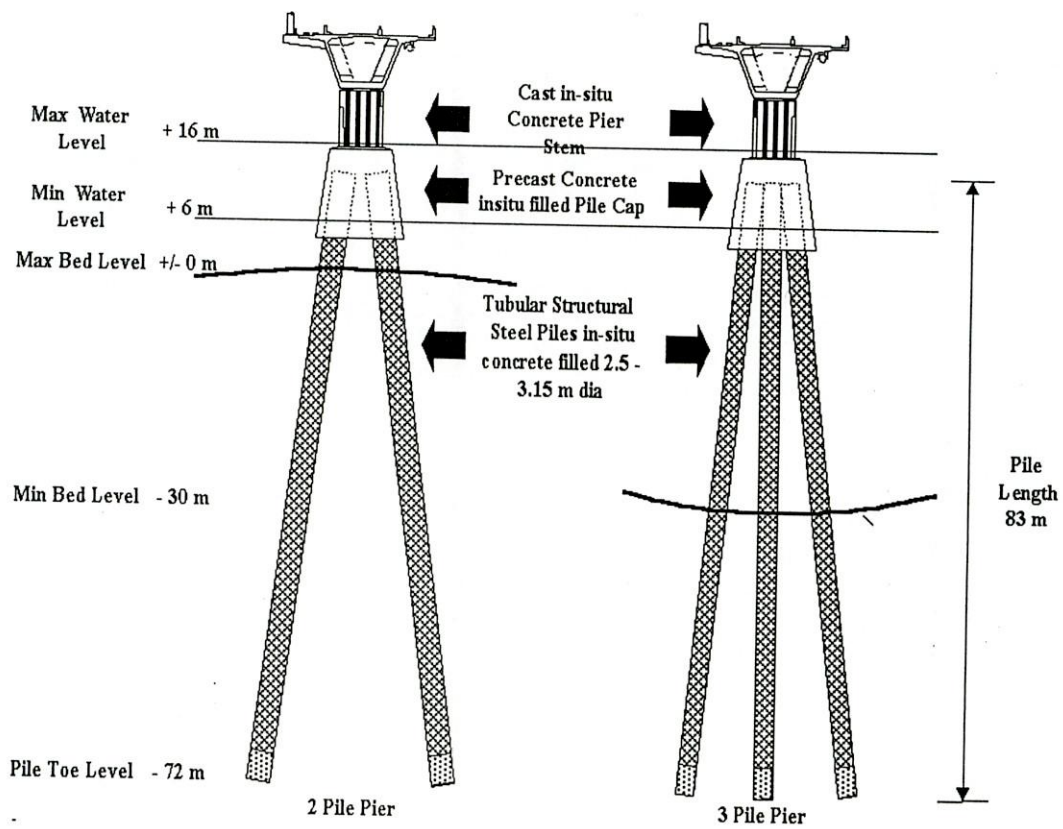


Fig. 3.2(c) General Arrangement of Piles.

3.5 DECK CONFIGURATION

The main bridge deck is a multi-span precast prestressed post-tensioned concrete segmental structure, constructed by the balanced cantilever method. Each cantilever has 12 segments (each 4 m long), joined to a pier head unit of 2 m long at each pier and by an *in-situ* stitch at mid span. The deck is internally prestressed and of single box section (Fig. 3.4). The width of the box section is 18.5 m but the depth of the box varies between 6.5 m at the piers and 3.25 m at mid-span. An expansion joint is provided every 7 spans by means of a hinge segment at approximately quarter span. The segments were precast and erected using a two-span erection gantry.

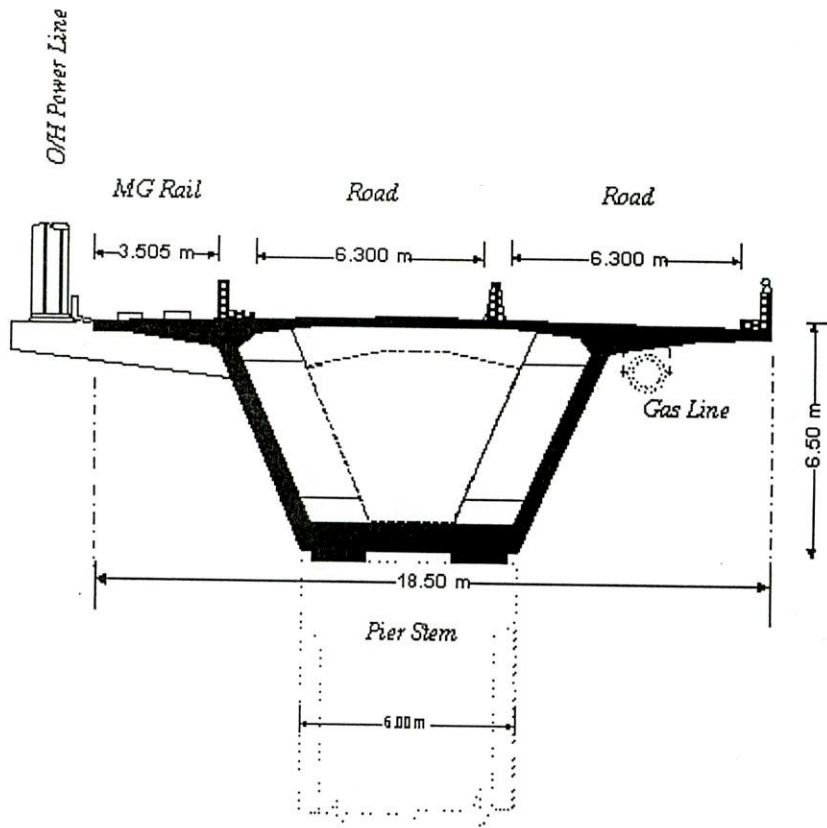


Fig. 3.4 A Typical Deck cross-section.

3.6 ISOLATION SYSTEM

Pin dissipating device (pintles) has been used as base-isolator for protection against earthquakes in JMB. Two types of dissipating device are used:

- pin elements dissipating device for fixed location (at 3-pile piers)
- pin elements and shock transmitter for the mobile locations (at 2-pile piers)

Figure 3.5 shows the schematic diagram of the device which comprises of the following elements: (FIP Industriale, 1995)

- A central body with pin dissipating elements (1)
- An upper (2) and a lower (3) plate, between which the pins are affixed. The top plate has an annular plate (4) to transmit the horizontal seismic loads from the superstructure to the pier.
- An external frame (5) with a tapered internal ring (6) affixed to the superstructure by means of bolts (9)
- An upper anchoring frame (7) with sockets (10)
- A ring (8) with an outer surface that is also tapered to match the taper of the element's (6) inner surface.

The dissipating device for the mobile locations comprises the same components as described for the fixed devices plus a shock transmitter unit made of:

- A one piece hydraulic cylinder
- Two bolted flanges that close the ends of the cylinder

A double headed piston is a rod that creates two chambers within the cylinder. The basic operation of the isolation device can be summarized as:

1. All horizontal loads other than those of sudden onset are accommodated by the elastic deformation of the pin elements in the fixed type devices at 3-pile piers.

2. Slowly applied movements, such as those resulting from thermal displacement of the bridge deck, are accommodated by the shock transmitter in (the mobile type devices at 2-pile piers.
3. Sudden onset loads such as earthquake are accommodated by the pin elements in both the fixed and mobile devices. The sharing of the sudden onset loads is achieved because the shock transmitter in the mobile locations Shocks up and transmits the loads to the pin element.

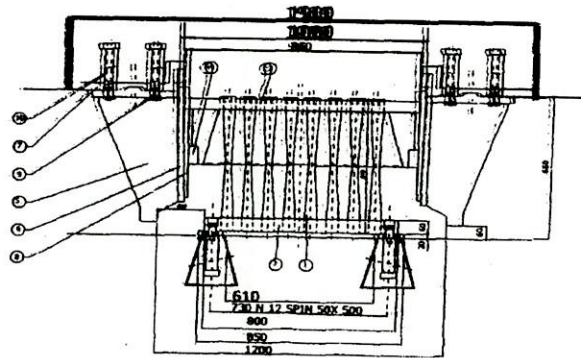
3.7 SEISMICITY OF BRIDGE SITE

Bolt, (1987) in his report on Seismicity Studies for Jamuna Bridge, Bangladesh, mentioned that the adopted site of the bridge (24.42°N , 89.75°E) could experience shaking from both great and moderate-sized distant earthquakes and from moderate near-site earthquakes during the lifetime (considered as 100 years) of the bridge structure.

Considering fault length, fault characteristics, earthquake records etc., the maximum magnitude (Richter scale) of earthquakes produced in different tectonic blocks affecting Bangladesh is given in Table-3.3. According to Bolt, (1987) only one seismic source needs to be considered in postulating strong ground shaking at the Jamuna Bridge site Zone D at a distance of 25 to 50 km. The design peak ground acceleration is 0.2g. Bolt mentioned that his work had been hampered by the lack of recordings from seismographic stations in the region. He recommended that several strong motion accelerometers should be near the bridge structure so that any local shaking can be measured accurately.

Table 3.3 Maximum Earthquake Magnitude in different Tectonic Blocks

Zone	Tectonic block	Magnitude of Earthquake	Distance from site (km)
A	Assam fault zone	8.0	120
B	Tripura fault zone	7.0	180
C	Sub Dauki fault zone	7.3	120
D	Bogra fault zone	7.0	25



3.5 (a) Schematic of Pin-Dissipating Device

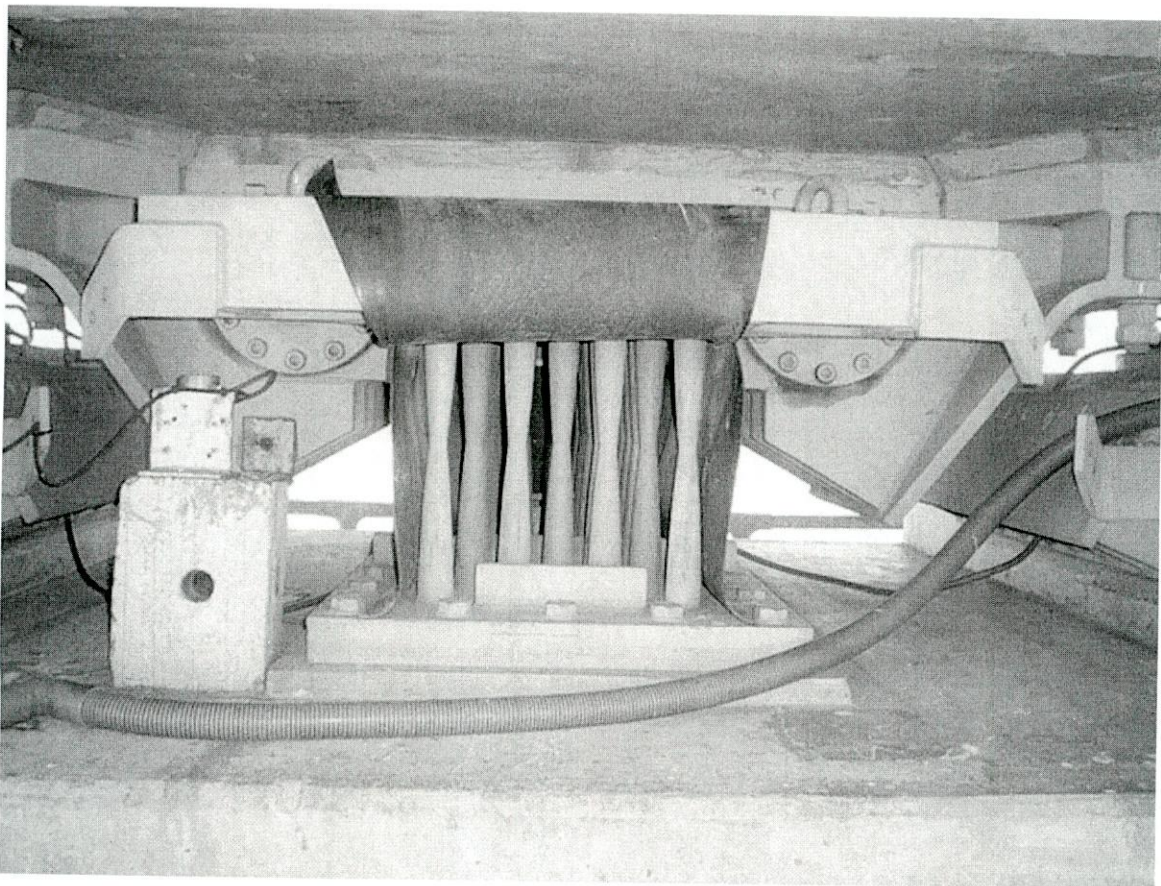


Fig. 3.5 (b) Plan of the Energy-Dissipating Device.

3.8 FREE-FIELD STATIONS

There are seven free-field stations to measure the ground motions. Each station (model ETNA) contains a triaxial accelerometer and a recorder built in a single unit. The six free-field stations are located at the two bridge ends and on office complexes of Local Government Engineering Department (LGED) in Gazipur, Mymensingh, Natore and Bogra districts. The stations are 70-90 km apart from one another forming an equilateral triangle as closely as possible on both the sides of the bridge. The portable triaxial accelerometer has been installed at the Bangladesh University of Engineering and Technology (BUET) Campus. In addition, one borehole sensor placed at the west end of the bridge. Figure 3.6 shows free-field instrumentation. Table 3.4 shows the locations and type of sensors used in free-field stations.

Table 3.4 Free-field Instruments

Model	Type	Location
ETNA	Triaxial Accelerometer (NS, EW, Vertical) plus Digital Recorder	LGED, Bogra
ETNA		LGED, Natore
ETNA		West-End
ETNA		East-End
ETNA		LGED, Mymensingh
ETNA		LGED, Gazipur
ETNA (Portable)		BUET

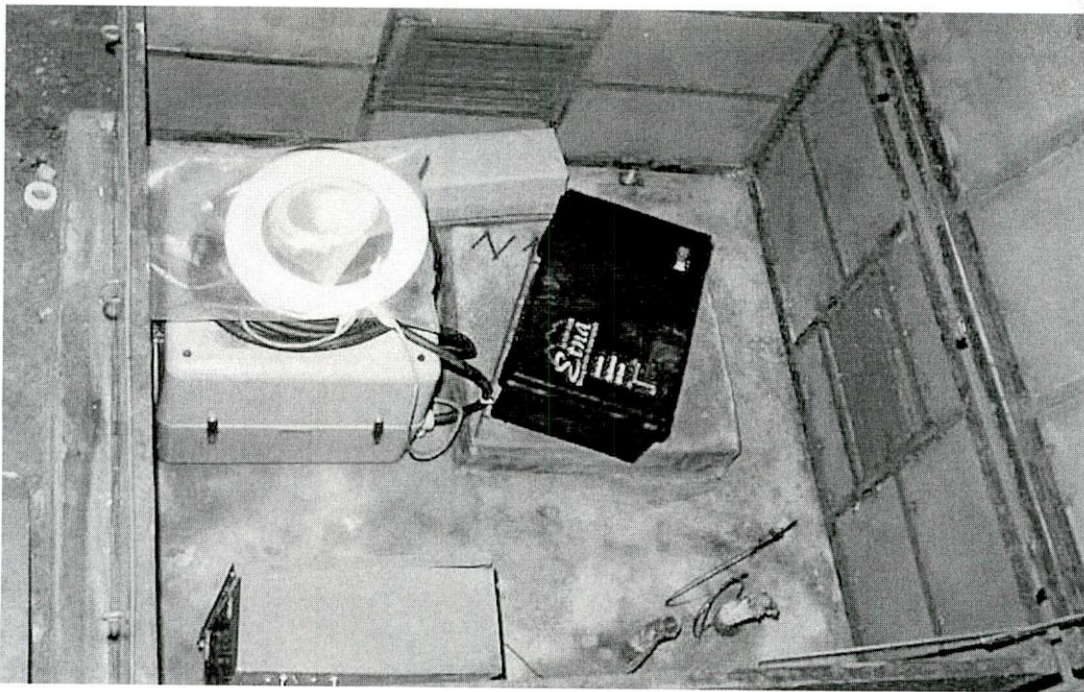


Fig. 3.6 Free-field Instrument Setup

3.9 SENSORS ON THE BRIDGE

Two triaxial, one biaxial and five uniaxial accelerometer (Model Episensor) sensors and three displacement sensors (Figs. 3.8) were installed on Module 1 of the bridge structure. There are thus 16 channels of data. These data are fed to three digital K2 data recorders labelled Jamuna, Meghna and Surma (Fig. 3.7). Each K2 recorder can support up to six channels of data. It was decided to place the three recorders and the communication enclosure close to one another within the box girder deck (Fig. 3.7) near Pier P10. The sensors and recorders installed on the bridge are listed in Table 3.5 along with location and direction of measurement. All the sensors were placed in their designated positions and each of them connected to one particular channel of a recorder. Locations of various accelerometer and displacement sensor in the Jamuna Bridge at pile, pier and deck are shown in Figures 3.9 and 3.10. These were connected to one communication enclosure for data transfer to the data control centre server through the 2.4 GHz wireless radio and antenna hoisted on a lamp post of the bridge. The system was set at Coordinated Universal Time (UTC) through a GPS.

Table 3.5 List of sensors and recorders installed on the bridge and bore-hole

K2 Data Recorder Label	Sensor Type	Channel Label	Orientation	Sensor Location
JAMUNA located inside bridge deck near Pier P10	Displacement	D1	X	Across Isolation System at Pier P10
	Displacement	D2	Y	
	Displacement	D3	Y	Across Expansion Joint between Piers P7 and P8
	EPI Uniaxial Accelerometer	BR9	Z	Pile Cap at Pier P9
	EPI Biaxial Accelerometer	BR10	X	Deck at Pier P9
BR11		Y		
MEGHNA located inside bridge deck near Pier P10	EPI Uniaxial Accelerometer	BR4	Z	Pile Cap at Pier P10
	EPI Uniaxial Accelerometer	BR8	Z	Deck at Pier P10
	EPI Uniaxial Accelerometer	BR12	X	Deck at Midspan between Piers P9 and P10
	EPI Uniaxial Accelerometer	BR13	X	Deck at Midspan between Piers P10 and P11
SURMA located inside bridge deck near Pier P10	EPI Triaxial Accelerometer	BR1	X	Pile Cap at Pier P10
		BR2	Y	
		BR3	Z	
	EPI Triaxial Accelerometer	BR5	X	Deck at Pier P10
		BR6	Y	
		BR7	Z	
PADMA located at west abutment	EPI Triaxial Accelerometer	AB1	X	West Abutment
		AB2	Y	
		AB3	Z	
	Borehole Triaxial Accelerometer	BH1	EW	Borehole near West End (58 m depth)
		BH2	NS	
		BH3	Z	

Note: X means orientation across to the bridge (transverse direction)
 Y means orientation parallel to the bridge (longitudinal direction)
 Z means vertical direction

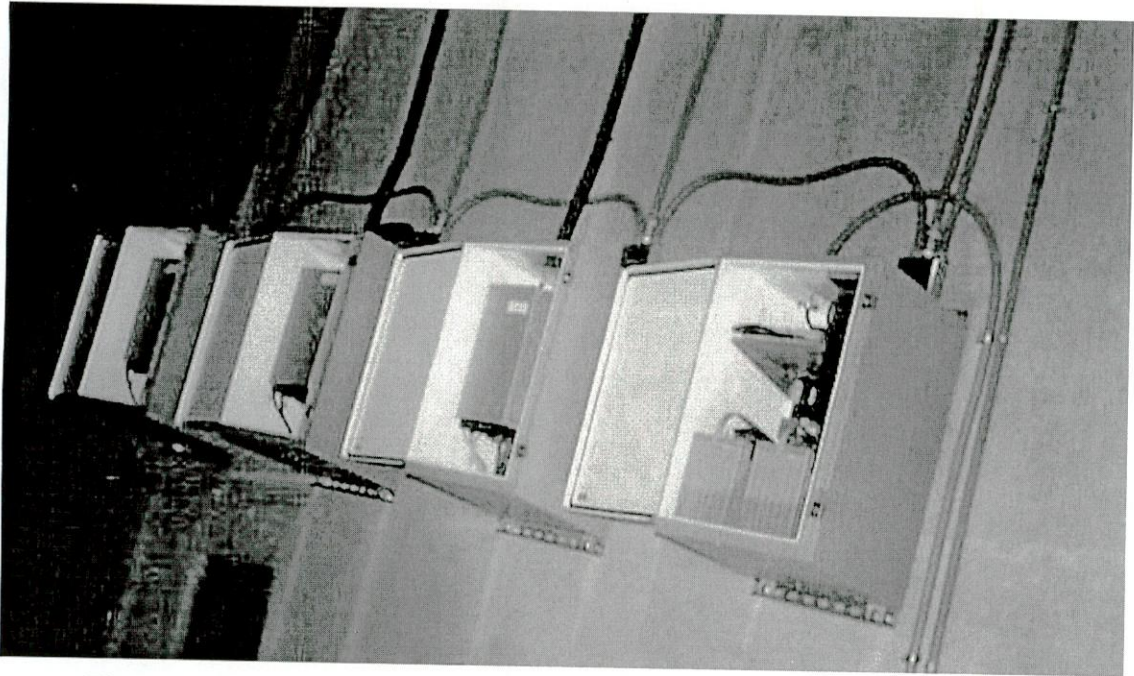


Fig. 3.7 Data Recorders and the Communication Enclosure within the Deck.

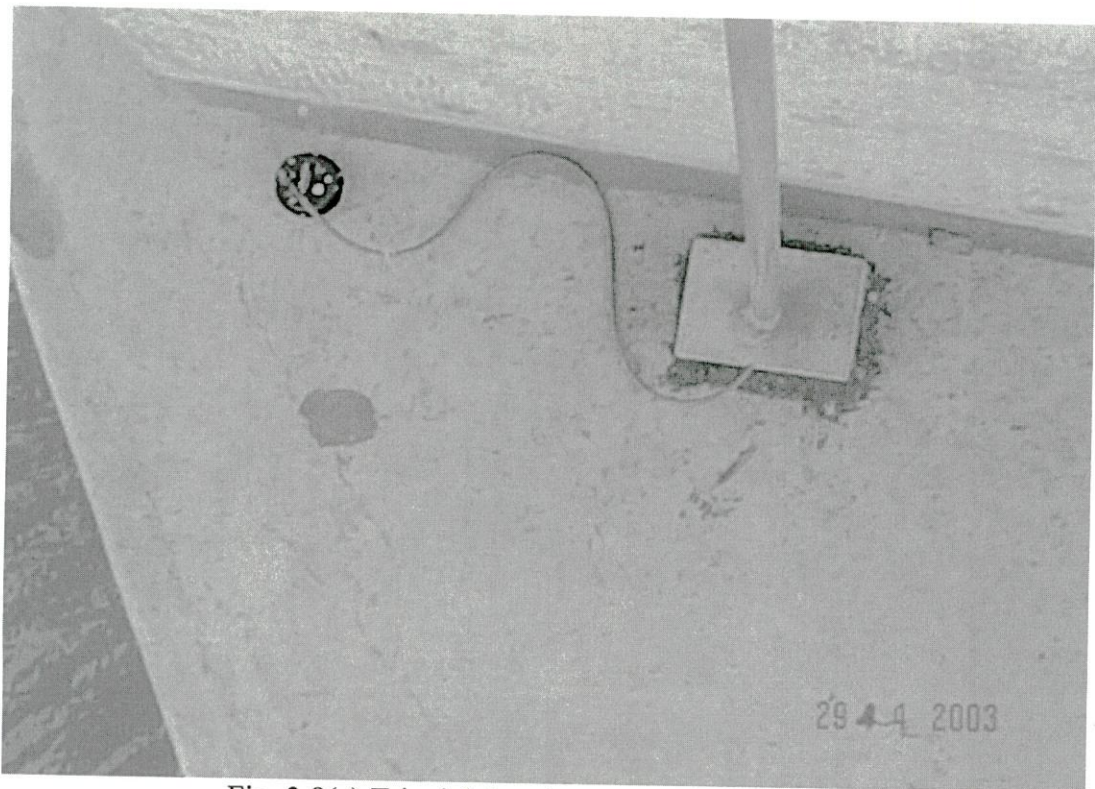


Fig. 3.8(a) Triaxial Accelerometer on the Pile Cap.

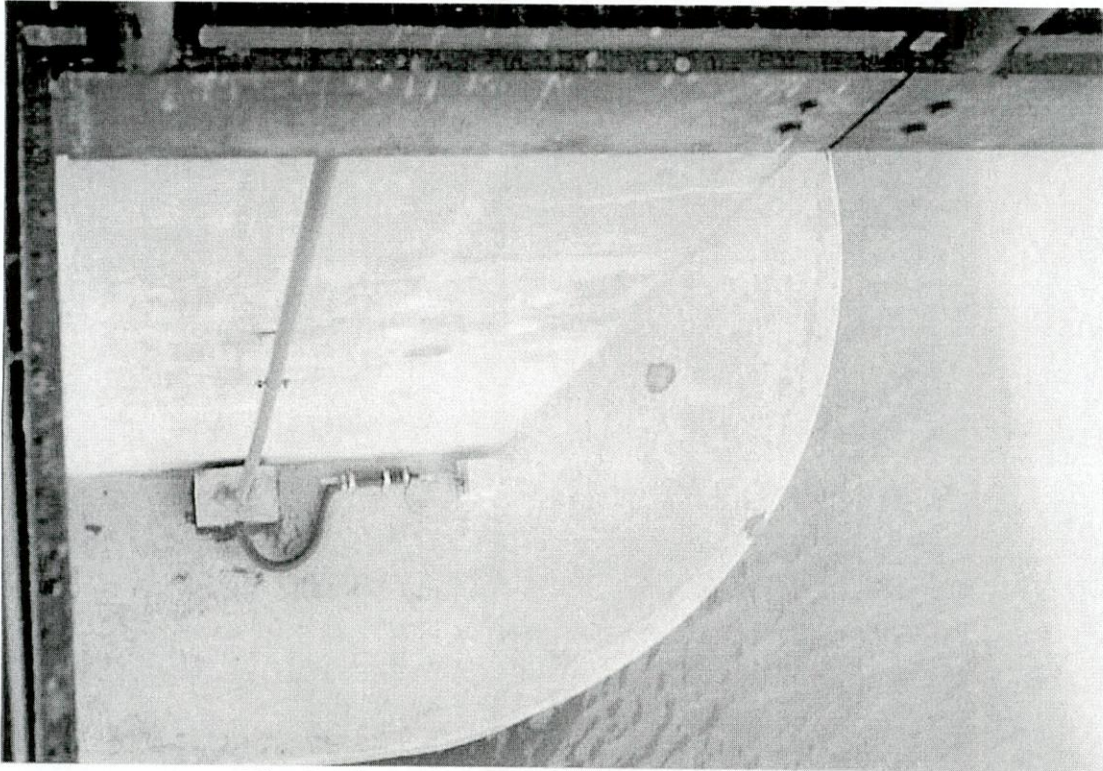


Fig. 3.8(b) Uniaxial Accelerometer on the Pile Cap.

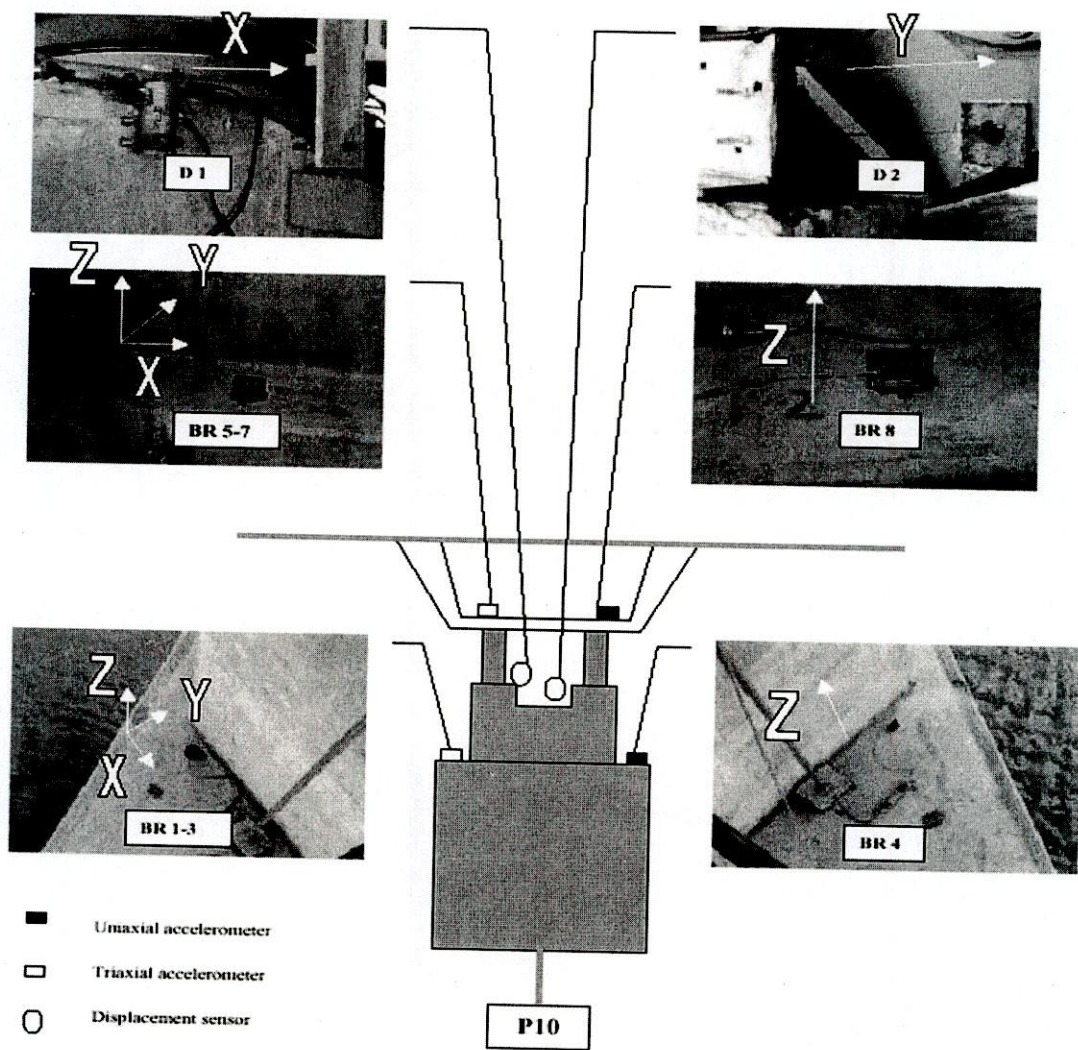


Fig. 3.9 Location of various Accelerometer and Displacement Sensors in the Jamuna Bridge at the pile caps and pier.

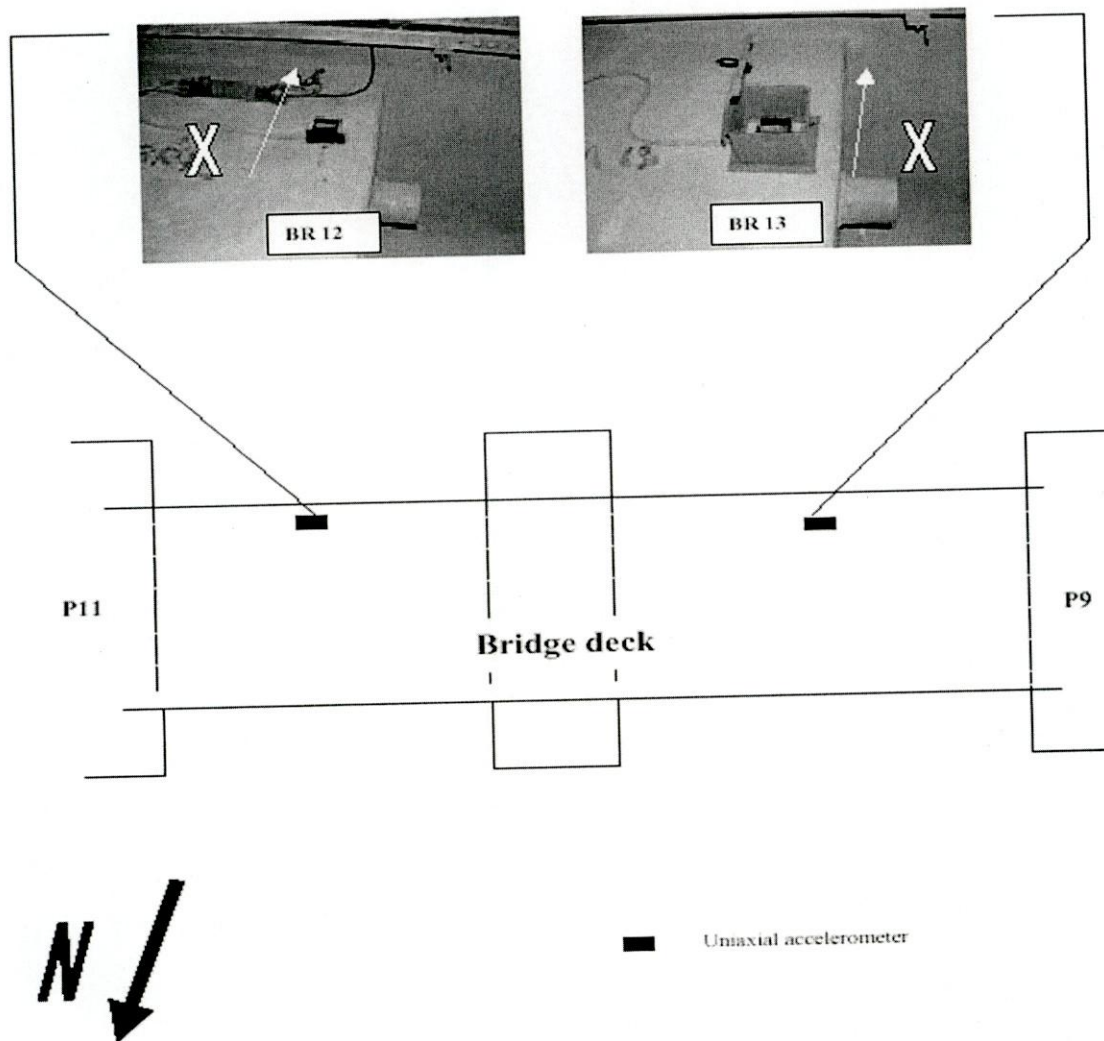


Fig. 3.10 Location of Various Accelerometers at Deck of Jamuna Bridge.

CHAPTER 4

SYSTEM IDENTIFICATION OF THE BRIDGE

4.1 GENERAL

Identification of system parameters from seismic accelerations recorded on a base-isolated bridge provides an excellent opportunity to examine the performance of various components of such bridge systems. The objective of this study is to analyze the dynamic system parameters of the Jamuna Bridge structure which would be useful in predicting response of the bridge due to earthquake.

4.2 MATHEMATICAL MODELING OF THE BRIDGE

Mathematical models are derived for better understanding of dynamic parameters of the bridge. At first formulations for single and two degrees of freedom systems are presented to compare dynamic parameters with ambient vibration of the bridge. Finally, Transfer Ratio (TR) is formulated for multi degrees of freedom system by using recorded earthquake.

4.3 SYSTEM IDENTIFICATION BY AMBIENT VIBRATION.

4.3.1 Ambient Vibration of The Pier-Deck System

Ambient vibration of the bridge is being constantly monitored with the installed sensors. Vibration of the bridge during train and road traffic movement is also being consciously recorded. A typical example of transverse vibration of pile-cap at BR1-X and corresponding vibration in the box-girder cum deck at BR5-X is shown in Figures 4.1 and 4.2. The Fourier spectrums of these noise data of ambient vibration are shown in Figures 4.3 and 4.4. From Figure 4.3 the predominant frequency of the input motion can be found approximately 1.58 Hz. In addition to this frequency, the major contribution in the deck vibration comes from the frequency level 1.37Hz and a secondary contribution from 1.1 Hz, as can be seen from Figure 4.4.

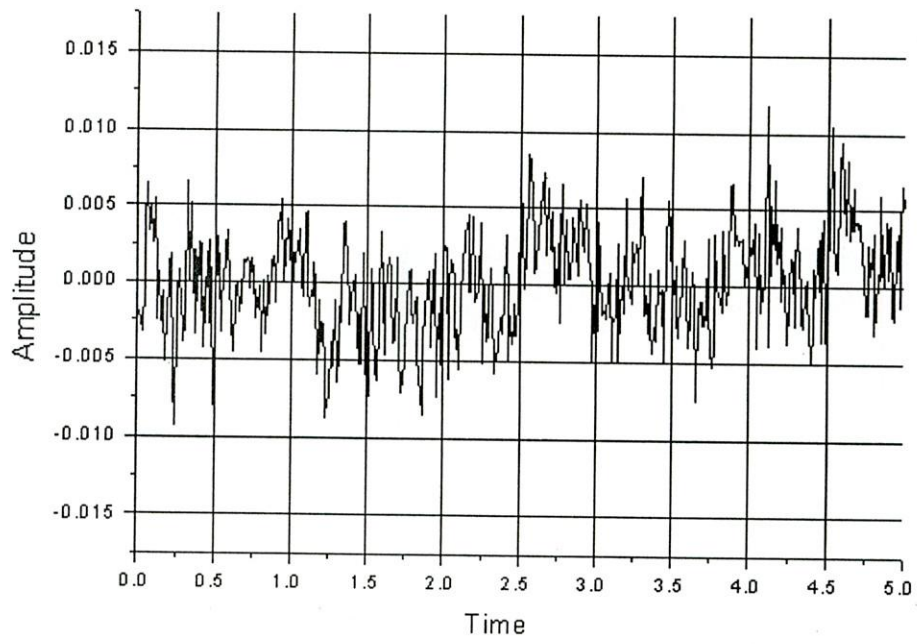


Fig. 4.1 Amplitude vs. Time (without traffic BR-1X).

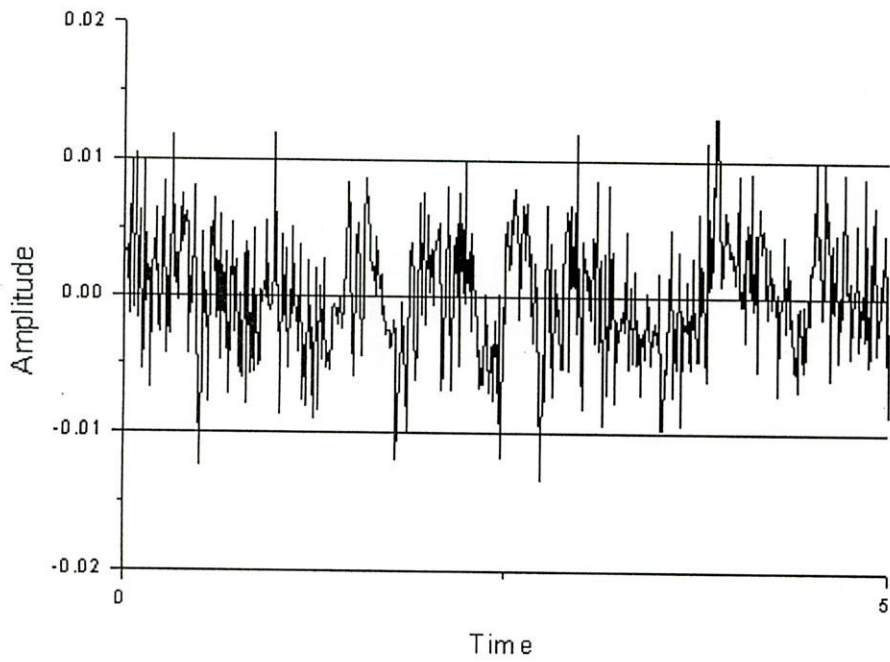


Fig. 4.2 Amplitude vs. Time (without traffic BR-5X).

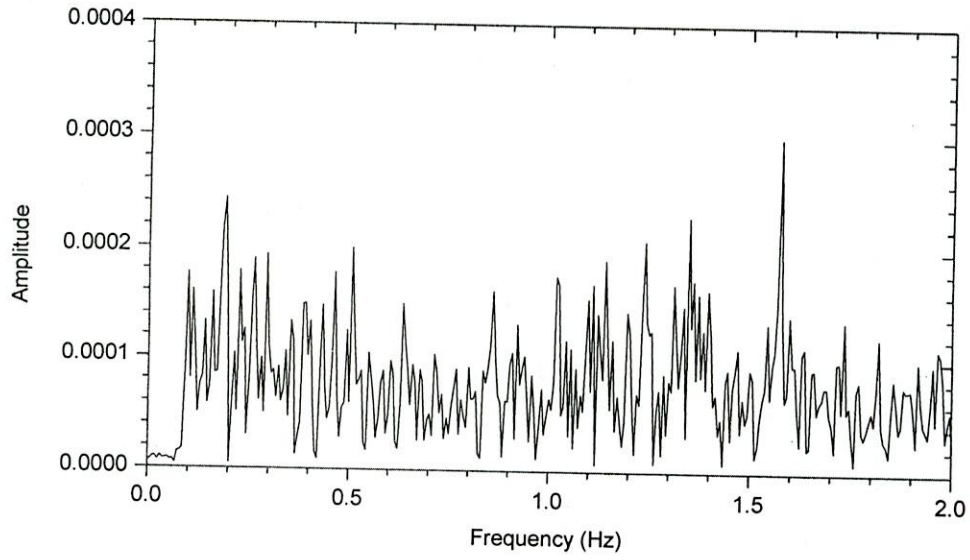


Fig. 4.3 FFT of BR-1X (without traffic).

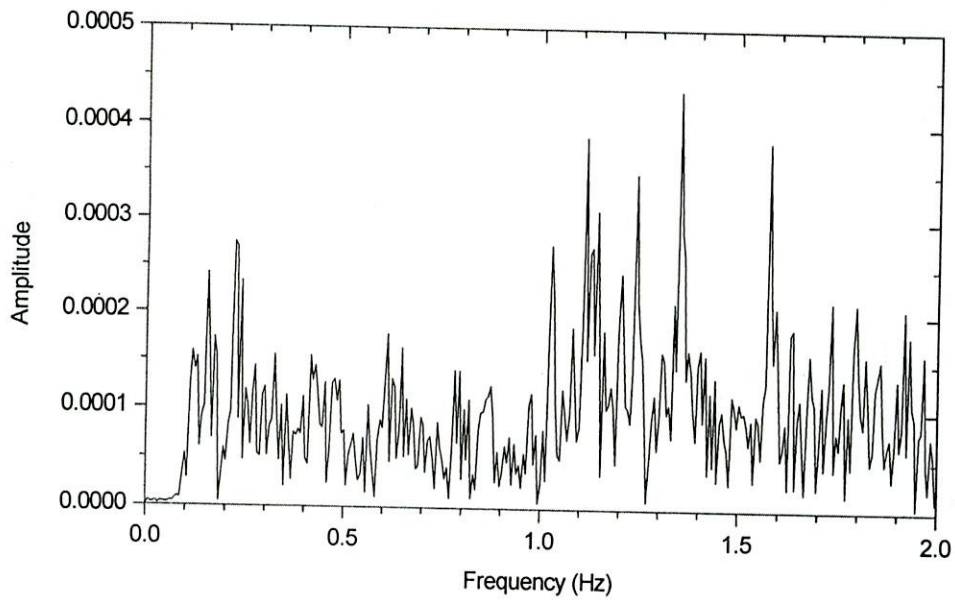


Fig. 4.4 FFT of BR-5X (without traffic).

4.3.2 Single Degree of Freedom Model (SDOF)

A Single degree of freedom system, of the pier and deck was studied in order to understand the dynamics of the system (Ahsan *et al.*, 2005). For this purpose, a 100 m segment of the deck is considered on a single pier and the curvature of the bridge is ignored. Although, the depth of the deck varies parabolically along the length, for simplicity a linear variation is assumed as shown in Figure 4.5. Instead of the complicated cross-section of the original deck, a simplified cross-section is assumed for calculation (Fig. 4.6). The mass of the deck of a 100 m segment is found to be 1.095×10^5 slug. Assuming a linear shape function of the pier, the total lumped mass of the SDOF system can be thought of deck mass plus one third of the pier mass, which amounts to 2.304×10^5 slug.

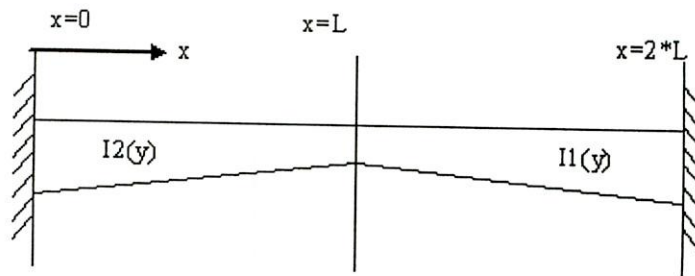


Fig. 4.5 Simplified deck profile.

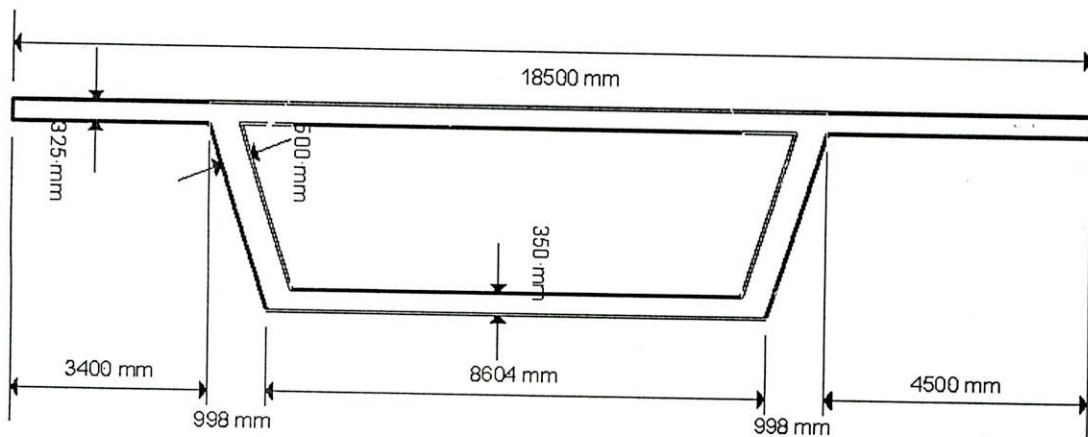


Fig. 4.6 Simplified deck cross section.

The stiffness of the pier is calculated 1.055×10^7 lb/in assuming the pier to act like a cantilever. Contribution of the deck stiffness is taken into account assuming that the 100 m segment of the deck is fixed at both ends. The total stiffness of the system becomes 1.67×10^7 lb/in. Hence, natural frequency of the SDOF model is 1.08 Hz which is very close to the secondary peak of the Fourier spectrum of the deck vibration i.e. 1.1 Hz (Fig4.4).

4.3.3 Two Degrees of Freedom Model (TDOF)

A single degree of freedom model although explains the secondary frequency, it fails to reflect the predominant frequency of 1.37 Hz. From Figure 4.3 three peaks are found of which 1.58 Hz is the contributing frequency of the ambient input vibration as shown in Figure 4.4. Two peaks suggest that the pier deck system can be better simulated as a Two degree of freedom system (Fig. 4.7).

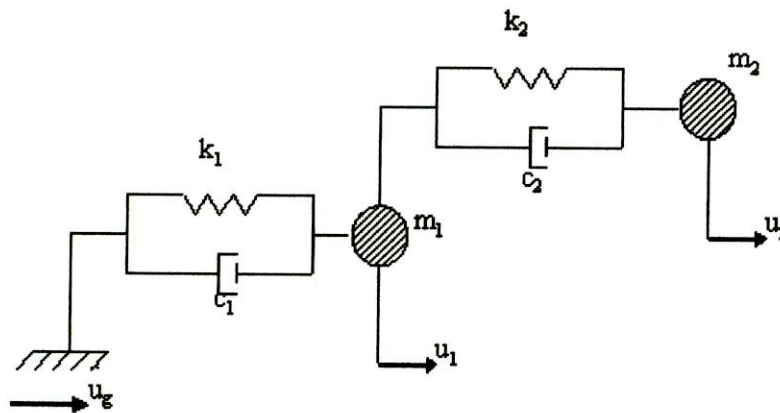


Fig. 4.7 TDOF model.

Now, the equation of motion, considering the equilibrium of mass m_1 is given by

$$m_1 \ddot{u}_1 + (k_1 + k_2)u_1 - k_2 u_2 + (c_1 + c_2) \dot{u}_1 - c_2 \dot{u}_2 = -m_1 \ddot{u}_g \dots \dots \dots (4.1)$$

Again, considering the equilibrium of mass m_2 ,

$$m_2 \ddot{u}_2 - k_2 u_1 + k_2 u_2 - c_2 \dot{u}_1 + c_2 \dot{u}_2 = -m_2 \ddot{u}_g \dots \dots \dots (4.2)$$

For undamped condition ($c=0$), Fourier transformation of Equations 4.1 and 4.2 yield,

$$(k_1 + k_2 - m_1\omega^2)\hat{u}_1 - k_2\hat{u}_2 + m_1\hat{u}_g = 0 \quad \dots\dots\dots (4.3)$$

$$-k_2\hat{u}_1 + (k_2 - m_2\omega^2)\hat{u}_2 + m_2\hat{u}_g = 0 \quad \dots\dots\dots (4.4)$$

From Equations 4.3 and 4.4

$$\frac{\hat{u}_1}{-k_2m_2 - m_1(k_2 - m_2\omega^2)} = \frac{\hat{u}_2}{-m_1k_2 - m_2(k_1 + k_2 - m_1\omega^2)} = \frac{\hat{u}_g}{(k_1 + k_2 - m_1\omega^2)(k_2 - m_2\omega^2) - k_2^2}$$

So the transfer function is

$$\frac{\hat{u}_1}{\hat{u}_g} = \frac{\omega^2 - \frac{k_1}{m_1} - \frac{k_2}{m_2}}{\omega^4 - \omega^2 \left(\frac{k_1}{m_1} + \frac{k_2}{m_1} + \frac{k_2}{m_2} \right) + \frac{k_1}{m_1} \cdot \frac{k_2}{m_2}}$$

and

$$\frac{\hat{u}_2}{\hat{u}_g} = \frac{\omega^2 - \left(\frac{k_1}{m_1} + \frac{k_2}{m_2} + \frac{k_2}{m_1} \right)}{\omega^4 - \omega^2 \left(\frac{k_1}{m_1} + \frac{k_2}{m_1} + \frac{k_2}{m_2} \right) + \frac{k_1}{m_1} \cdot \frac{k_2}{m_2}}$$

For resonance, $\frac{\hat{u}_1}{\hat{u}_g} = \frac{\hat{u}_2}{\hat{u}_g} = \infty = \frac{1}{0}$

Therefore the dominator of the transfer function becomes,

$$\omega^4 - \omega^2 \left(\frac{k_1}{m_1} + \frac{k_2}{m_1} + \frac{k_2}{m_2} \right) + \frac{k_1}{m_1} \cdot \frac{k_2}{m_2} = 0 \quad \dots\dots\dots (4.5)$$

Solving equation 4.5 the predominant frequency for the system can be calculated.

Now, for the pier stiffness k_1 , mass m_1 will be the deck mass and one-third of the pier mass, i.e. 2.23×10^5 slug. For the deck stiffness k_2 , mass m_2 will be one-third of the deck mass 7.33×10^4 slug.

The frequency parameters of Equation 4.5 are calculated, $\frac{k_1}{m_1} = 74.07$, $\frac{k_2}{m_2} = 0.27$ and

$$\frac{k_2}{m_1} = 0.09$$

Now, from Equation 4.5, $\omega^2 = \left\{ \begin{matrix} 74.16 \\ 0.27 \end{matrix} \right\}$.

Ignoring the long period vibration the predominant frequency is $\omega = 8.61$ radian/sec or $f = 1.37$ Hz which coincides with the predominant frequency of the ambient vibration of the deck (Fig. 4.4).

4.4 SYSTEM IDENTIFICATION BY TRANSFER RATIO

While identifying system parameters from ambient vibration, recorded data were only compared with derived parameters. The records were not used in deriving the parameters. Moreover in that derivation simplified geometry and deflection pattern of the bridge were assumed. With the concept of Transfer Ratio (TR), actual recorded data can be used to determine the system behavior and no simplified assumption is required regarding the geometry of the bridge. However, in order to understand the form of the transfer function a mathematical derivation of TR for three degrees of freedom system is first presented.

4.4.1 Formulation of Three Degree of Freedom System

The essential physical properties of any linearly elastic structural or mechanical system subjected to an external source of excitation or dynamic loading are its mass, elastic properties (flexibility or stiffness), and energy-loss mechanism or damping (Clough and Penzien, 1975). A mathematical representation of a multiple degree of freedom system is shown in Figure 4.8.

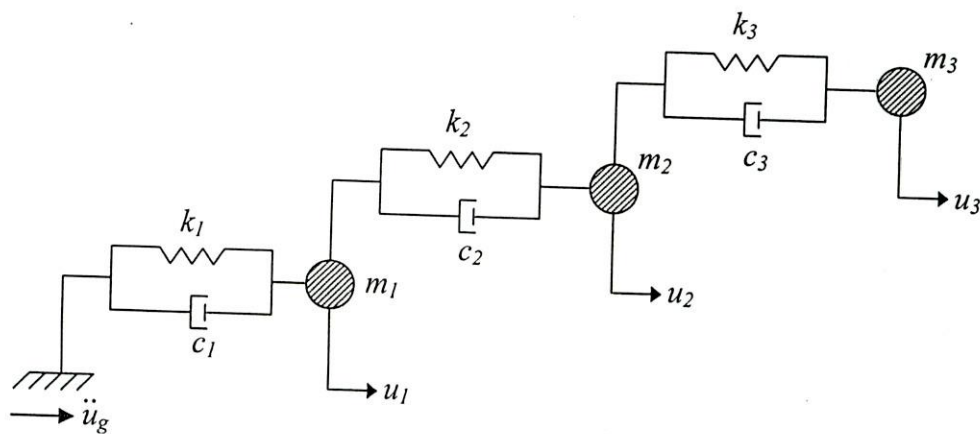


Fig. 4.8 Ideal multiple degree of freedom system.

Where,

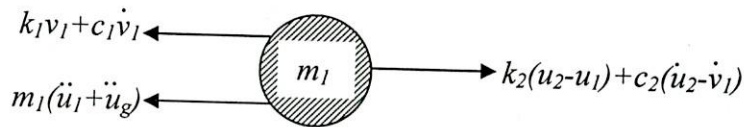
m_1, m_2 and m_3 = concentrated masses of the system

c_1, c_2 and c_3 = damper of the masses m_1, m_2 and m_3 respectively

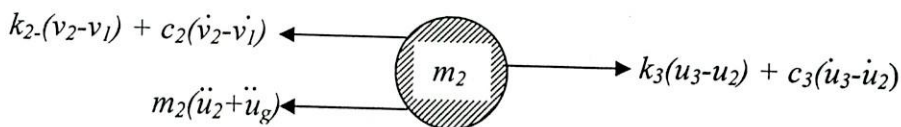
k_1, k_2 and k_3 = stiffness of the masses m_1, m_2 and m_3 respectively

u_1, u_2 and u_3 = displacements of the masses m_1, m_2 and m_3 respectively

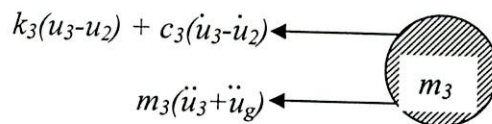
\ddot{u}_g = ground acceleration due to external source of excitation



(a)



(b)



(c)

Fig. 4.9. (a) Free body diagram of masses, (b) Free body diagram of mass m_2 ,
(c) Free body diagram of mass m_3 .

Considering equilibrium of mass m_1 (Fig. 4.9) the equation of motion is

$$m_1(\ddot{u}_1 + \ddot{u}_g) + k_1 u_1 + c_1 \dot{u}_1 - k_2(u_2 - u_1) - c_2(\dot{u}_2 - \dot{u}_1) = 0$$

$$\Rightarrow -\omega^2 m_1 \hat{u}_1 + m_1 \hat{u}_g + k_1 u_1 - i\omega c_1 \hat{u}_1 - k_2 \hat{u}_2 + k_2 \hat{u}_1 + i\omega c_2 \hat{u}_2 - i\omega c_2 \hat{u}_1 = 0$$

by Fourier Transformation

$$\Rightarrow \hat{u}_1 [-\omega^2 m_1 + (k_1 + k_2) - i\omega(c_1 + c_2)] + (i\omega c_2 - k_2) \hat{u}_2 + m_1 \hat{u}_g = 0 \dots \dots \dots (4.7)$$

Considering equilibrium of mass m_2 (Fig. 4.9) the equation of motion is

$$m_2(\ddot{u}_2 + \ddot{u}_g) + k_2(u_2 - u_1) + c_2(\dot{u}_2 - \dot{u}_1) - k_3(u_3 - u_2) - c_3(\dot{u}_3 - \dot{u}_2) = 0$$

$$\Rightarrow -\omega^2 m_2 \hat{u}_2 + m_2 \hat{\ddot{u}}_g + k_2 \hat{u}_2 - k_2 \hat{u}_1 - i\omega c_2 \hat{u}_2 + i\omega c_1 \hat{u}_1 - k_3 \hat{u}_3 + k_3 \hat{u}_2 + i\omega c_3 \hat{u}_3 - i\omega c_3 \hat{u}_2 = 0$$

(by Fourier Transformation)

$$\Rightarrow \hat{u}_3(i\omega c_3 - k_3) + \hat{u}_2[-\omega^2 m_2 + (k_2 + k_3) - i\omega(c_2 + c_3)] + \hat{u}_1(i\omega c_2 - k_2) + m_2 \hat{\ddot{u}}_g = 0 \quad (4.8)$$

Considering equilibrium of mass m_3 (Fig. 4.9) the equation of motion is

$$m_3(\ddot{u}_3 + \ddot{u}_g) + k_3(u_3 - u_2) + c_3(\dot{u}_3 - \dot{u}_2) = 0$$

$$\Rightarrow -\omega^2 m_3 \hat{u}_3 + m_3 \hat{\ddot{u}}_g + k_3 \hat{u}_3 - k_3 \hat{u}_2 - i\omega c_3 \hat{u}_3 + i\omega c_3 \hat{u}_2 = 0 \quad \text{(by Fourier Transformation)}$$

$$\Rightarrow \hat{u}_3(-\omega^2 m_3 + k_3 - i\omega c_3) + \hat{u}_2(i\omega c_3 - k_3) + m_3 \hat{\ddot{u}}_g = 0$$

$$\Rightarrow \hat{u}_3 = \frac{-m_3 \hat{\ddot{u}}_g - \hat{u}_2(i\omega c_3 - k_3)}{-\omega^2 m_3 + k_3 - i\omega c_3} \quad \dots\dots\dots (4.9)$$

Where,

\hat{u}_1 = FFT of the displacement of mass m_1

\hat{u}_2 = FFT of the displacement of mass m_2

\hat{u}_3 = FFT of the displacement of mass m_3

ω = Angular frequency = $2\pi\nu$

ν = Oscillating frequency

$\hat{\ddot{u}}_g$ = FFT of the ground acceleration

From using Equations (4.7), (4.8) & (4.9), finally we get

$$\frac{\hat{u}_1}{\hat{\ddot{u}}_g} = \frac{\omega^4 + i\omega^3 A + \omega^2 B + i\omega C + D}{\omega^6 + i\omega^5 K + \omega^4 L + i\omega^3 M + \omega^2 N + i\omega U + V} \quad \dots\dots\dots (4.10)$$

and

$$\frac{\hat{u}_2}{\hat{\ddot{u}}_g} = \frac{\omega^4 + i\omega^3 P + \omega^2 Q + i\omega R + S}{\omega^6 + i\omega^5 K + \omega^4 L + i\omega^3 M + \omega^2 N + i\omega U + V} \quad \dots\dots\dots (4.11)$$

Where,

$\frac{\hat{u}_1}{\hat{\ddot{u}}_g}$ or $\frac{\hat{u}_2}{\hat{\ddot{u}}_g}$ are Transfer ratio (TR) for degrees of freedom u_1 and u_2 respectively.

Detail calculations are shown in appendix.

4.4.2 Calculation of Transfer Ratio

Transfer Ratio (TR) is the ratio of the FFT of the displacement of the bridge deck to the FFT of the ground acceleration due to the earthquake. Here, TR is calculated using the FFT of the displacement recorded at BR-5X (i.e. displacement of the bridge at the deck at pier P10 in the NS direction) and the FFT of the ground acceleration recorded at the west-end free-field station in the north-south direction.

$$\begin{aligned}
 \therefore \text{TR} &= \frac{\hat{u}}{\hat{u}_g} \\
 &= \frac{c + id}{a + ib} \\
 &= \frac{A_1 e^{i\theta_1}}{A_2 e^{i\theta_2}} \\
 &= \frac{A_1}{A_2} e^{i(\theta_2 - \theta_1)} \\
 &= T e^{i\theta_1} \\
 &= T_R + iT_I \quad \dots\dots\dots (4.12)
 \end{aligned}$$

Where,

\hat{u} = FFT of the displacement of the bridge at the deck at pier P10 in the NS direction; i.e. at BR5X

\hat{u}_g = FFT of the ground acceleration recorded at the west-end free-field station in the north-south direction

c = Real value of the FFT of the displacement of the bridge at the deck at pier P10 in the NS direction; i.e. at BR5X

d = Imaginary value of the FFT of the displacement of the bridge at the deck at pier P10 in the NS direction; i.e. at BR5X

a = Real value of the FFT of the ground acceleration recorded at the west-end free-field station in the north-south direction

b = Imaginary value of the FFT of the ground acceleration recorded at the west-end free-field station in the north-south direction

$A_1 =$ Absolute value of the FFT of the displacement of the bridge at the deck at pier P10 in the NS direction; i.e. at BR5X = $\sqrt{c^2 + d^2}$

$\theta_1 =$ Phase angle of the FFT of the displacement of the bridge at the deck at pier P10 in the NS direction; i.e. at BR5X = $\tan^{-1} d/c$

$A_2 =$ Absolute value of the FFT of the ground acceleration recorded at the west-end free-field station in the north-south direction = $\sqrt{a^2 + b^2}$

$\theta_2 =$ Phase angle of the FFT of the ground acceleration recorded at the west-end free-field station in the north-south direction = $\tan^{-1} b/a$

$T = A_1/A_2 =$ Absolute value of TR = $\sqrt{T_R^2 + T_I^2}$

$\theta_t = \theta_1 - \theta_2 =$ Phase angle of TR = $\tan^{-1} T_I/T_R$

$T_R =$ Real value of TR = $T * \cos \theta_t$

$T_I =$ Imaginary value of TR = $T * \sin \theta_t$

The displacement recorded at BR-5X (i.e. displacement of the bridge at the deck at pier P10 in the NS direction) due to the earthquake on June 17, 2004 at 5:36:53 hrs BST has been shown in Figure 4.10 and the corresponding FFT has been shown in Figure 4.11. The ground acceleration recorded at the west-end free-field station in the north-south direction during this earthquake and the corresponding FFT have been shown in Figures 4.12 and 4.13 respectively. The Transfer ratio TR and phase angle θ_t are plotted against the corresponding frequency are shown in Figures 4.14 and 4.15.

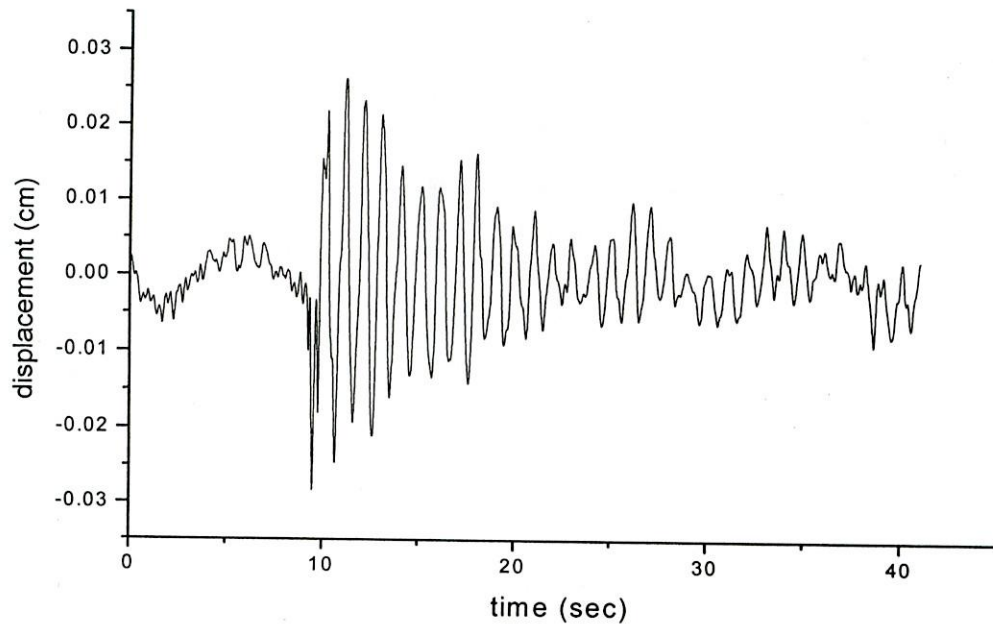


Fig. 4.10 Displacement of the bridge at BR-5X due the earthquake, June 17, 2004.

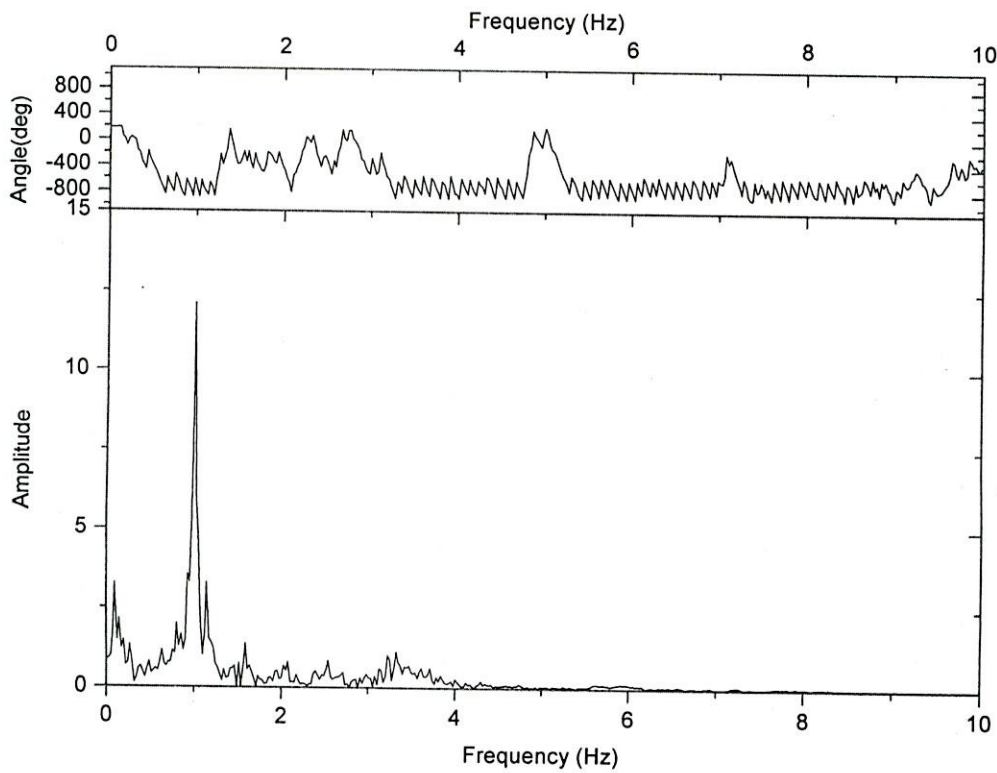


Fig. 4.11 FFT of the displacement of the bridge due the earthquake, June 17, 2004.

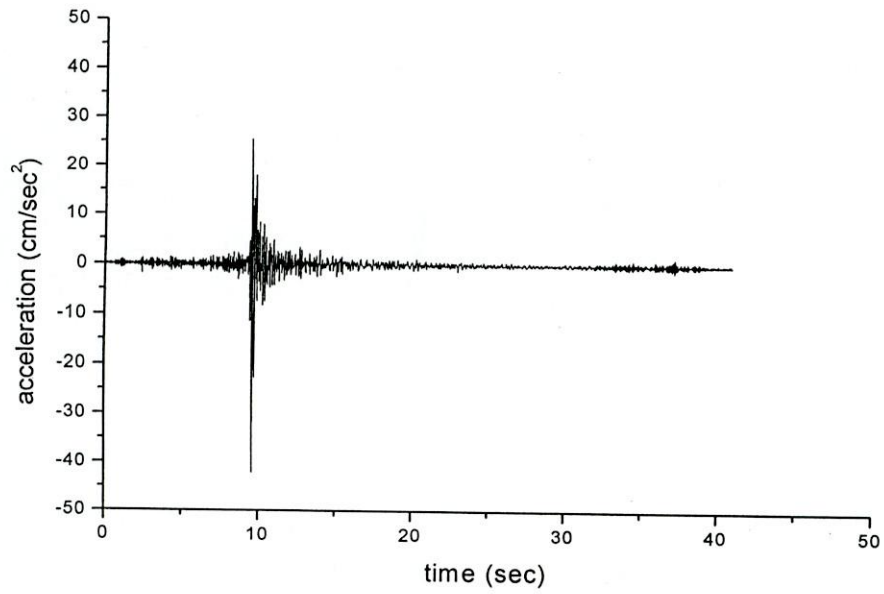


Fig. 4.12 Ground motion of the earthquake, June 17, 2004

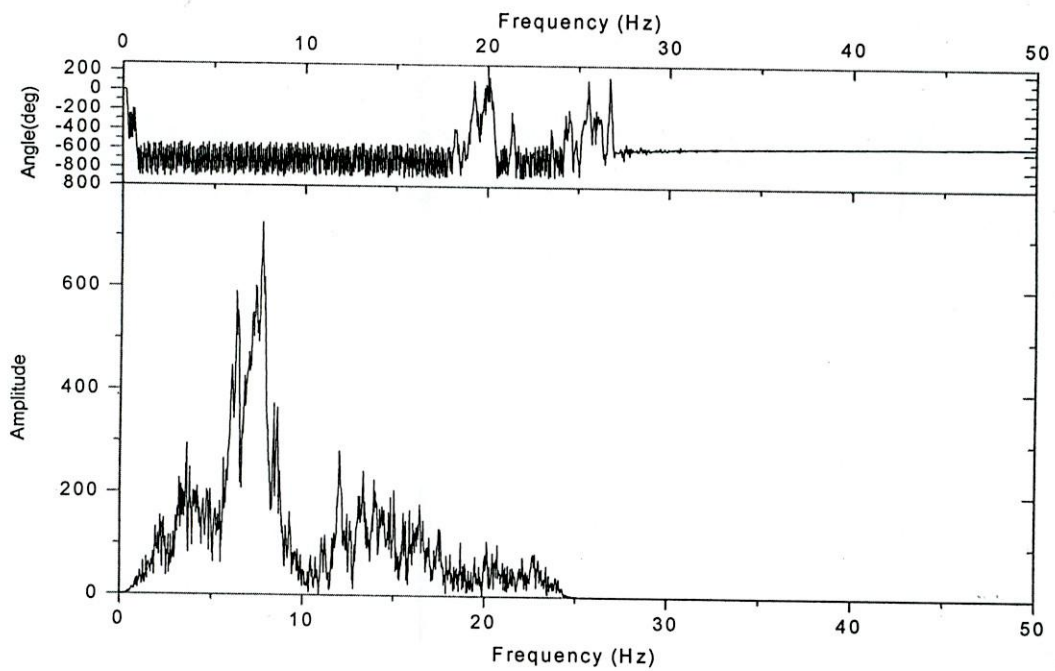


Fig. 4.13 FFT of the ground motion of the earthquake, June 17, 2004.

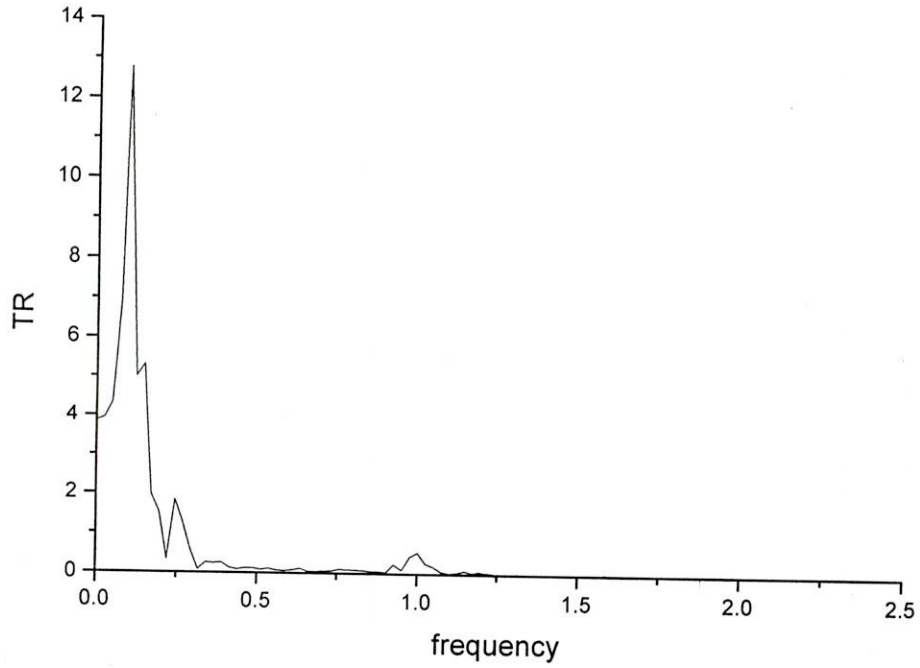


Fig. 4.14 TR vs. frequency plot

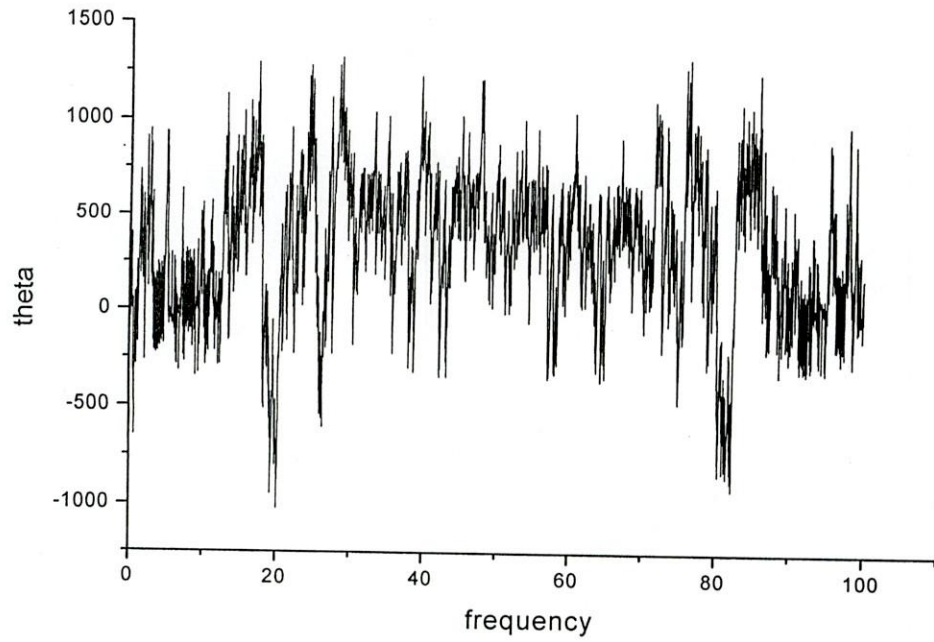


Fig. 4.15 Theta vs. frequency plot

4.5 APPLICATION OF THE TRANSFER RATIO

The calculated Transfer Ratio is used to observe the response of the Jamuna Multipurpose Bridge for earthquakes of different magnitude and thereby, predict any possible damage of the bridge. The TR values obtained are multiplied by the values of the ground accelerations of different earthquakes to find the probable displacement of the bridge deck at pier P10 in the NS direction. The obtained displacement represents the response of the bridge due to the applied earthquake force and thus, helps to take remedial measures in this regard.

We know,

$$TR = Te^{i\theta_1}$$

Let,

$$\begin{aligned} \hat{a}'_g &= \text{FFT of the ground acceleration of the applied earthquake} \\ &= Ge^{i\theta_g} \end{aligned}$$

Now, to get the desired response of the applied earthquake, the TR value and FFT of the ground acceleration of the earthquake is multiplied.

$$\begin{aligned} TR * \hat{a}'_g &= Te^{i\theta_1} * Ge^{i\theta_g} \\ &= (T * G) * e^{i(\theta_1 + \theta_g)} \\ &= Re^{\theta_R} \\ &= R_R + iR_I \dots\dots\dots(4.13) \end{aligned}$$

Where,

- G = Absolute value of the FFT of the ground acceleration of the applied earthquake
- θ_g = Phase angle of the FFT of the ground acceleration of the applied earthquake
- R = Absolute value of the FFT of the response of the bridge to the applied earthquake = $\sqrt{R_R^2 + R_I^2}$

- θ_R = Phase angle of the FFT of the response of the bridge to the applied earthquake = $\tan^{-1} \frac{R_I}{R_R}$
- R_R = Real value of the response of the bridge to the applied earthquake = $R * \cos \theta_R$
- R_I = Imaginary value of the response of the bridge to the applied earthquake = $R * \sin \theta_R$

When the values of R_R and R_I are obtained, Inverse Fast Fourier Transformation (IFFT) is applied to get the values of the displacement (u') of the bridge at the deck at pier P10 in the NS direction; i.e. at BR5X due to the applied earthquake. Thus, the response of the Jamuna Multipurpose Bridge has been studied through the displacement found by the IFFT.

4.6 VERIFICATION OF THE TRANSFER RATIO

The calculated values of the TR are first applied to the data of the earthquake occurred on June 17, 2004 to compare the response of the Jamuna Multipurpose Bridge, obtained from calculation with the original data of the displacement recorded at BR-5X during the earthquake. The TR values are multiplied with the FFT values of the ground accelerations of the earthquake. From this multiplication, the values of R_R and R_I are obtained and after IFFT, the magnitude of the displacements of the Jamuna Multipurpose Bridge at the deck at pier P10 in the NS direction; i.e. at BR-5X is found Figure 4.16, which was exactly similar to the displacement values recorded (Fig. 4.17).

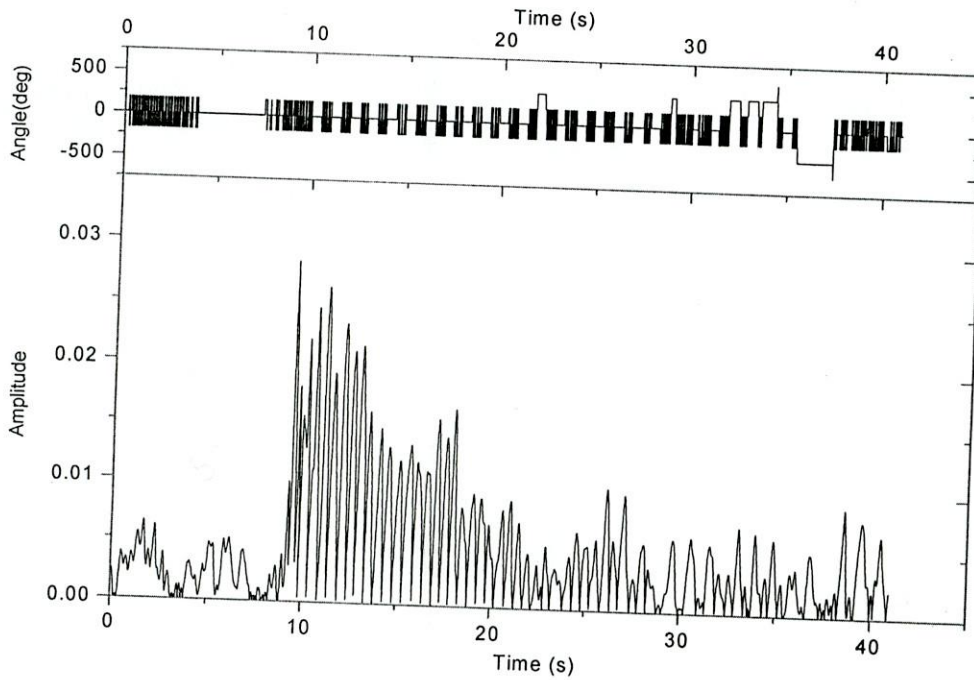


Fig. 4.16 IFFT of the response of the bridge due to the earthquake, June 17, 2004

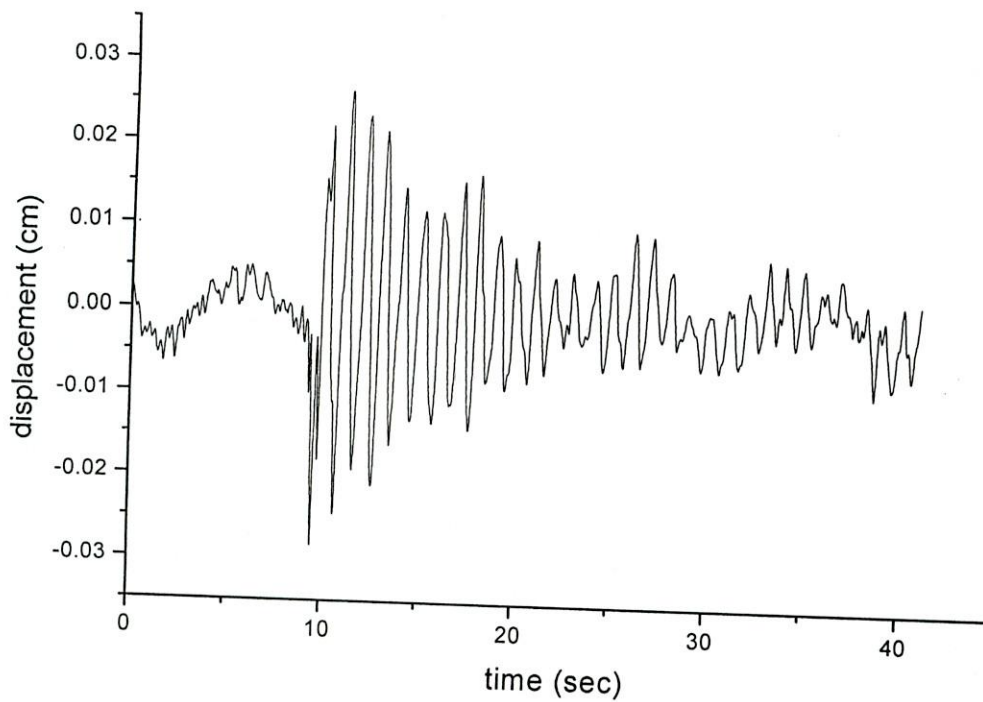


Fig. 4.17 Displacement of the bridge due to the earthquake, June 17, 2004.

4.7 RESPONSE OF BRIDGE UNDER TRANSFER RATIO.

The calculated TR can be used to find out the response under various earthquake loadings. The Jamuna Multipurpose Bridge is located in an active Bogra fault zone (Bolt, 1987). The free-field stations of the both side of bridge recoded local small ground motions. Although the threshold value of the sensors in the bridge is high to omit noise, the TR can verify the response of bridge under local ground motion which are recorded in west-end free-field station.

4.7.1 Application TR under Local Earthquake

The calculated values of the TR are applied on the recorded earthquake data, February 14, 2006 to study the response of the Jamuna Multipurpose Bridge. The ground acceleration and the corresponding FFT have been shown in Figures 4.18 and 4.19.

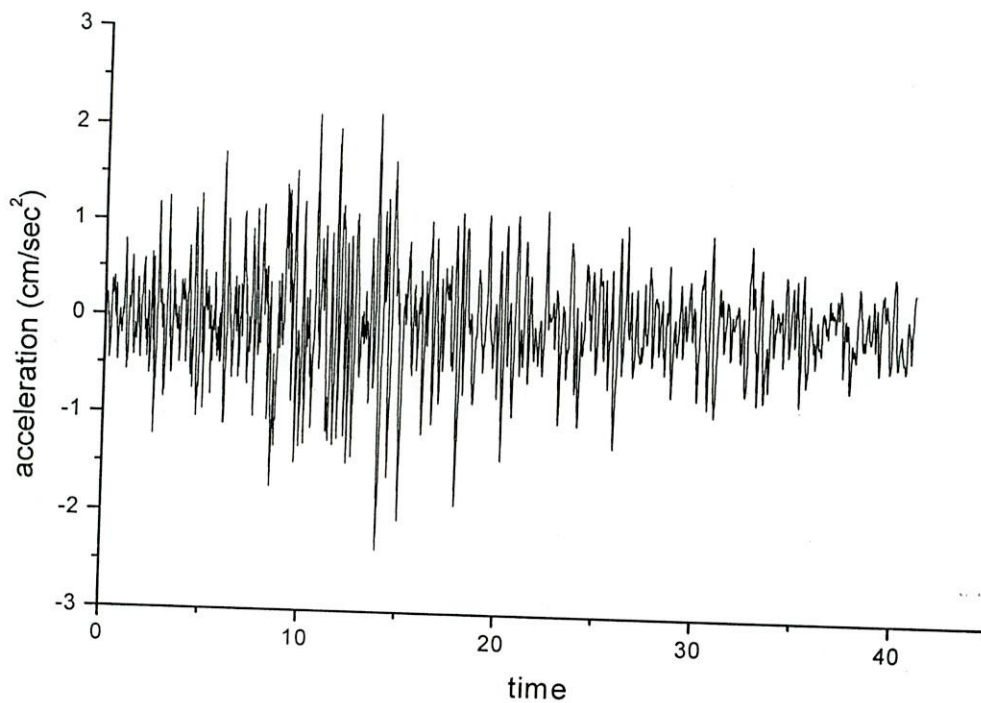


Fig. 4.18 Ground motion of the earthquake, February 14, 2006.

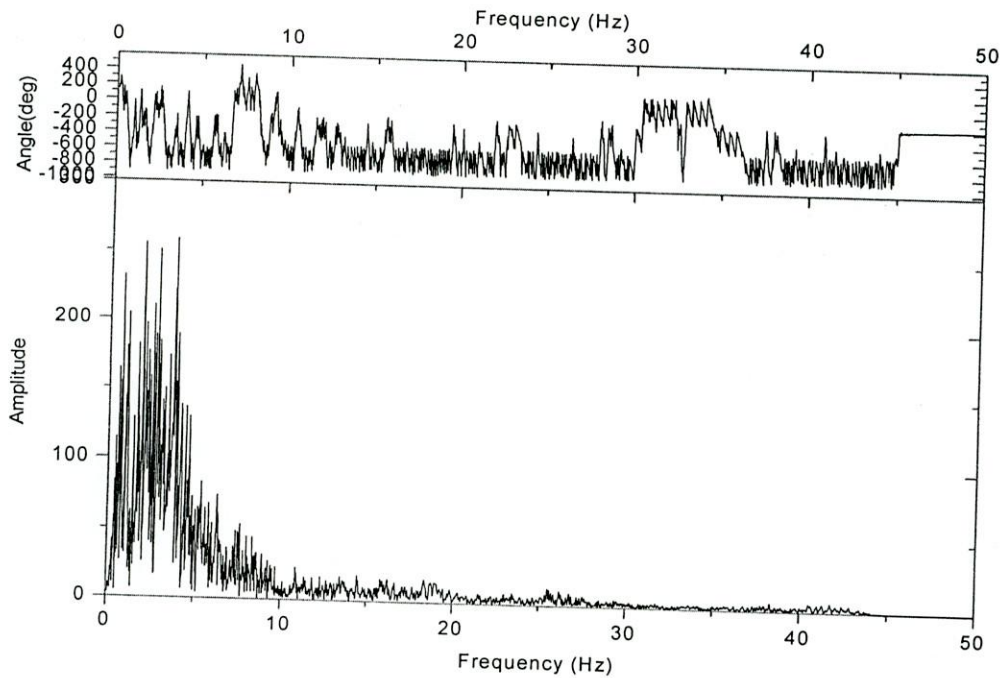


Fig 4.19 FFT of ground motion of the earthquake, February 14, 2006.

The TR values obtained are multiplied with the FFT values of the ground accelerations of the applied earthquake. From this multiplication, the values of R_R and R_I are obtained and after IFFT, the magnitude of the displacements of the Jamuna Multipurpose Bridge at the deck at pier P10 in the NS direction; i.e. at BR-5X is found. The IFFT and the obtained displacement have been shown in Figures 4.20 and 4.21.

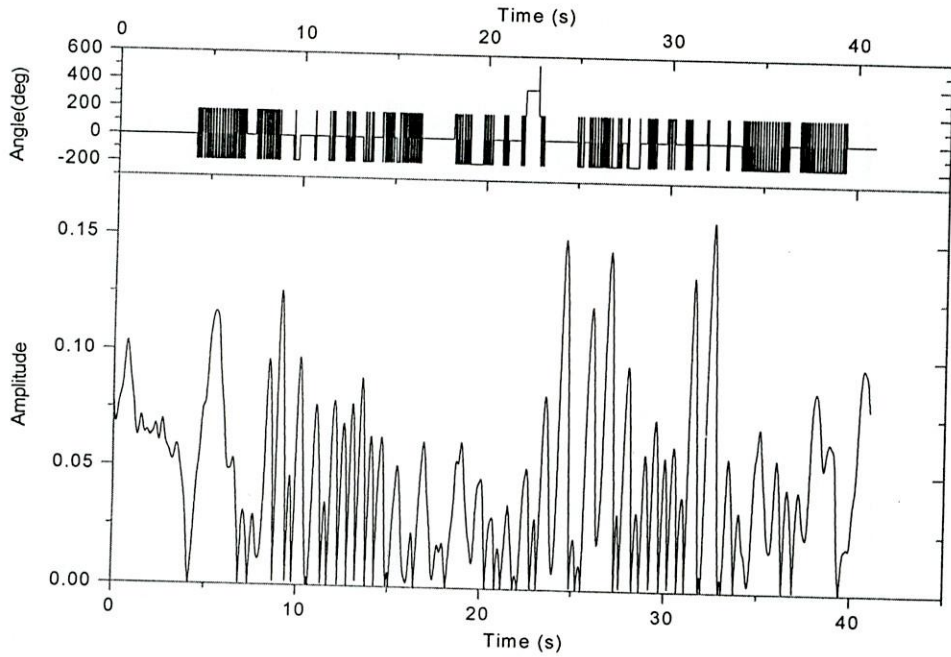


Fig. 4.20 IFFT of the response of the bridge due to the earthquake,
February 14, 2006.

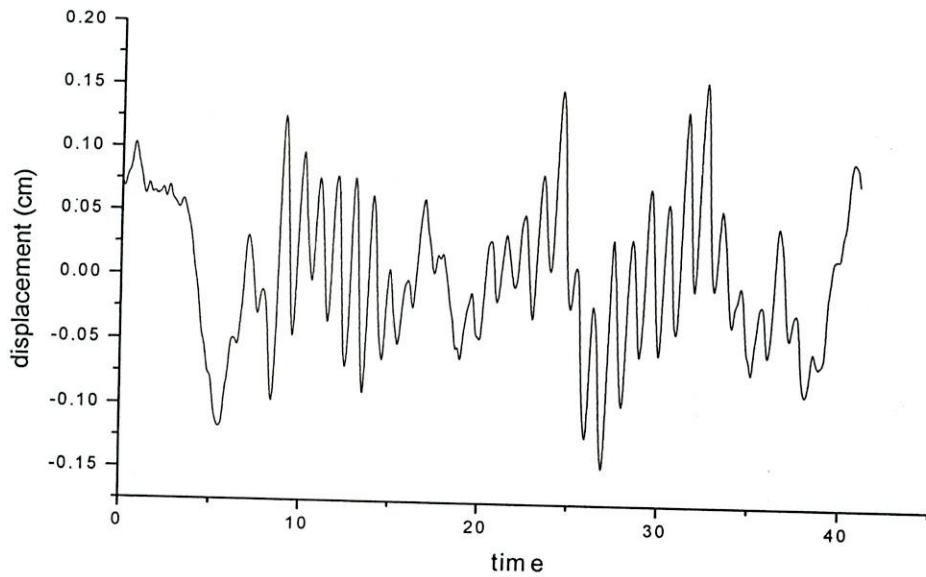


Fig 4.21 Displacement of the bridge due to the due to the earthquake,
February 14, 2006.

Another local earthquake data on August 05, 2006 was recorded which is used in the study to determine the response of the Jamuna Multipurpose Bridge using TR. The ground acceleration and the corresponding FFT have been shown in Figures 4.22 and 4.23.

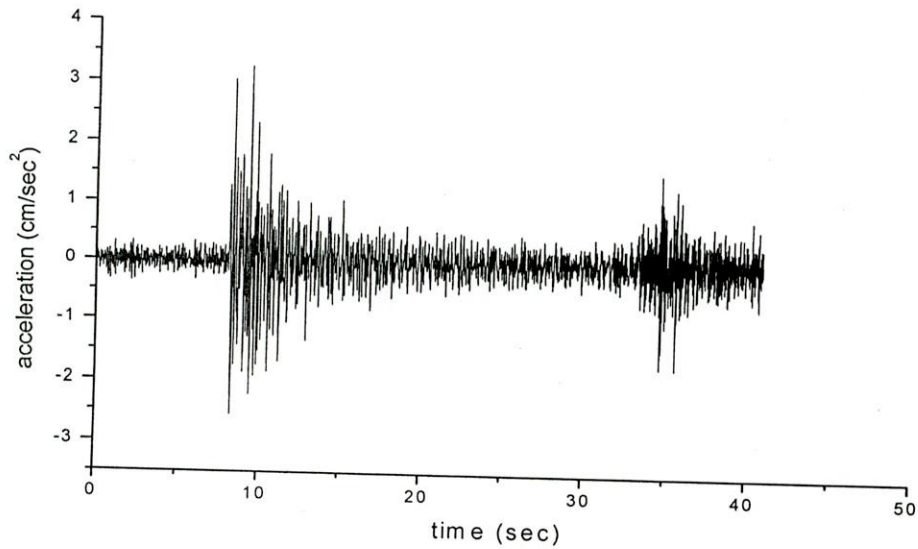


Fig. 4.22 Ground motion of the earthquake, August 05, 2006.

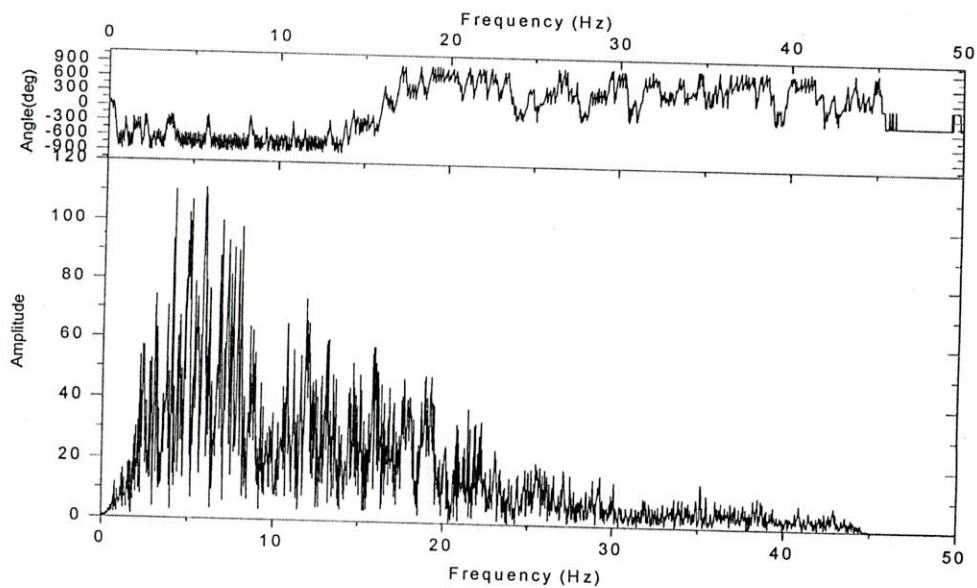


Fig 4.23 FFT of ground motion of the earthquake, August 05, 2006.

The magnitude of the displacements of the Jamuna Multipurpose Bridge at the deck at pier P10 in the NS direction is shown in Figure 4.24.

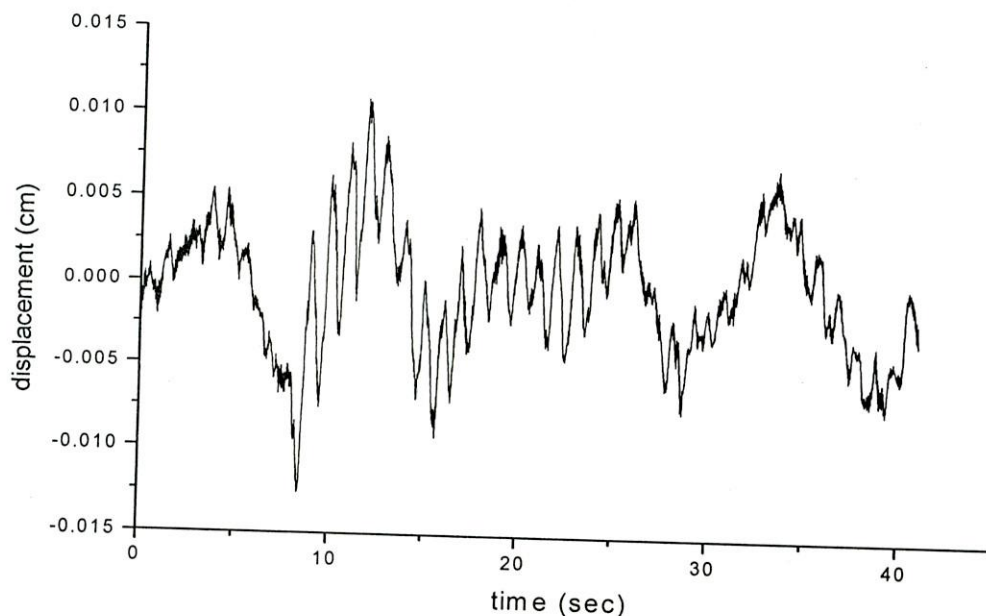


Fig. 4.24 Displacement of the bridge due to the earthquake, August 05, 2006.

Applying TR function, the maximum displacement of deck at pier 10 is found to be 0.15855 cm and 0.01204 cm from the above study, which is lower than the trigger level set for starting the device to record earthquake data in bridge sensors. Therefore, no earthquake data was recorded in the bridge.

4.7.2 Application of TR under the El Centro Earthquake, Imperial Valley, California, USA, 1940

The earthquake data of the El Centro site, Imperial Valley Irrigation District, California, USA, 1940 was applied on the TR function to study the response of the Jamuna Multipurpose Bridge. The ground motion of the earthquake and the corresponding FFT has been shown in Figures. 4.25 & 4.26 respectively. The maximum acceleration of the applied earthquake is 340.202 cm/sec^2 . TR values obtained using Equation 4.16 were multiplied with the ground accelerations of the applied earthquake occurred. After IFFT the displacement (Fig. 4.27) of the Jamuna Bridge due to the applied earthquake was

found. The maximum displacement due to earthquake was found to be 20.3284 cm is shown in Figure 4.28.

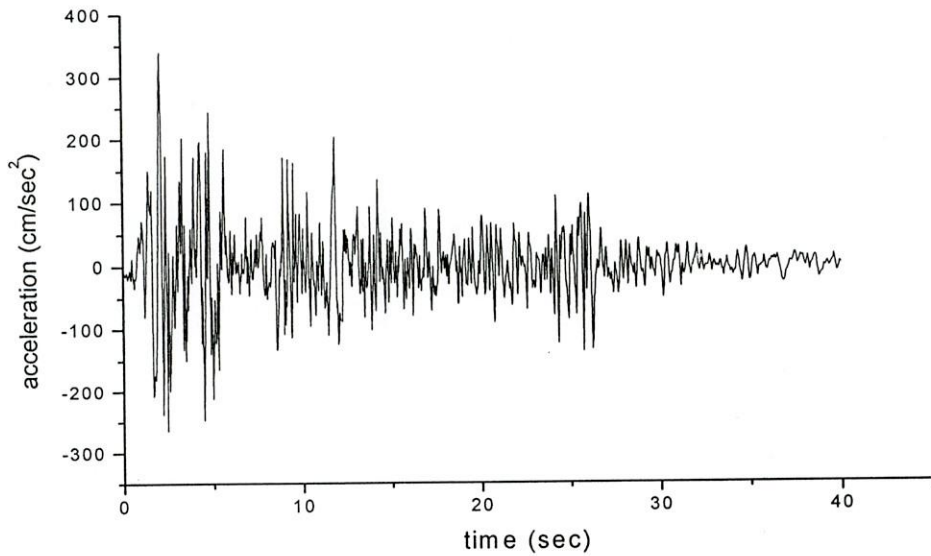


Fig. 4.25 Ground motion of the El Centro Earthquake, Imperial Valley, California, USA, 1940

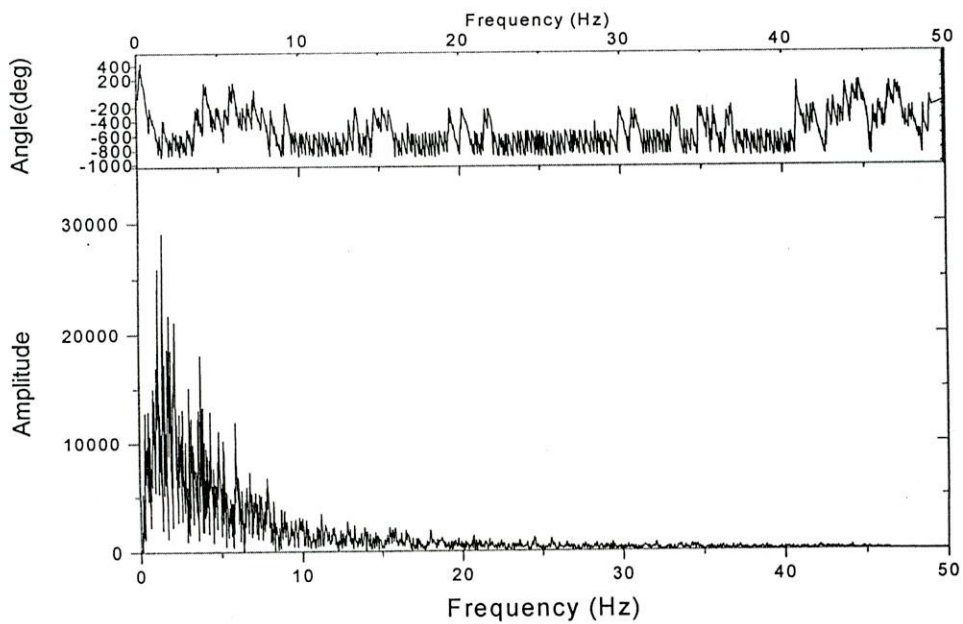


Fig.4.26 FFT of ground motion of the El Centro Earthquake, Imperial Valley, California, USA, 1940

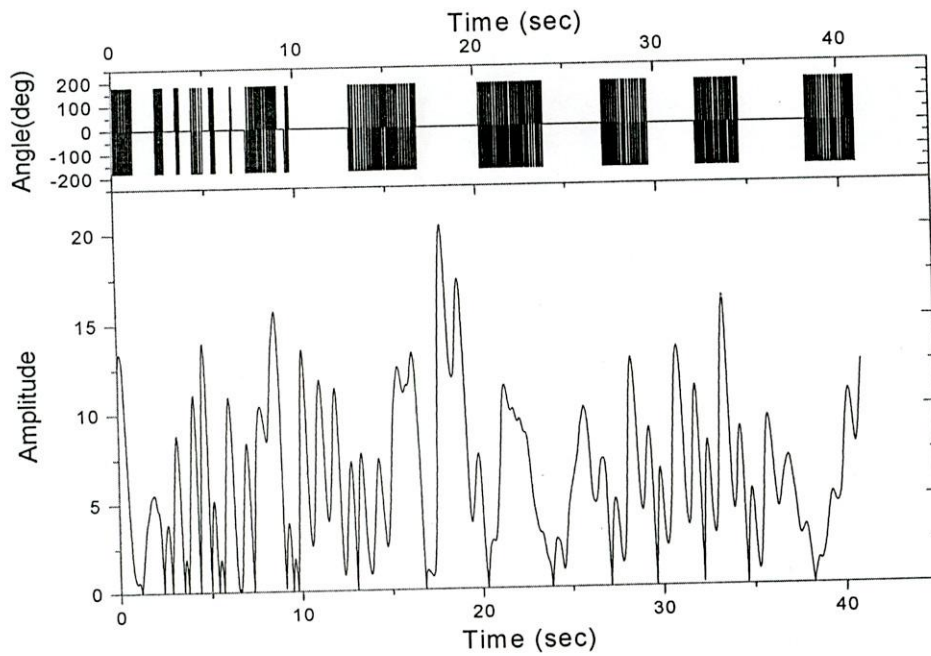


Fig. 4.27 IFFT of the response of the bridge due to the El Centro Earthquake, Imperial Valley, California, USA, 1940.

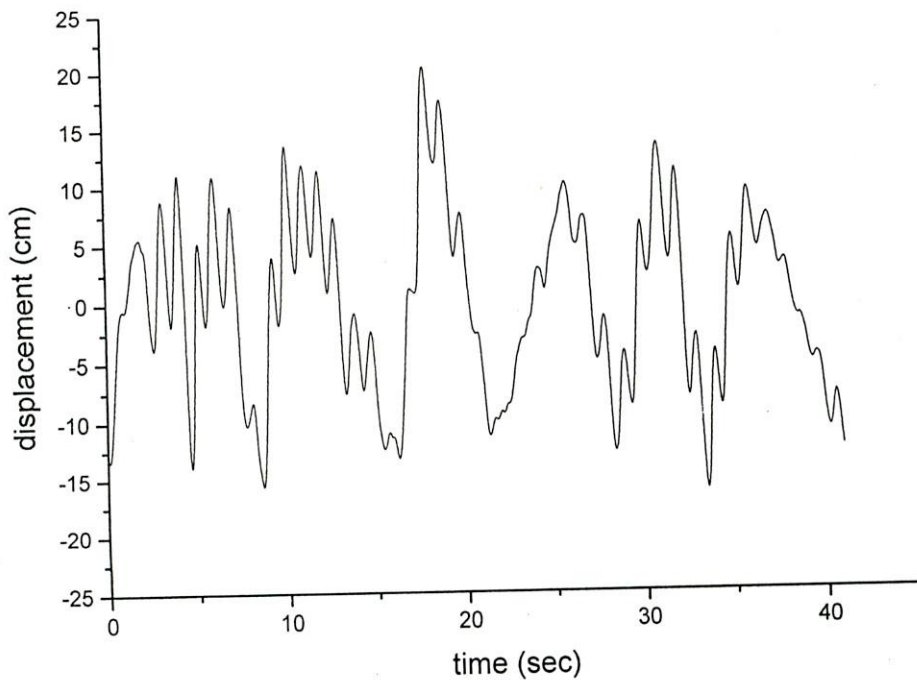


Fig. 4.28 Predicted displacement of the bridge due to the El Centro Earthquake, Imperial Valley, California, USA, 1940

4.7.3 Application of the Mexico City Earthquake, September 19, 1995

The calculated values of the TR are applied to the data of the earthquake of Mexico City, Station I, September 19, 1995 to study the response of the Jamuna Multipurpose Bridge due to this earthquake. The ground acceleration and the corresponding FFT have been shown in Figures 4.29 and 4.30.

The maximum acceleration of the applied earthquake is 167.918 cm/sec^2 and from Figure 5.14, the predominant frequency is found to be 0.48828 Hz . The TR values obtained are multiplied with the FFT values of the ground accelerations of the applied earthquake. From this multiplication, the values of R_R and R_I are obtained, the magnitude of the displacements of the Jamuna Multipurpose Bridge at the deck at pier P10 in the NS direction; i.e. at BR5X is found. The IFFT and the obtained displacement have been shown in Figures 4.31 and 4.32.

The maximum displacement due to earthquake of this magnitude is estimated from this study to be 37.35531 cm

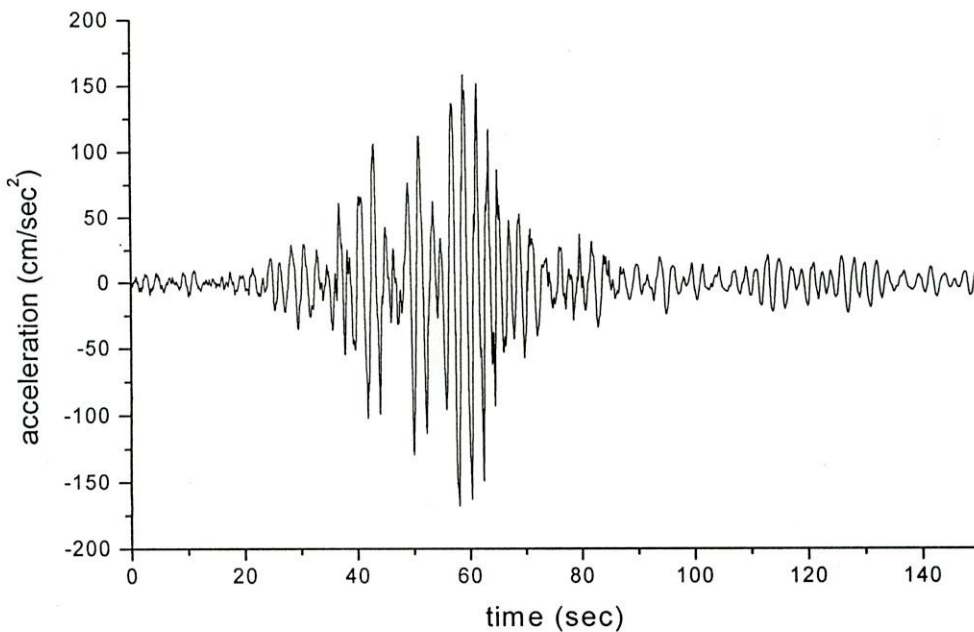


Fig. 4.29 Ground motion of the Mexico City Earthquake, September 19, 1995

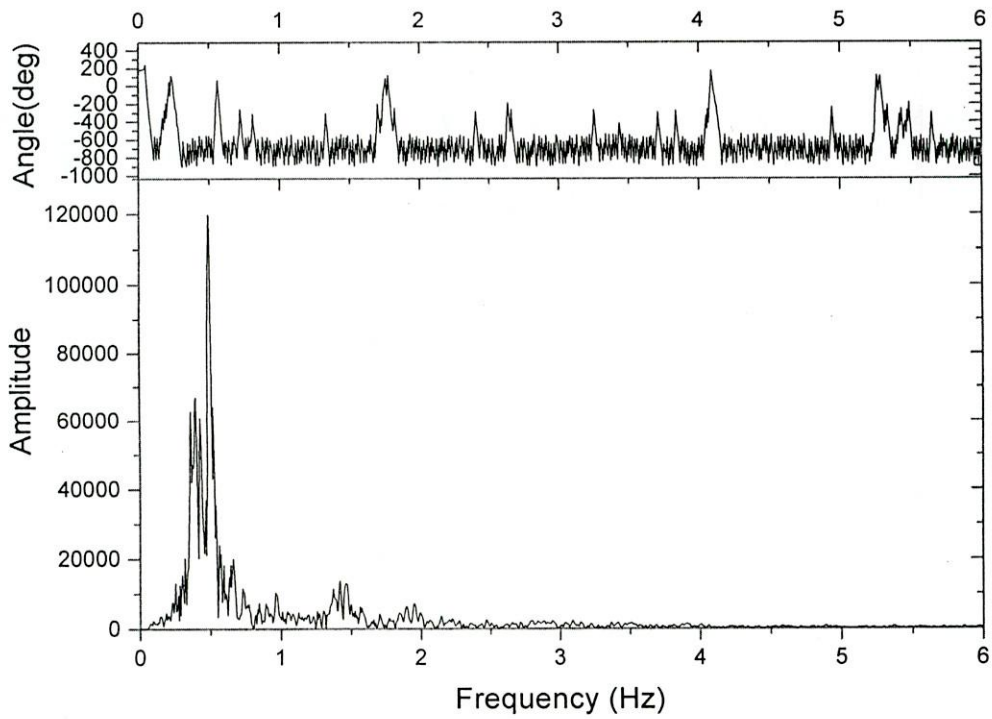


Fig. 4.30 FFT of ground motion of the Mexico City earthquake, September 19,1995

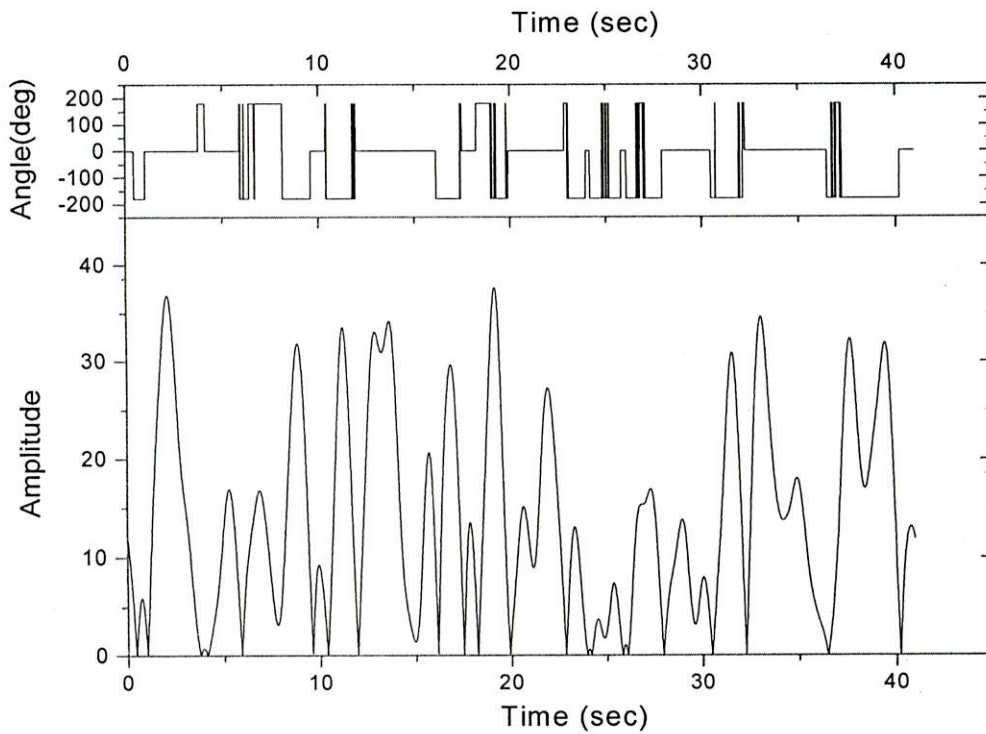


Fig. 4.31 IFFT of the response of the bridge due to the Mexico City earthquake, September 19,1995

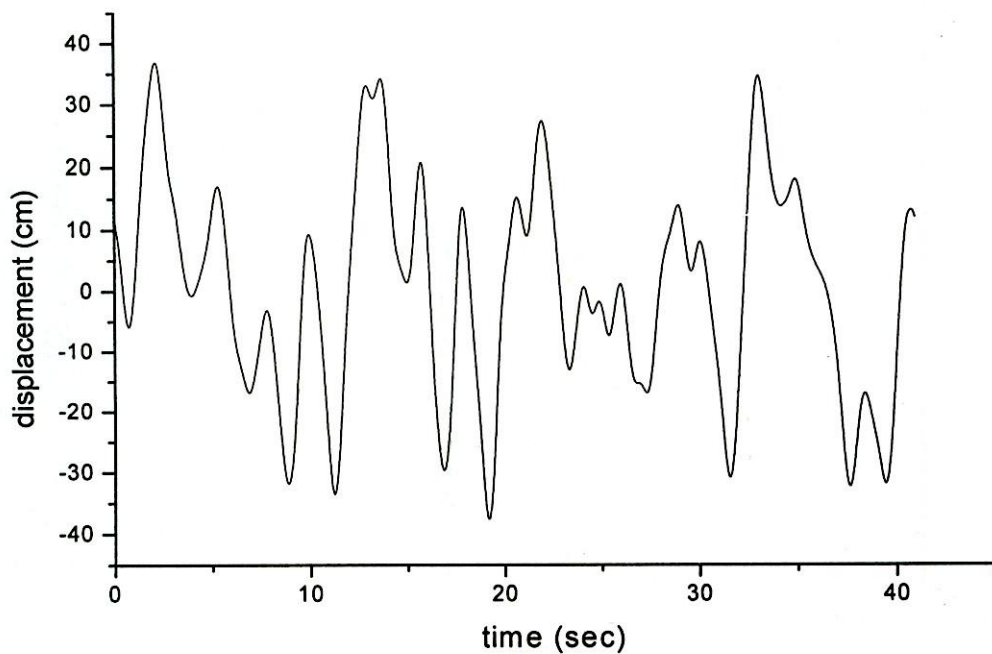


Fig. 4.32 Predicted displacement of the bridge due to the Mexico City earthquake, September 19,1995

CHAPTER 5

FINITE ELEMENT MODELING OF THE SYSTEM

5.1 GENERAL

This research embarks upon modal analysis with the objective of developing a better understanding of the complex dynamic behavior of the Jamuna Multipurpose Bridge. A finite element program is used to study the seismic response of the bridge. In the present analysis the structural behavior of the bridge was assumed to be linear ignoring material and other non-linearity. Brief descriptions are provided in this chapter of the main features of this program.

5.2 FINITE ELEMENT MODELING OF THE BRIDGE

5.2.1 Salient Features for Modeling of the Bridge

A seven-span module of bridge is modeled by SAP 2000. The length of module is 695.625m. This module consists of six equal spans with seven piers and two extended portions. The 26.325m extended portion is directed towards east-side (Tangail) and the 73.05 extended portions are directed towards west-side (Shirajgonj). This extended portion is called hinge of the bridge. Figure 5.1 shows the 3-D view of bridge module.

5.2.2 Bridge Layout Line

The studied bridge have curvatures in both horizontal and vertical directions. There is a circular horizontal curve of radius of 12000 m. On the other hand, the vertical curvature is composite, first 1460m is a straight line of .05 percent gradient and then a circular curve which has a length of 1880 m. and then again a straight line of same length and gradient as in the previous. In the present study, the second module from the northern side is modeled which lies on the straight line vertical gradient only. Figures 5.2 and 5.3 show the procedure of providing input data for horizontal and vertical layout.

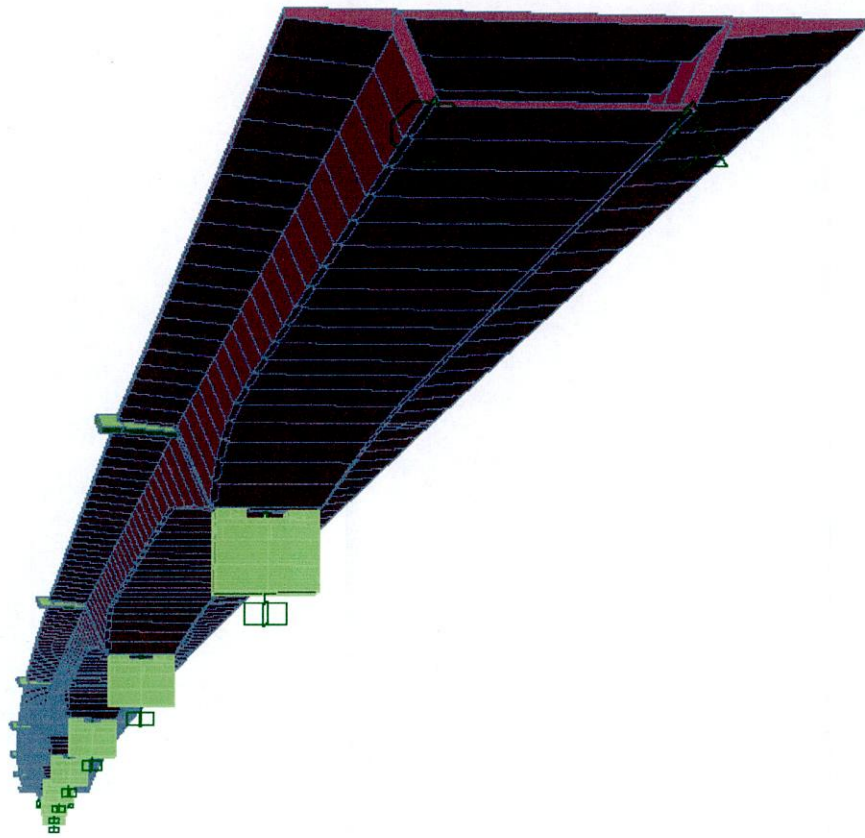


Fig. 5.1 3D view of the Finite Element Bridge Model.

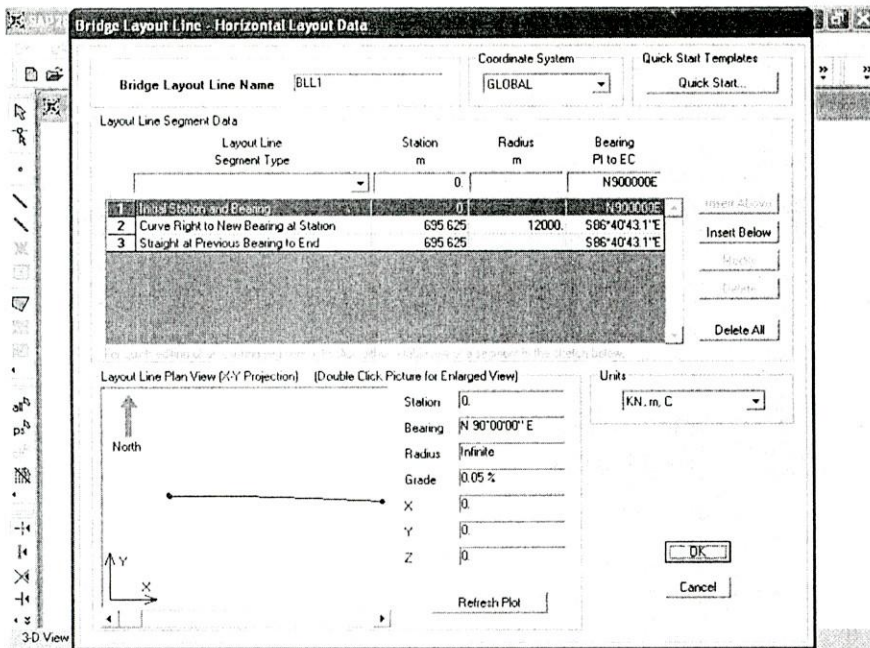


Fig. 5.2 Sap window for horizontal layout line.

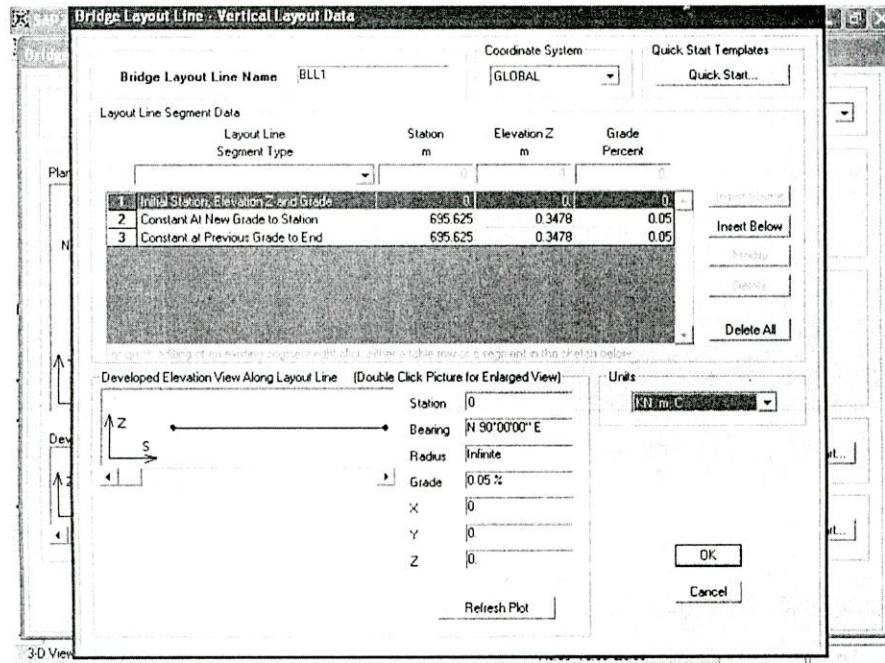


Fig. 5.3 Sap window for vertical layout line.

5.2.3 Deck Section

Jamuna Multipurpose Bridge has a complex Deck system which is a box girder type. Therefore, deck section has two types of parabolic variation in width of deck and as well as thickness. Deck consists of a thicker thickness in pier section and a thin thickness in mid section. The mid section is wider width than the pier section. The typical cross-sectional characteristics and dimensional properties are shown in the Figure 5.4.

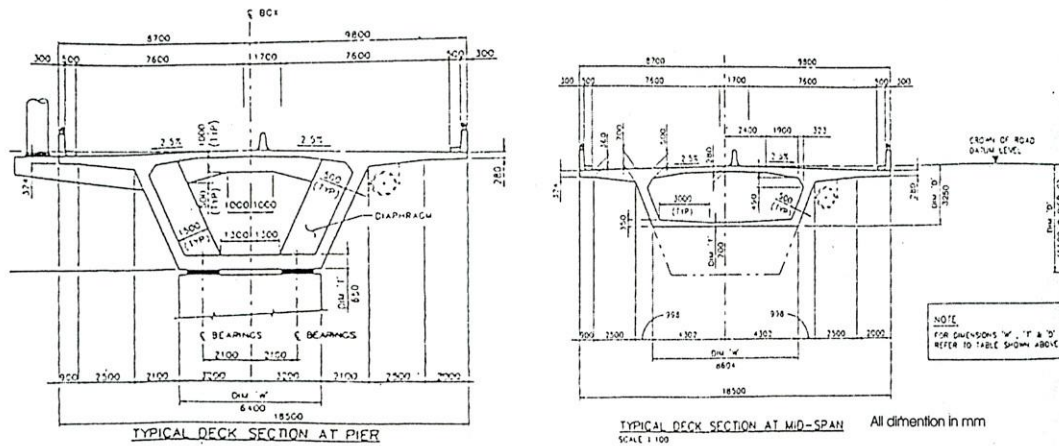


Fig. 5.4 Typical Deck section at pier and at mid span respectively.

The following three variations have been considered while modeling deck section and the thickness in various parts of the deck section in the model. Figures 5.5 to 5.7 show the Sap input thickness data variation of various span length.

- Parabolic variation in depth (5.5m. at pier and 3.05 m. at mid span)
- Parabolic variation in the thickness of bottom slab (0.65 m. at pier and 0.2 m. at mid span)
- Parabolic variation in bottom slab width (6.4 m. at pier and 8.604 m. at mid span)

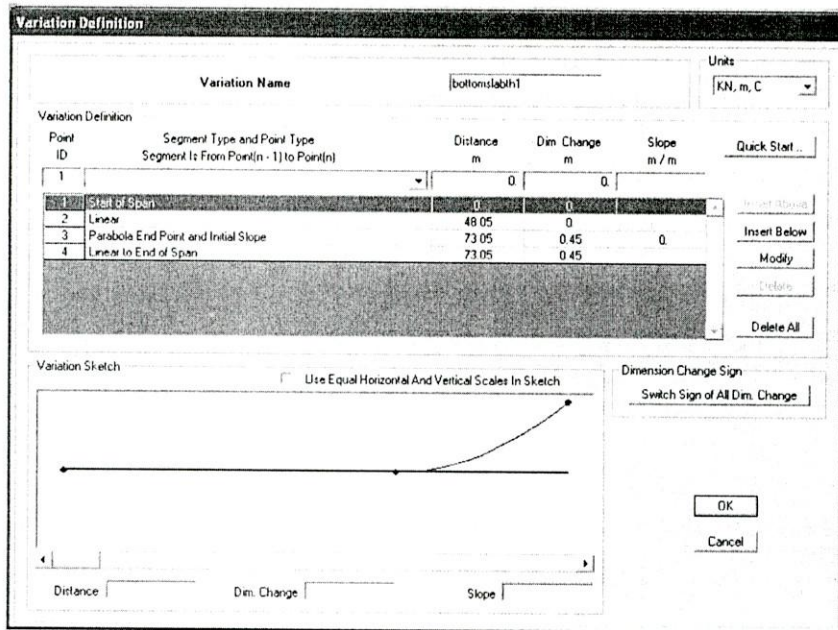


Fig. 5.5 Sap window shows parametric variation for the thickness of bottom slab of the 64.6875 m. hinge segment

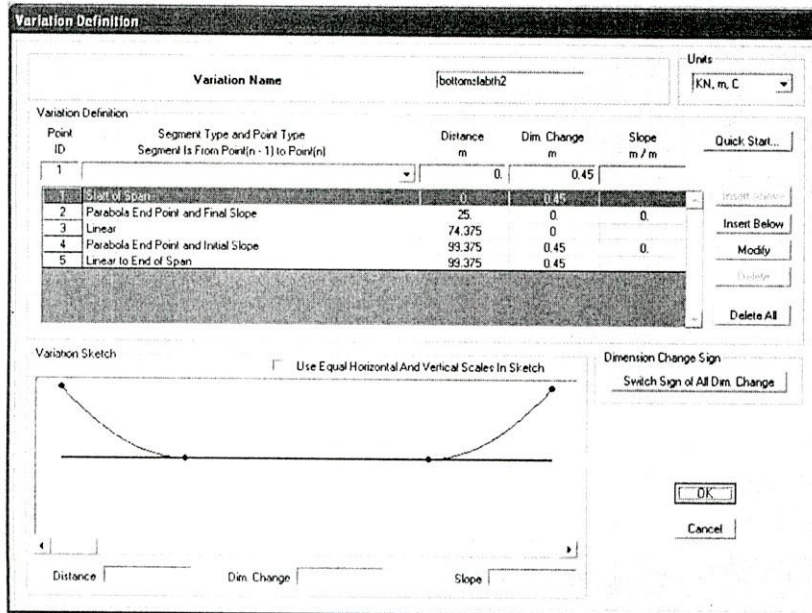


Fig. 5.6 Sap window shows parametric variation for the thickness of the bottom slab of the 99.375 m. span

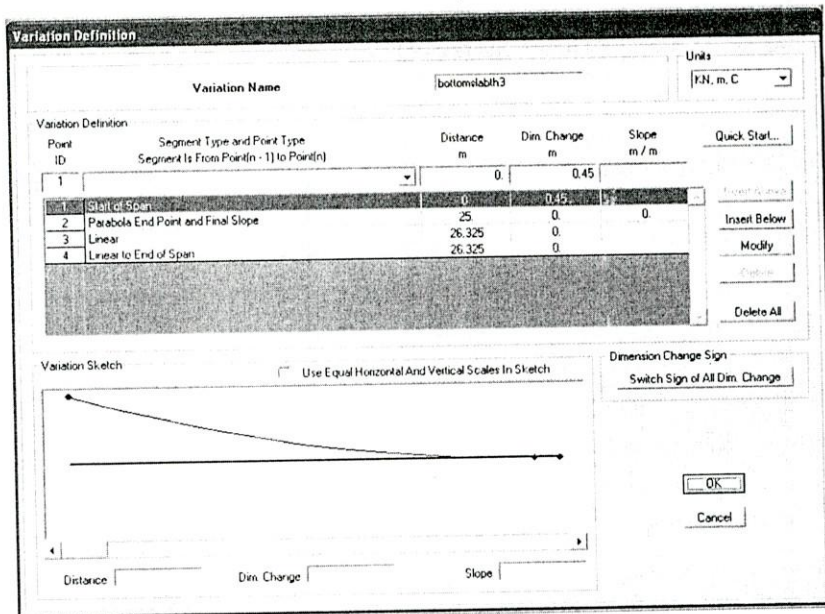


Fig. 5.7 Sap window shows parametric variation for the thickness of the bottom slab of the 26.325 hinge segment.

5.2.4. Pier, Diaphragm, Exterior Rail Girder

The pier dimension is 6 m. width and 2.5 m. thick. One of the most challenging parts of modeling of the bridge is to model the pier as it has a notch at the top (0.54 m.) and it has a solid portion (3 m.) at the bottom. But the middle of the pier is hollow and its height varies linearly 0.298 m. This model consists of all variation of piers considering its solid, hollow and notch portions. There is an exterior rail girder and a diaphragm in each pier above. The diaphragm girder is 2.5 m. thick, its top portion is 1 m, the bottom is 0.5 m and the side is 1.5 m in depth. The exterior rail girder is 2.5 m. thick and it starts at a depth of 1.11 m. and ends at a depth of 0.75 m. In the model, the diaphragm and exterior rail girder is used as shell and frame elements. Figure 5.8 shows complete view of piers, internal diaphragm and rail exterior girder of the bridge.

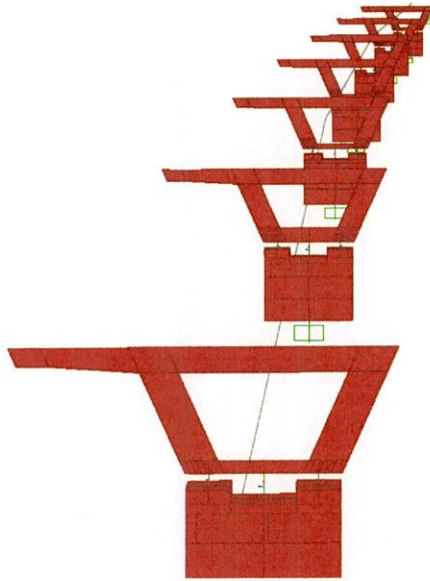


Fig. 5.8 3D View of pier, diaphragm and exterior girder.

5.2.5. Bearing and Restraint

As the model consists of a 7-span module, it has seven piers. Each of the piers has three bearing points, one at the mid point of the pier and the other two at the edges. In the edges of the pier, the bearings are multi directional and the mid point bearings are of two types. Three piers of each sides of the span have horizontal restraint with shock transmission device and the one at the mid span is horizontal restraint without shock transmission device. Deck bearing and restraint system layout are shown in Figure 5.9. The bearing system without and with transmission device is shown in Figure 5.10

In Figure 5.11 Sap window shows link or support data for mid points of the pier for all piers except the 4th pier which has a horizontal restraint with a shock transmission device. The symbol u1 indicates vertical direction, u2 indicates longitudinal direction of the bridge and u3 is lateral direction of the bridge. Vertical direction is free to move.

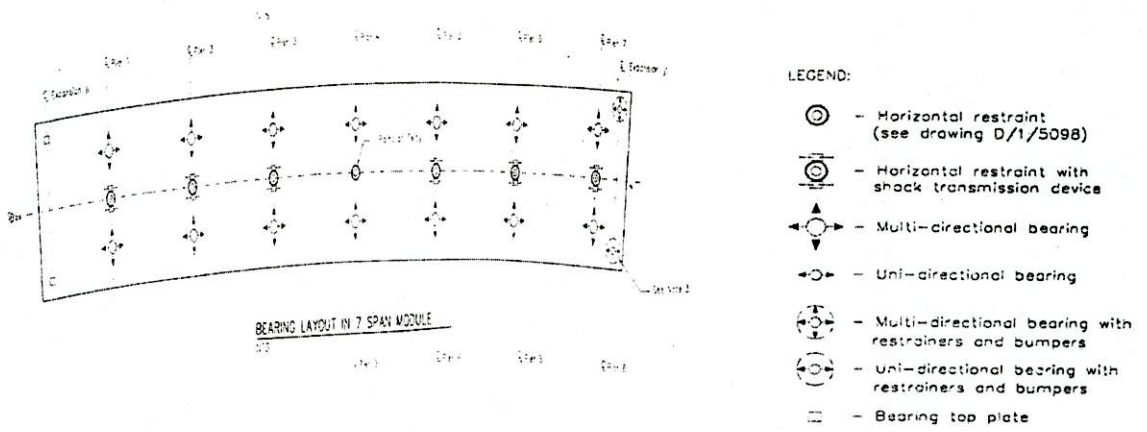


Fig. 5.9 Bearing and restraint layout

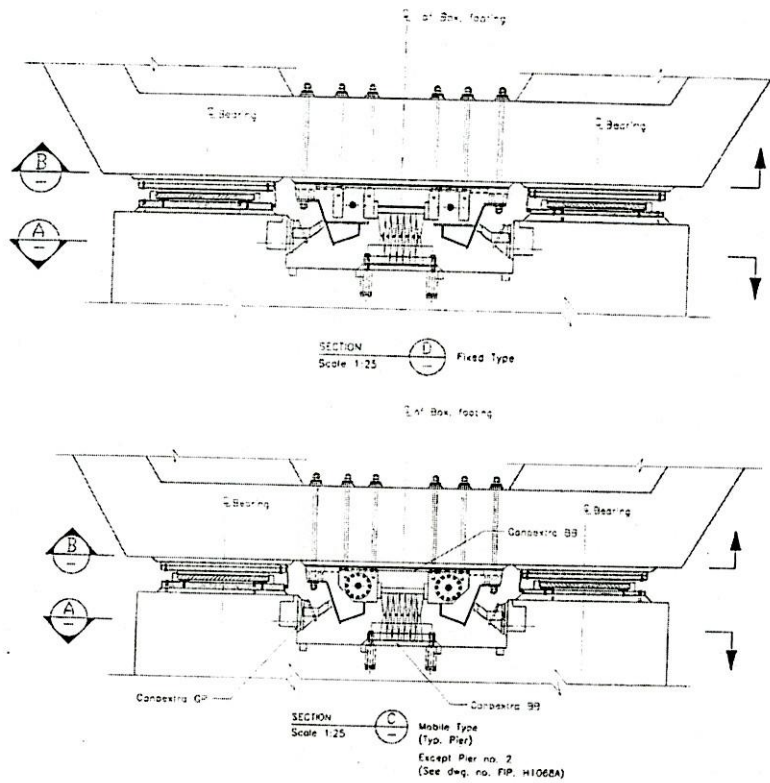


Fig. 5.10 Bearing and shock transmission device of Jamuna Bridge (fixed and mobile type).

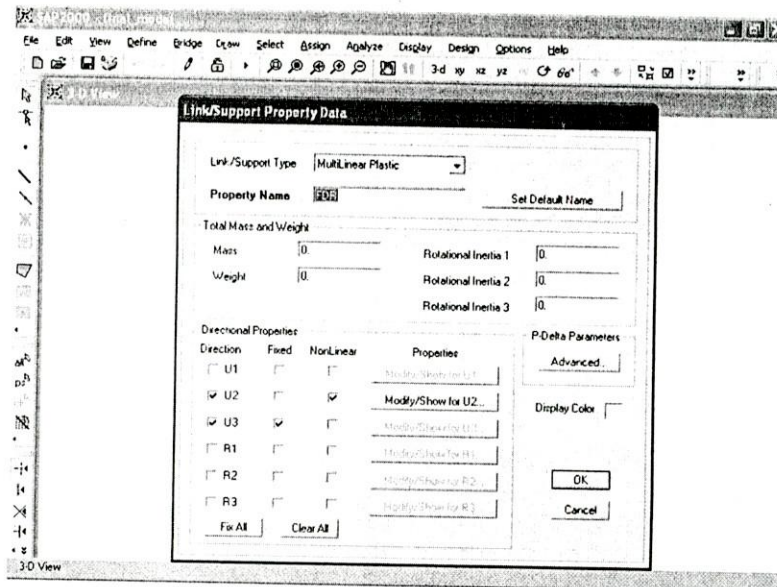


Fig. 5.11 Sap window shows link or support conditions

5.2.6 Applying Lateral Prestressing to the Deck

The bridge is prestressed in both directions laterally and longitudinally. The longitudinal prestressing is more complex in application of modeling. Therefore only lateral prestressing is considered in the model. A typical lateral prestressing layout is shown in Figure 5.12. The Figures 5.13 to 5.15 show the procedure of applying prestressing in the bridge deck. The complete lateral prestressing of the finite element modeling is shown in Figure 5.16

The following criteria are followed during applying prestressing to deck system.

- ◆ The average spacing of the prestress is .665m and the module is 695.625 m. Hence 1046 tendons need to apply.
- ◆ Every tendon has 18 parameters because of the bridge has a horizontal curvature and a longitudinal gradient.
- ◆ The adjacent two tendons are different that is if one has a dead end to the right then the other has dead end to the left and the variation is all through the same.
- ◆ Area of the tendon is 0.7258 sq. mm
- ◆ Applied load is from one end and that is 755kN.

- ◆ Curvature coefficient is .2
- ◆ Wobble coefficient is .002 per meter
- ◆ Anchorage slip is taken as 2 mm.

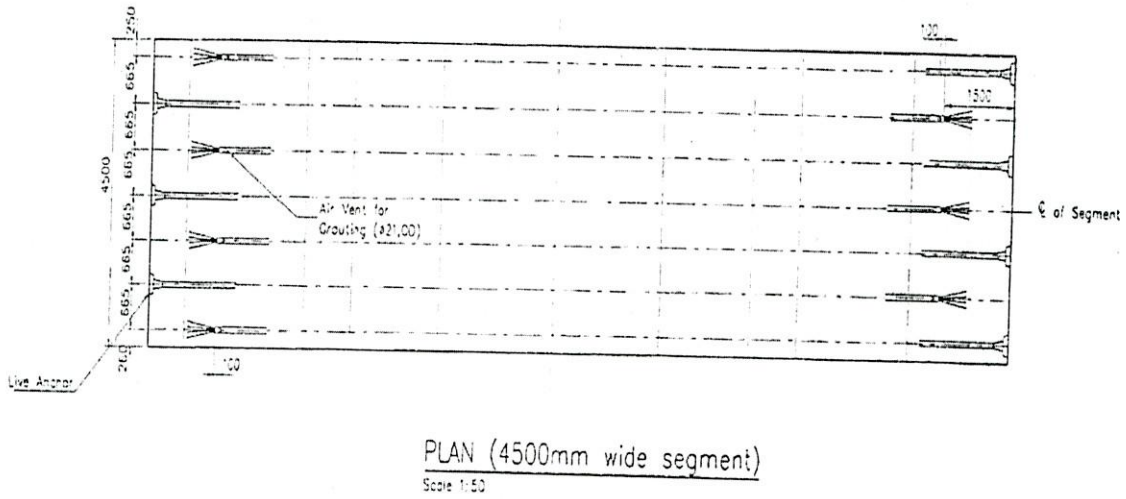


Fig. 5.12 Typical lateral prestressing layout for deck section.

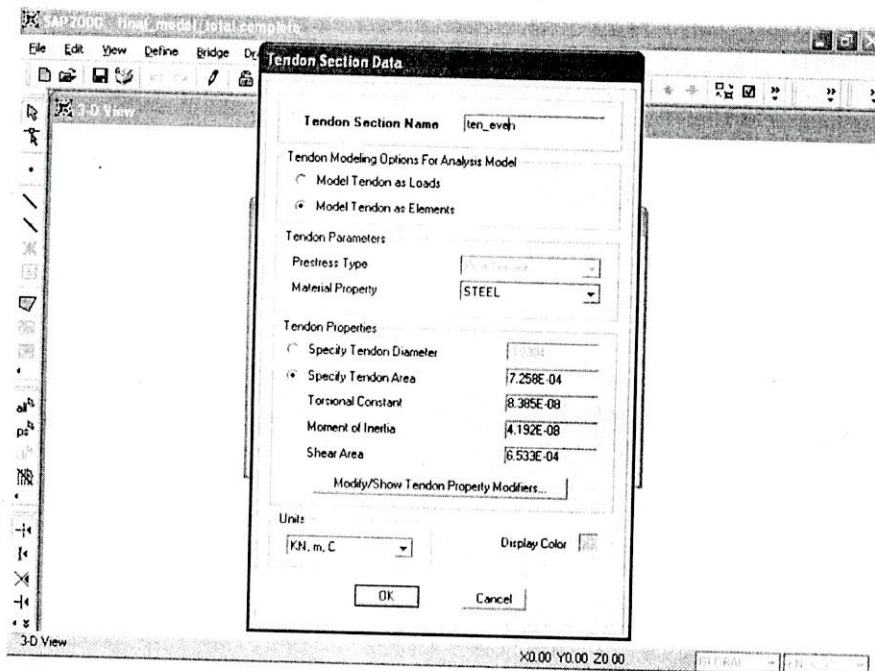


Fig. 5.13 Sap window shows tendon is modeled as element.

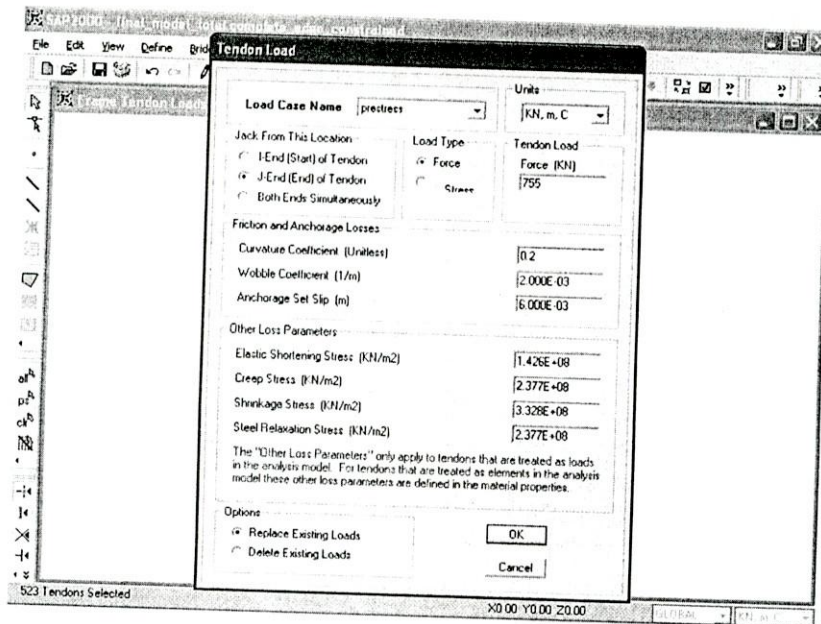


Fig. 5.14 Sap window shows prestressing is done for odd number of tendon and the jacking end is J-end.

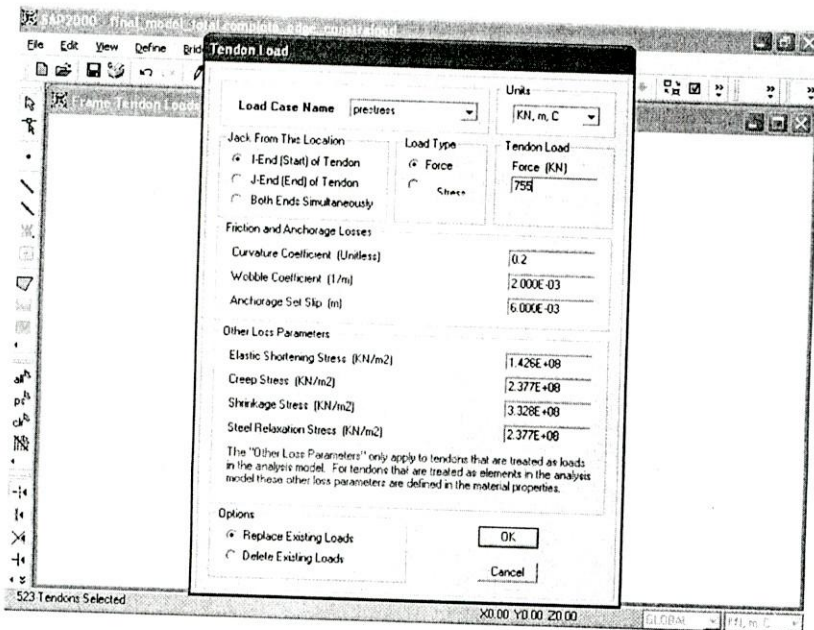


Fig. 5.15 Sap window shows prestressing are done for odd number of tendon and the jacking end is I-end.



Fig. 5.16 3D View of the lateral prestressing tendon.

CHAPTER 6

MODAL ANALYSIS

6.1 GENERAL

System identification for the transverse vibration of the Jamuna Multipurpose Bridge is performed in three ways in this present study. In order to check the validity of the Finite Element Model, a modal analysis is performed and the modal frequencies or periods are compared with the recorded data and the mathematical model. The Finite Element Model once verified can be used to predict the response of the bridge by incorporating non-linear parameters.

6.2 INTERPRETATION OF VARIOUS MODELS

Eight types of Finite Element Model have been generated as discussed in chapter 5. Their descriptions are as follows:

- ◆ Model-1. The model does not consider prestressing, pier system, diaphragm, exterior rail girder and longitudinal curvature. Vertical curvature is considered in this model. Supports and restraints are provided by hinge and roller as per actual condition.
- ◆ Model-2. The model does not consider prestressing and the pier system. Supports and restraint are provided by hinge and roller as per actual condition. Internal diaphragm and exterior rail girder are modeled with shell element.
- ◆ Model-3. The model does not considering prestressing and the pier system. Supports and restraints are provided by hinge not as per actual condition, i.e. the direction of restrains are not considered in this model. Internal diaphragm and exterior rail girder are modeled with shell element.
- ◆ Model-4. The model does not consider prestressing in the deck. Pier system is modeled with solid elements. Hollow sections at the top of the piers are not considered. Internal diaphragm and exterior rail girder are modeled with shell elements.

- ◆ Model-5. The model does not consider prestressing in the deck. Pier system is modeled with solid elements. Hollow sections at the top of the piers are also considered. Internal diaphragm and exterior rail girder are modeled with frame elements.
- ◆ Model-6. The model does not consider prestressing in the deck. Pier system is modeled with shell elements. Hollow sections at the top of the piers are not considered. Internal diaphragm and exterior rail girder are modeled with shell elements.
- ◆ Model-7. The model does not consider lateral prestressing in the deck. Pier system is modeled with solid element. A hollow section at the top of the piers is also modeled. Internal diaphragm and exterior rail girder are modeled with shell element.
- ◆ Model-8. The model considers lateral prestressing in the deck. Pier system is modeled with solid element. A hollow section at the top of the piers is also modeled. Internal diaphragm and exterior rail girder are modeled with shell element.

6.3 MODAL ANALYSIS OF THE SYSTEM

Modal analysis involves determination of natural frequencies and vibration modes of the structure by eigenvector or ritz-vector method. Graphical presentation of time period vs. mode number for various model are presented in Figure 6.1.

In Figure 6.1 it can be clearly seen that the graph is all about same for with prestressing and without prestressing (that is model-8 and model-7). On the other hand it can be said that if everything remain same for model-7 and only the hollow section is not considered then it has a very little effect in the time period or the frequency(that is in the model-4). Again there is a little effect if every thing remains same as the model-4 (previous one) and the pier is made using shell element and in that case the time period slightly decreases (that is in the model-6). From graph of model-2 and model-3 it can be easily said that the time period reduces significantly because of not considering the bearing and restraint condition. From the graph of model-5 it can be said that using frame element in

diaphragm and exterior girder (other things remain same as in the model-7) it increases the time period slightly. From the graph of the model-1 it can be said that the time period is very high at initial modes and the very low at the 12th mode. The probable reason may be not considering the important parameter of the bridge.

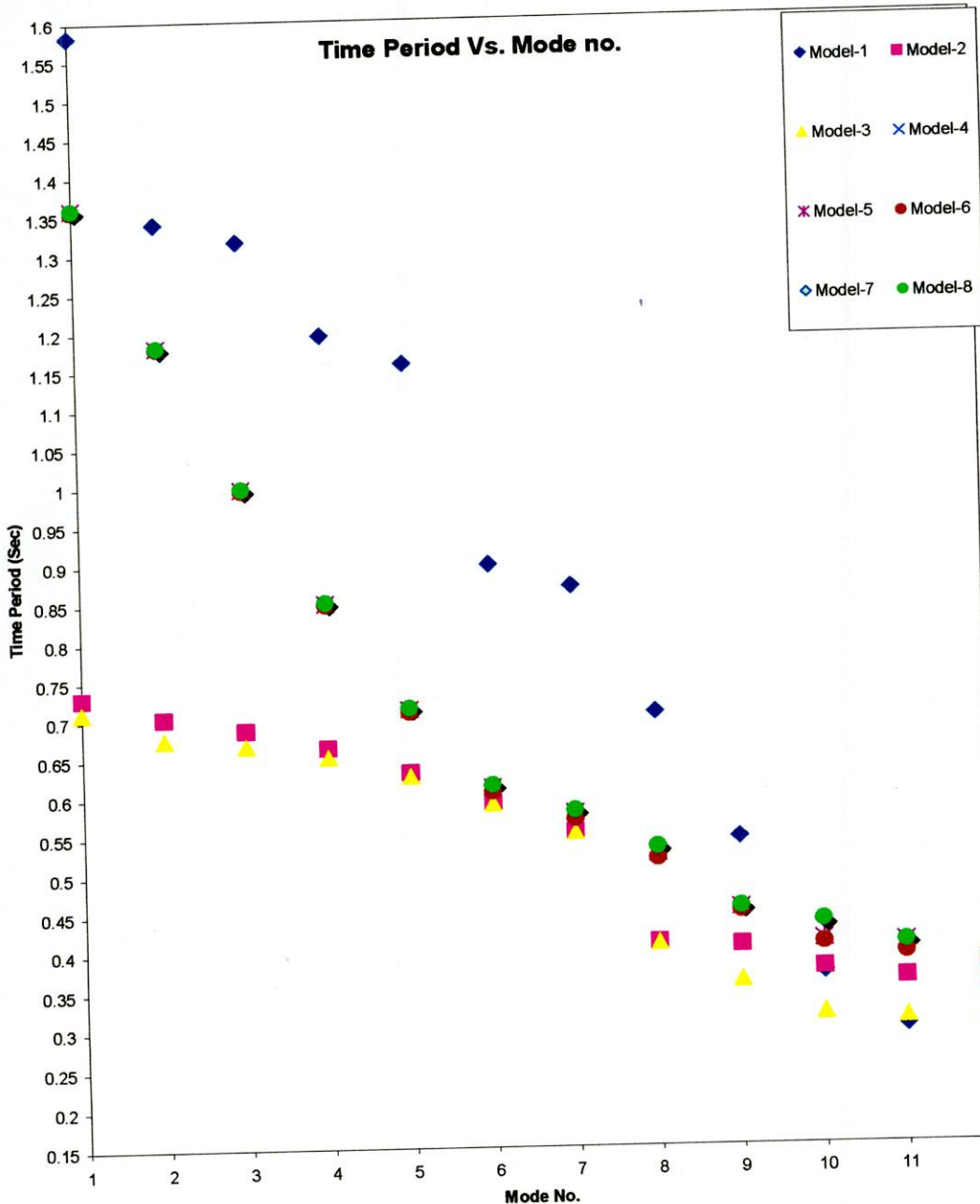


Fig. 6.1 Time period vs. mode no. of different model

6.4 GRAPHICAL DESCRIPTION OF VARIOUS TRANSVERSE MODELS

Model-8 as described in the previous section is the most sophisticated model compared to others developed in the present study. Various mode shapes as obtained by modal analysis of Model-8 are described here. The main concern of this study is to identify the modal parameter of transverse vibration of the bridge. After Modal analysis of the bridge, mode 1 and mode 2 show the longitudinal vibration and their respective frequencies are 0.735Hz and 0.846Hz. Corresponding mode shapes are shown in Figures 6.2 and 6.3. The first transverse vibration appears in the finite element model under mode 3 and its respective frequency is 1.001747Hz. The mode shape is shown in Figure 6.4. This modal frequency almost matches with 1.000976Hz of FFT of BR-5X (Fig. 4.11) and 1.00098Hz of Transfer Ratio function (Fig. 4.14). Mode 4 of the model shows both longitudinal and transverse vibration and its modal frequency is 1.175Hz. Figure 6.5 shows the mode shape of mode 4. Under mode 5, mode 6, and mode 7 the bridge vibrates in higher combined modes which is shown in Figures 6.6, 6.7 and 6.8. The entire deck of bridge vibrates transversely under mode 8 which is shown in Figure 6.9. The transverse vibration with torsional effect are observed in mode 9 and shown in Figure 6.10. The complex modal shape appears in mode 10, mode 11 and mode 12 which are shown in Figures 6.11, 6.12 and 6.12 respectively.

Mode 1

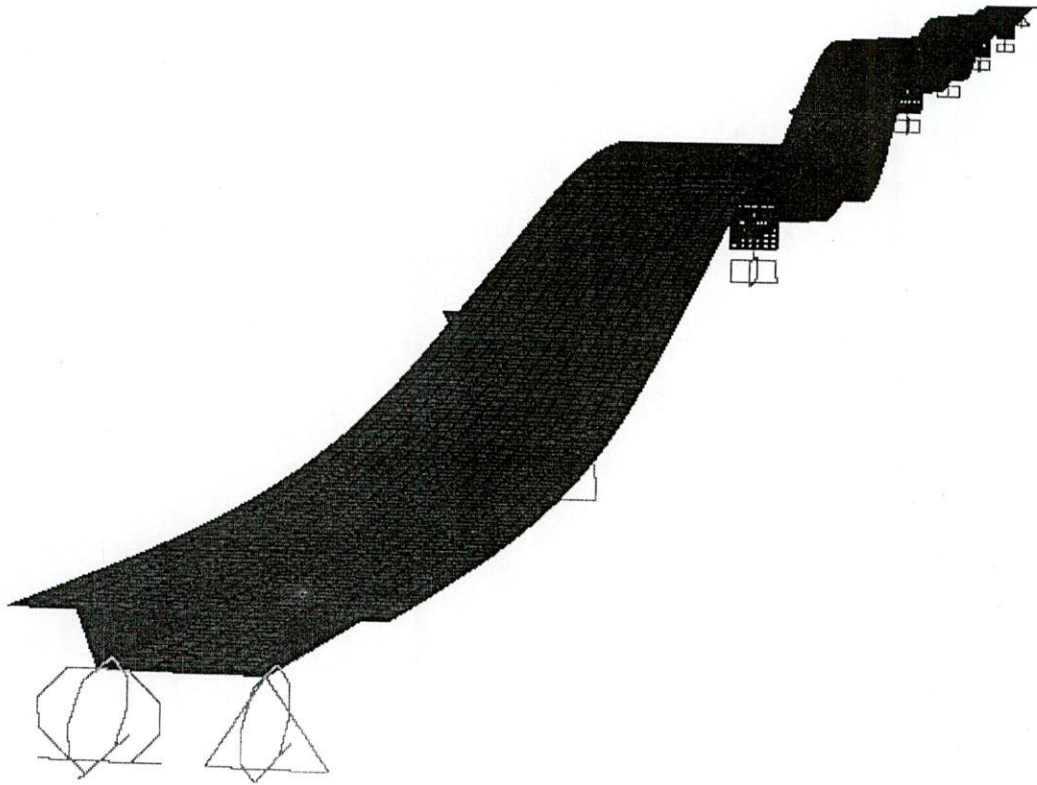


Fig. 6.2 Deformed shape of the mode 1

Mode 2

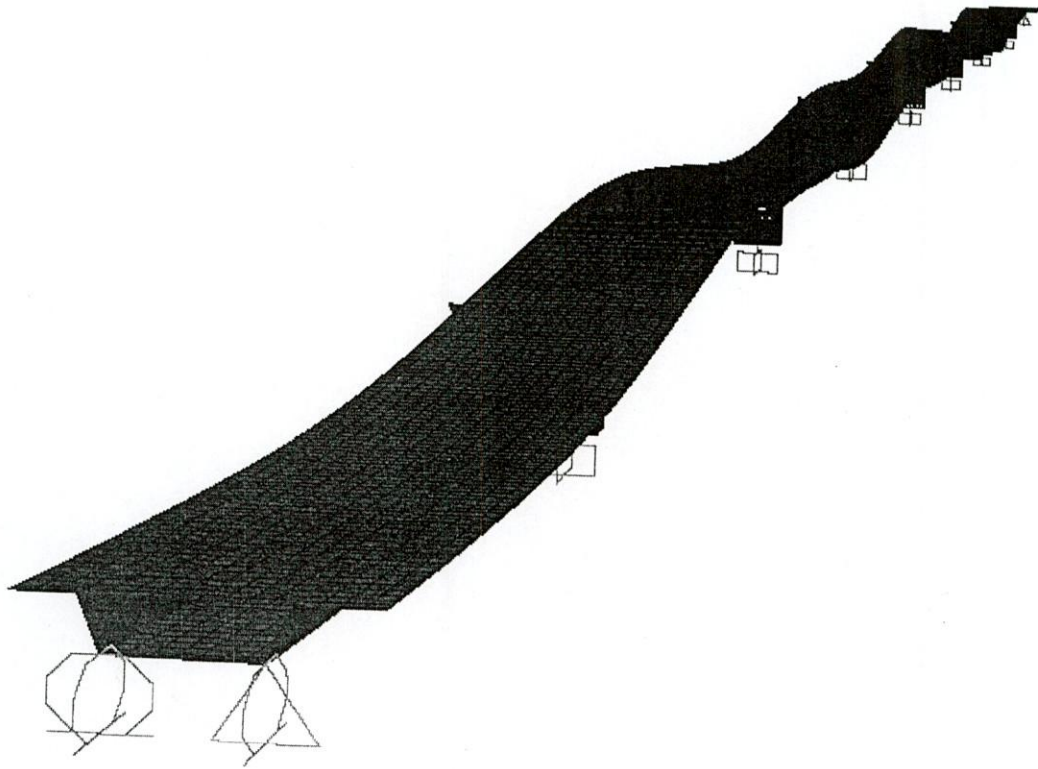


Fig. 6.3 Deformed shape of the mode 2

Mode 3

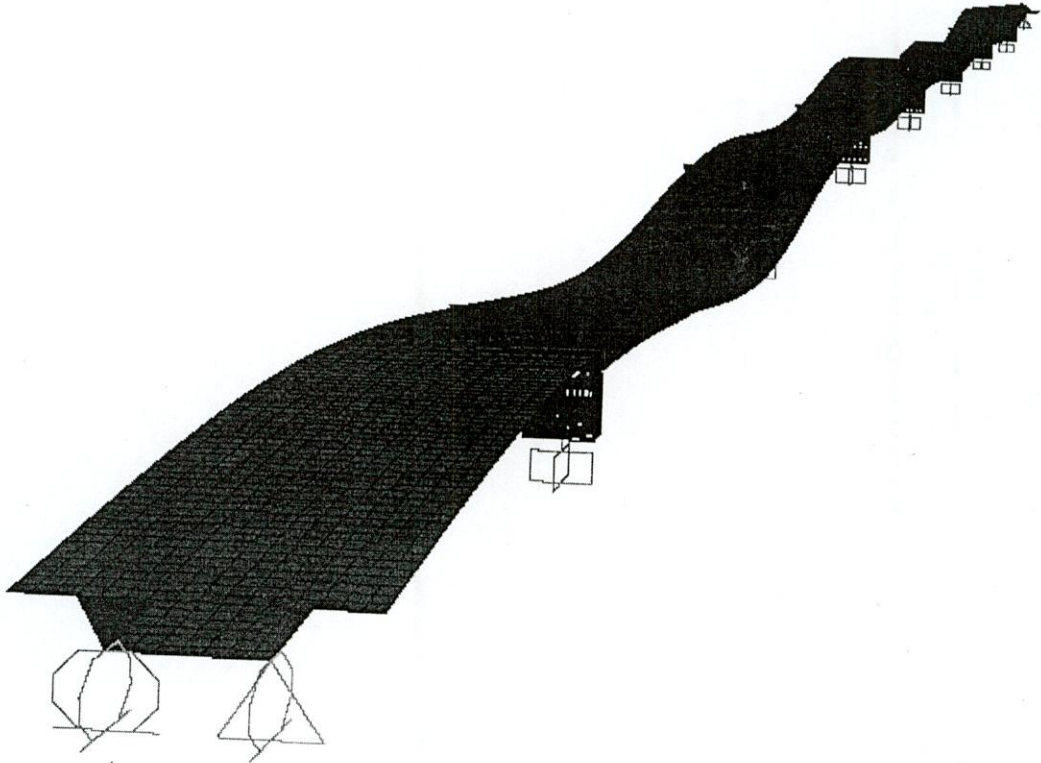


Fig. 6.4 Deformed shape of the mode 3

Mode 4

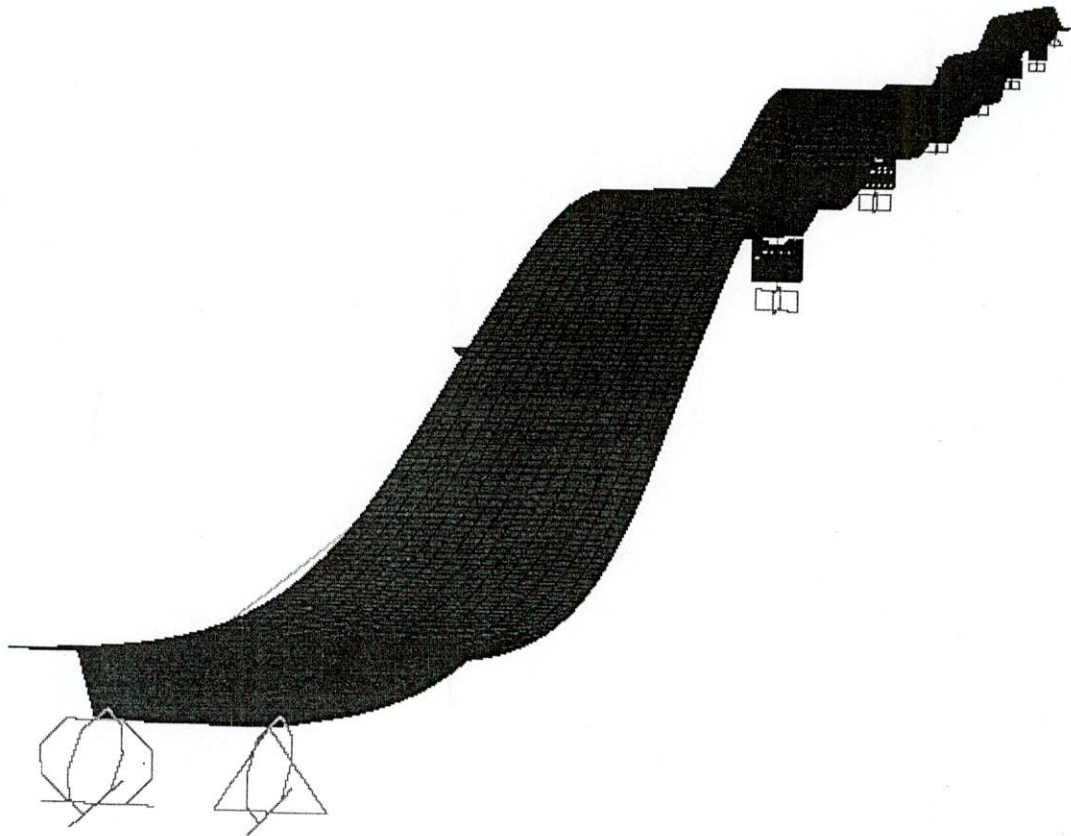


Fig. 6.5 Deformed shape of the mode 4

Mode 5

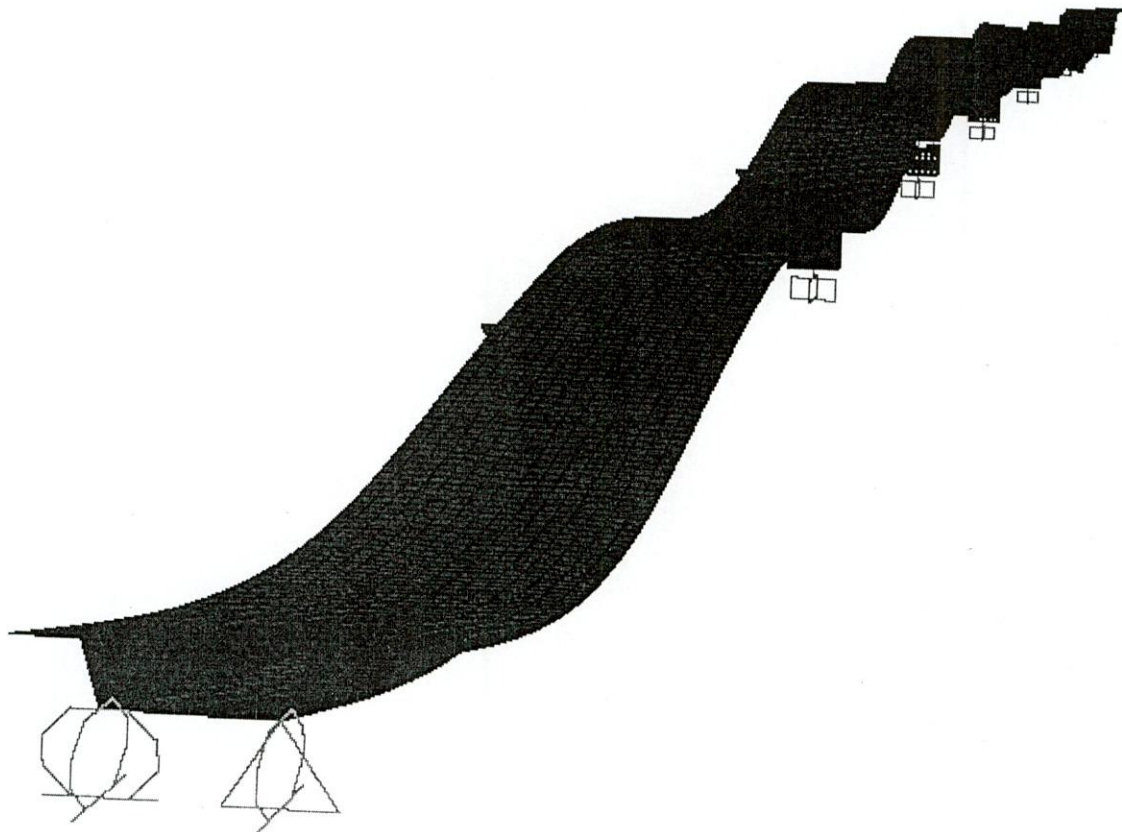


Fig. 6.6 Deformed shape of the mode 5

Mode 6

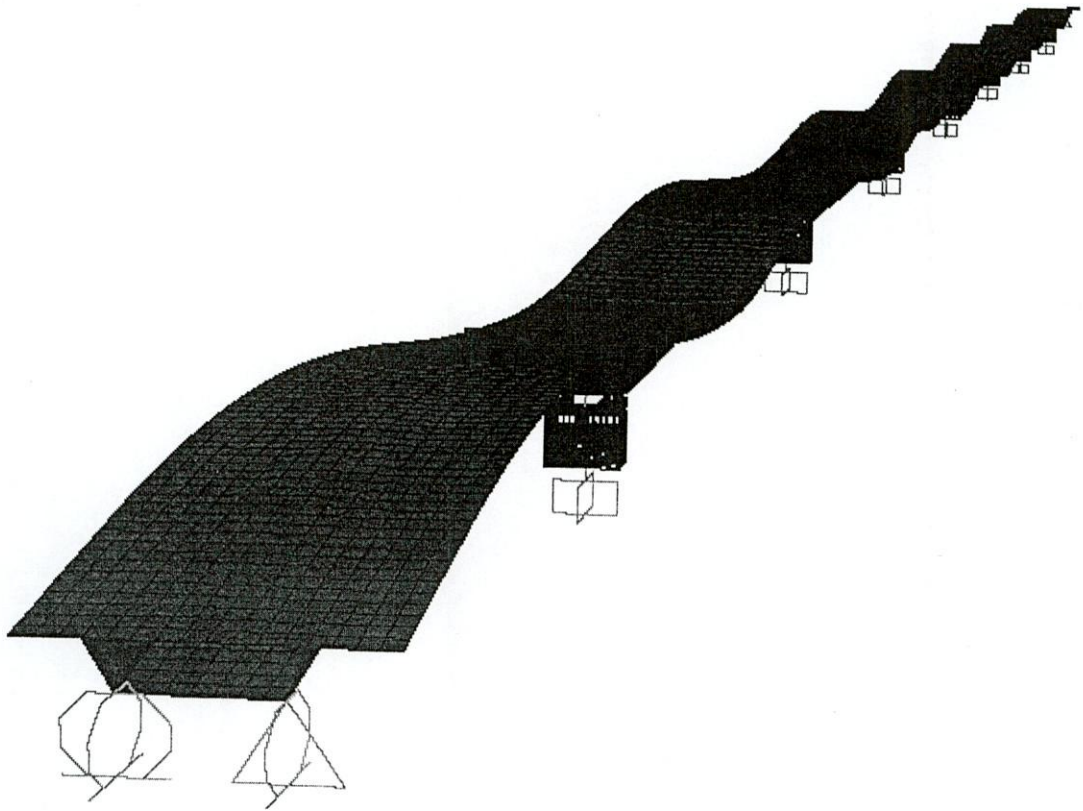


Fig. 6.7 Deformed shape of the mode 6

Mode 7

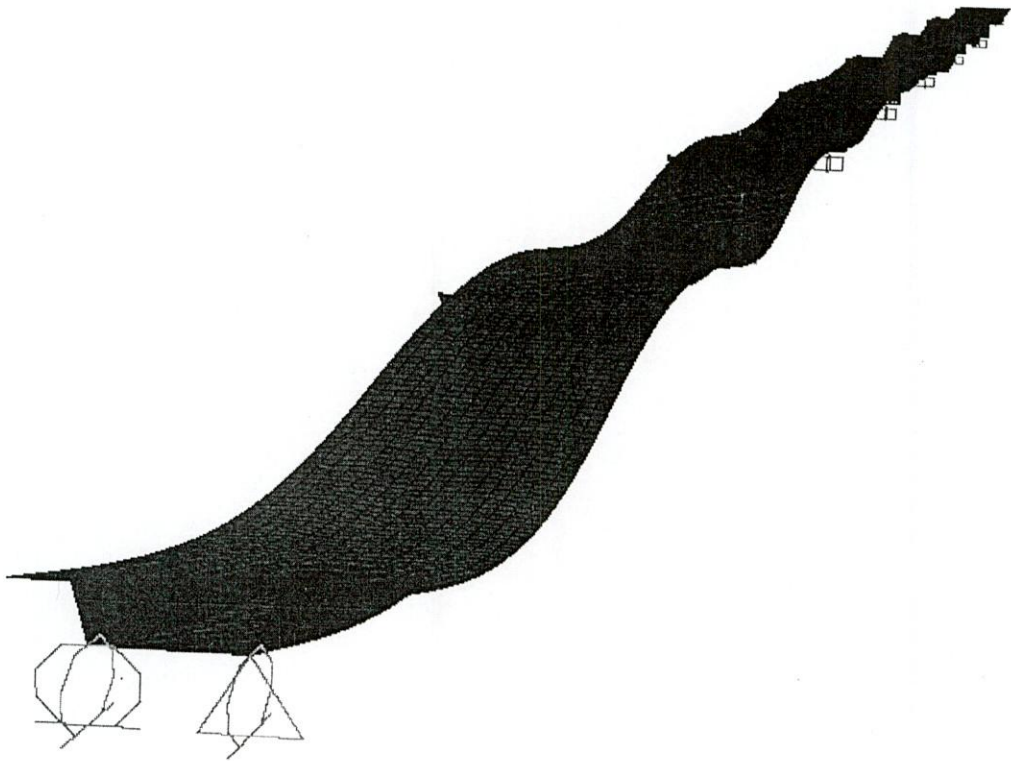


Fig. 6.8 Deformed shape of the mode 7

Mode 8

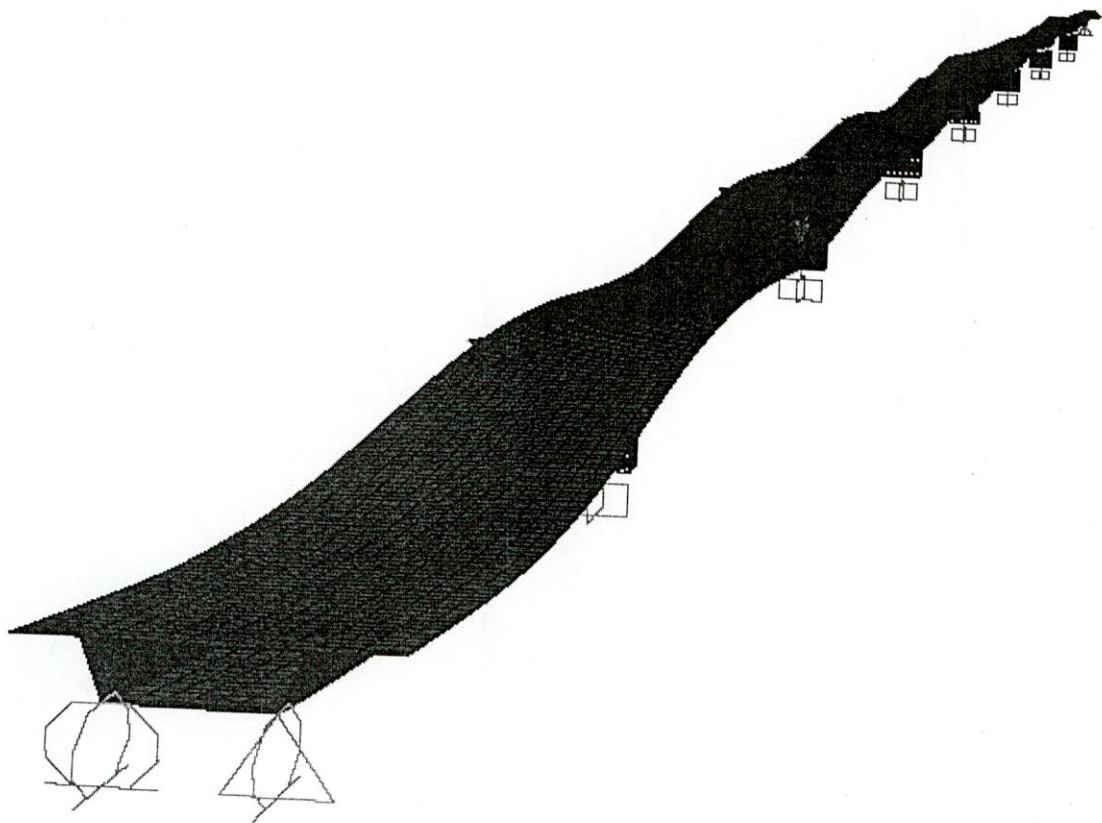


Fig. 6.9 Deformed shape of the mode 8

Mode 9

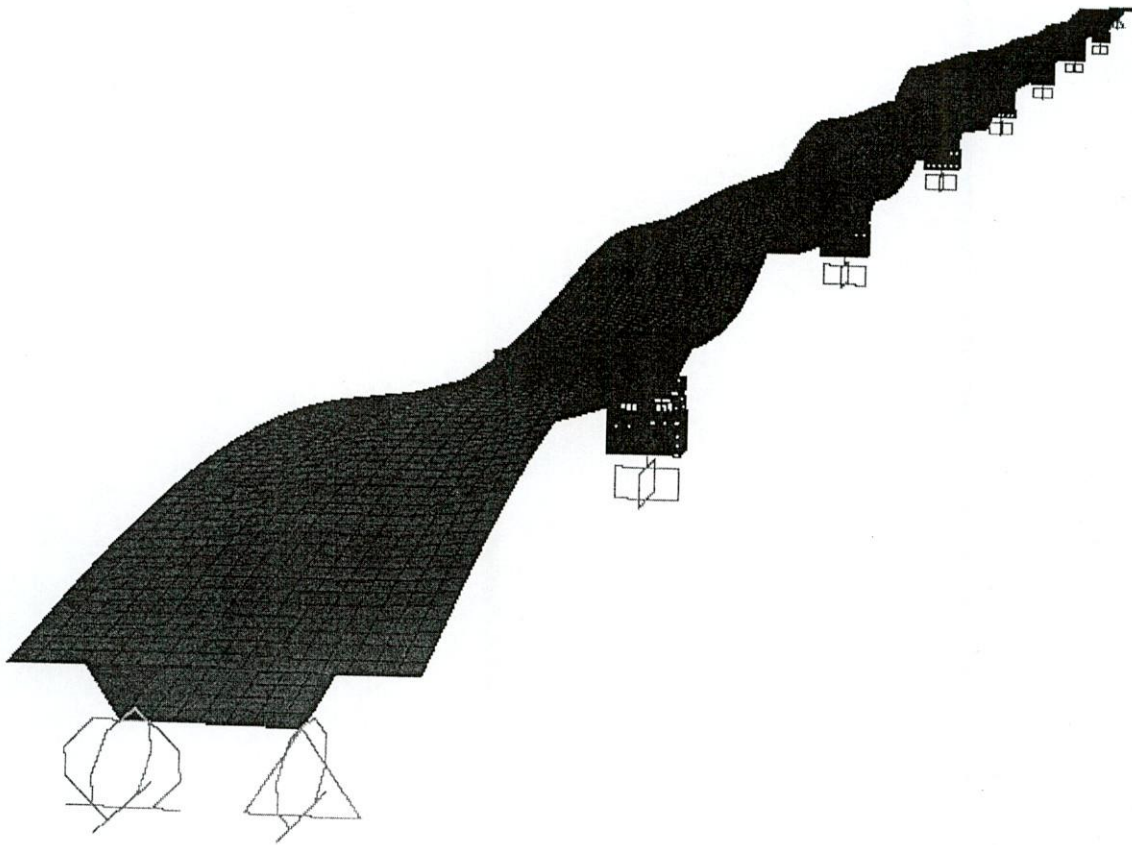


Fig. 6.10 Deformed shape of the mode 9

Mode 10

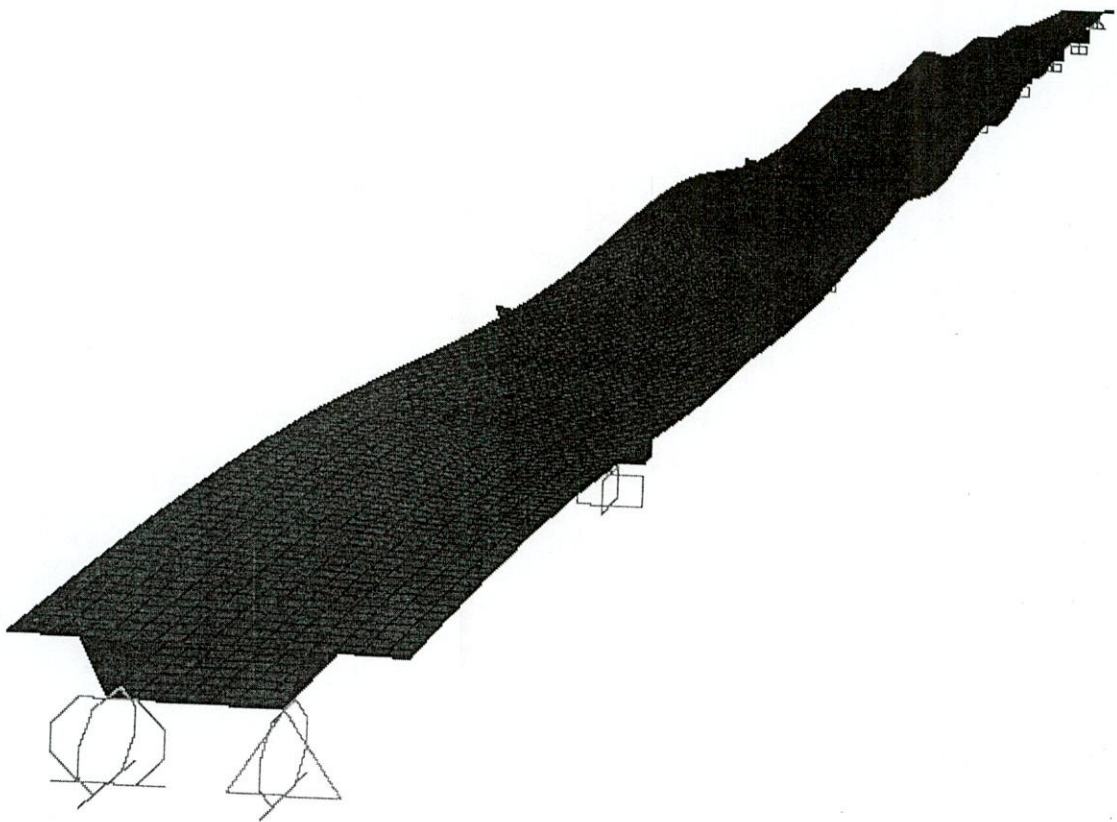


Fig. 6.11 Deformed shape of the mode 10

Mode 11

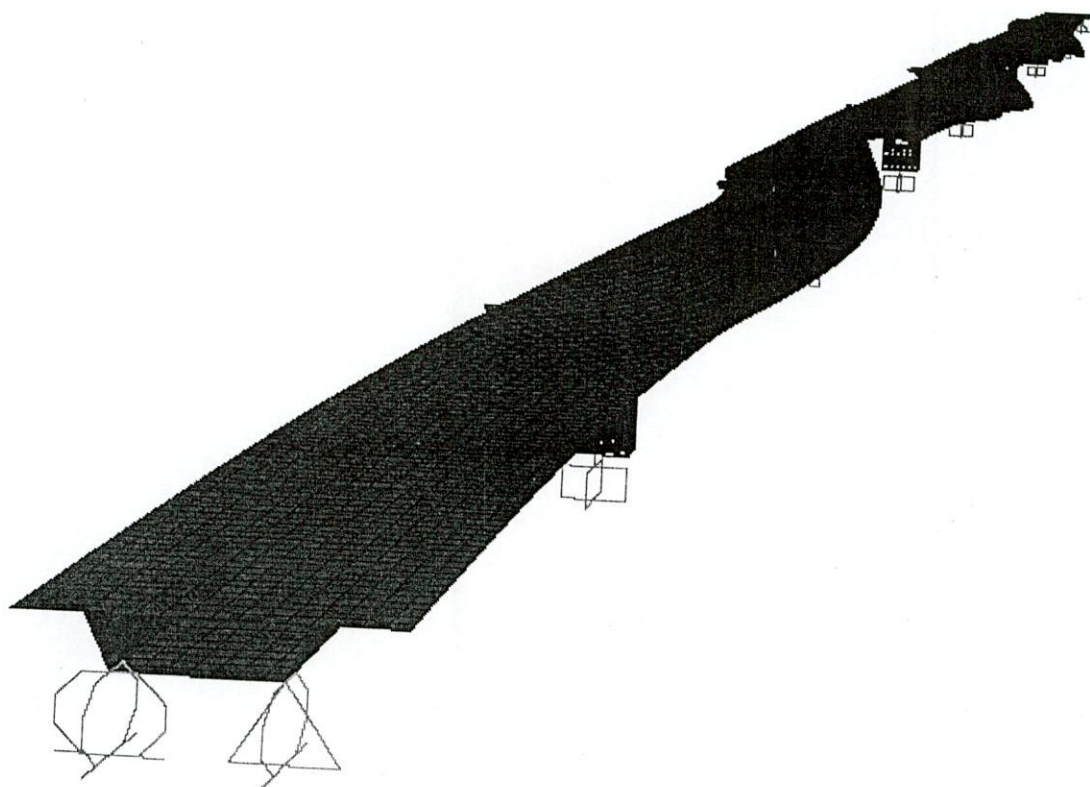


Fig. 6.12 Deformed shape of the mode 11

Mode 12

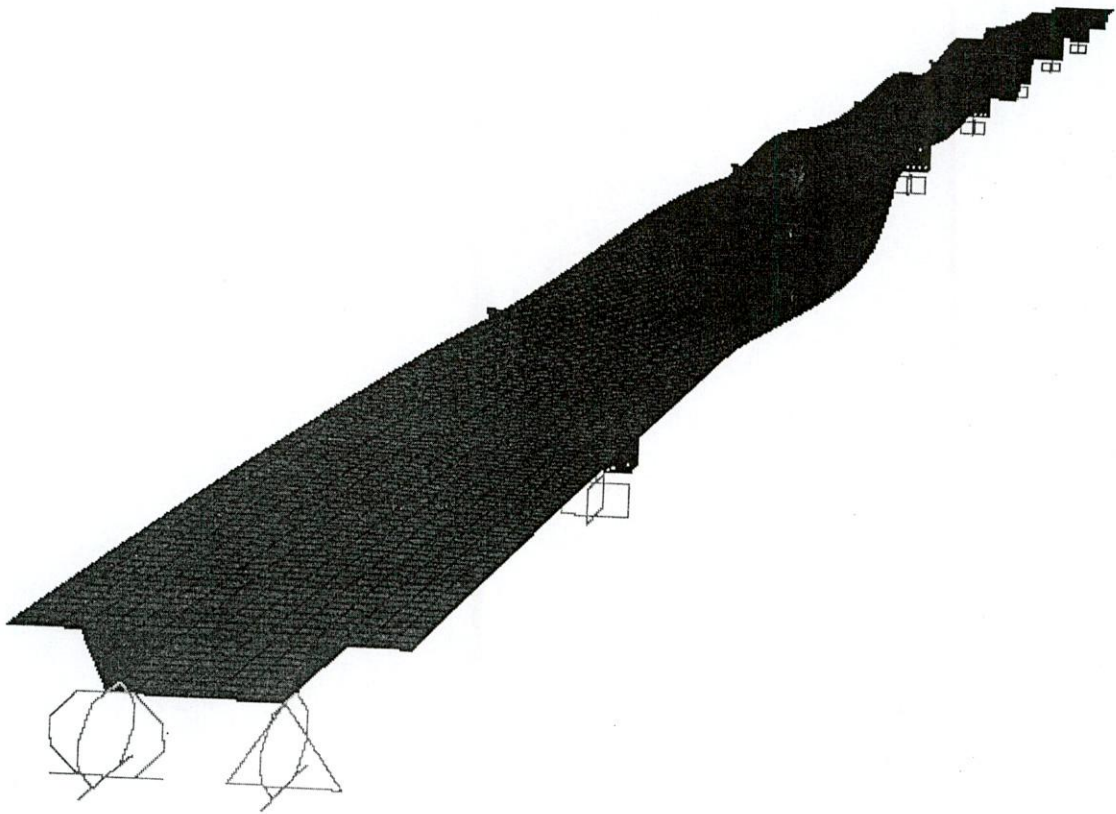


Fig. 6.13 Deformed shape of the mode 12

CHAPTER 7

BRIDGE BEHAVIOR UNDER VARIOUS DYNAMIC LOADS

7.1 GENERAL

An earthquake was detected on June 17, 2004 at 05:36:53 hrs BST, (23:36:53 hrs GMT, June 16, 2004) at the Bridge West End free-field station. All accelerometers inside the bridge and bridge west-end, east-end and Mymensingh free-field stations were active at that time. Other four free-field stations were not activated which may be due to the fact that the intensity of ground motion at those sites being lower than the trigger level set for starting the devices. Epicenter of this earthquake lies close to the bridge site.

7.2 EARTHQUAKE PARAMETERS

The strong motion instruments recorded the time of occurrence of the earthquake through GPS. Using the recorded ground motions, the time of first arrivals of S and P waves, epicentral location, magnitude were estimated.

The estimated epicentral parameters are as follows:

Magnitude: $M_L=2.5$

Epicentre: Approximately 50 to 60 km from the bridge site.

Depth: 33 km

7.3 TIME HISTORY OF EARTHQUAKE DATA

The processed information of time histories of ground motion is shown in Figures 7.1 to 7.6. In the time history records, pre-event is 10 seconds and post event is 30 seconds. Duration of the earthquake records at Bridge West-End and Bridge East-End is around 43 sec and 42 sec respectively. Each plot of time history shows acceleration, velocity and displacement in the three directions for each station. The maximum ground acceleration 42.208cm/sec^2 in east-west direction of the west end free field station. Whereas the maximum ground acceleration of east end of the bridge is 12.614 cm/sec^2 in east-west direction. The peak values of these accelerograms are given in Table 7.1.

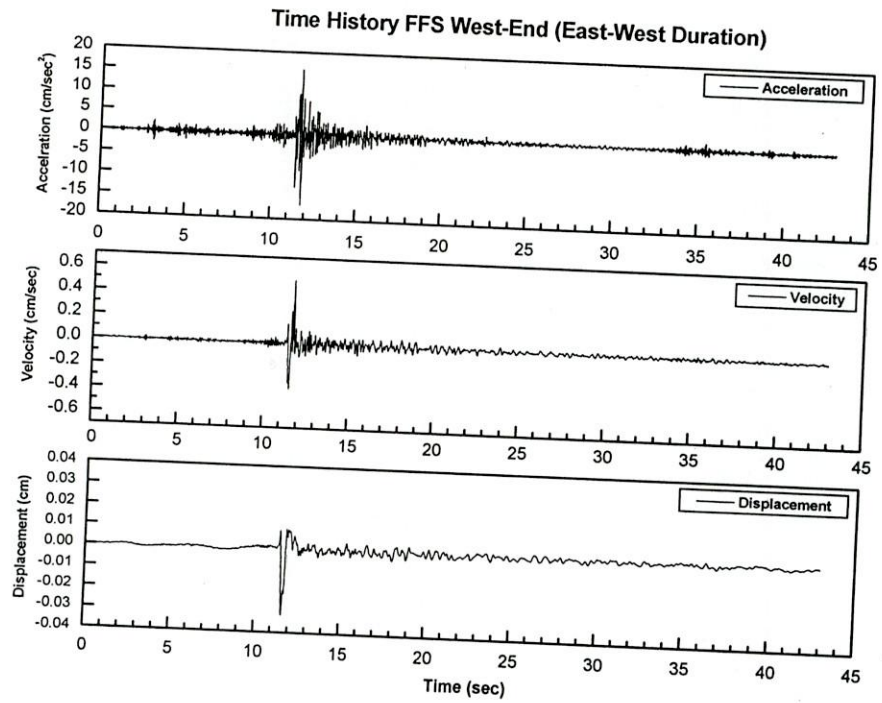


Fig.7.1 Time History of West -End Source (E-W Direction)

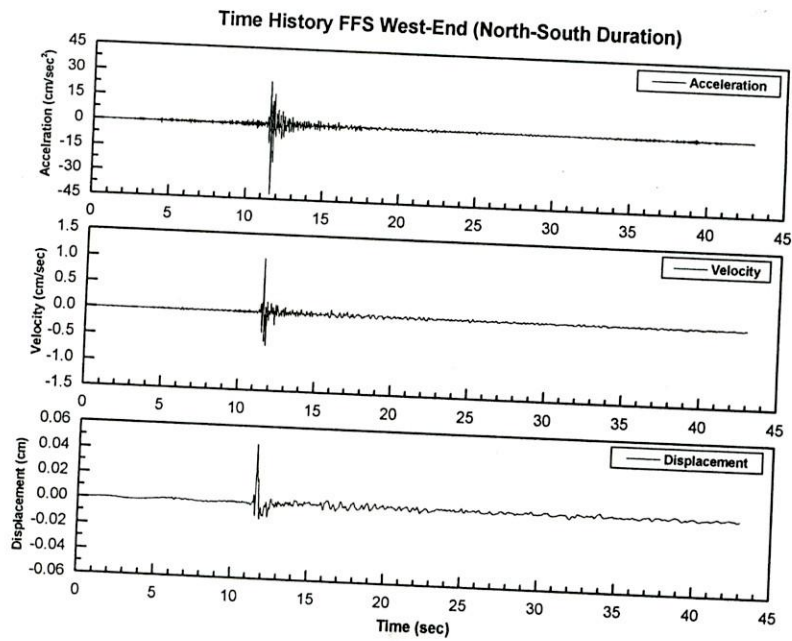


Fig. 7.2 Time History of West-End Source (N-S Direction)

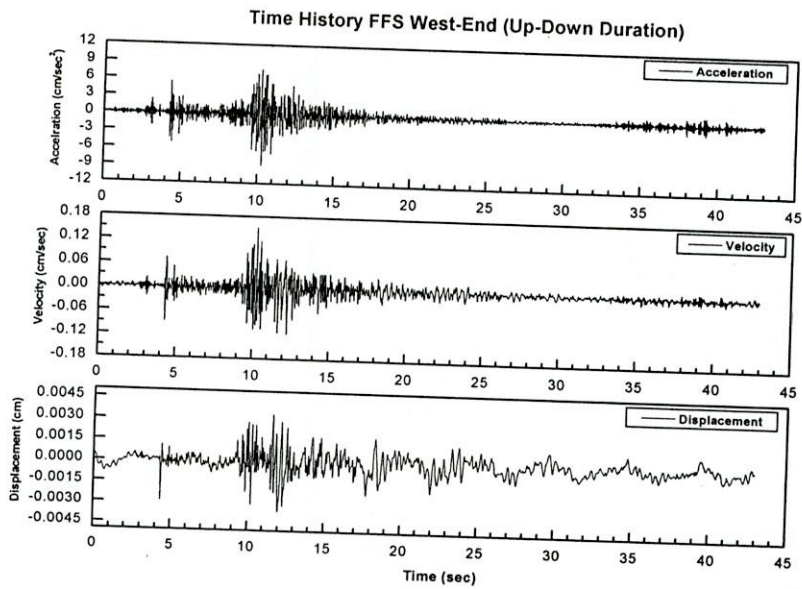


Fig. 7.3 Time History of West-End Source (Up-Down Direction)

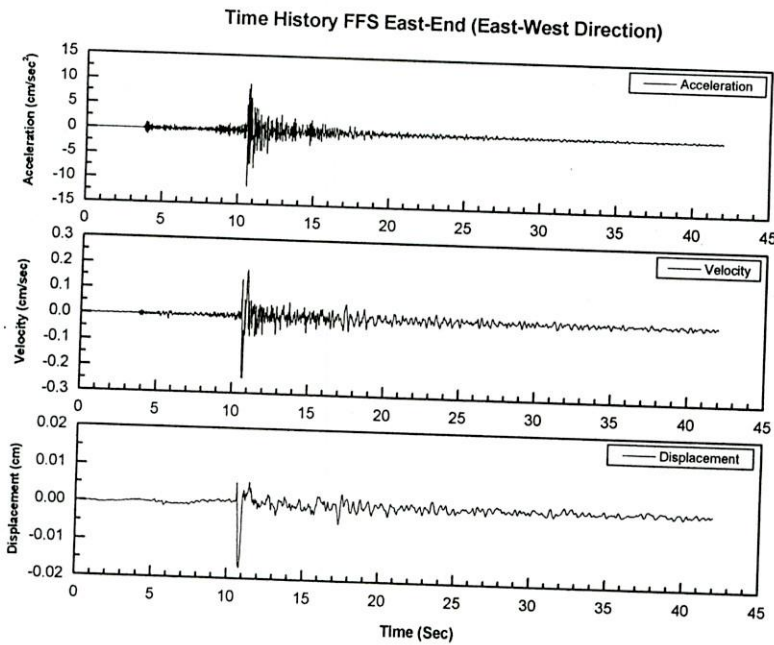


Fig. 7.4 Time History of East-End Source (East-West Direction)

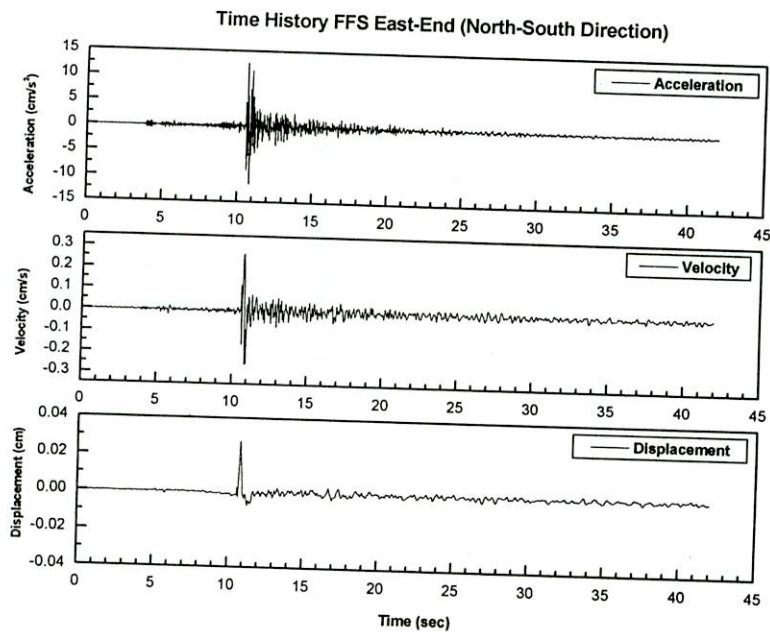


Fig. 7.5 Time History of East-End Source (North-South Direction)

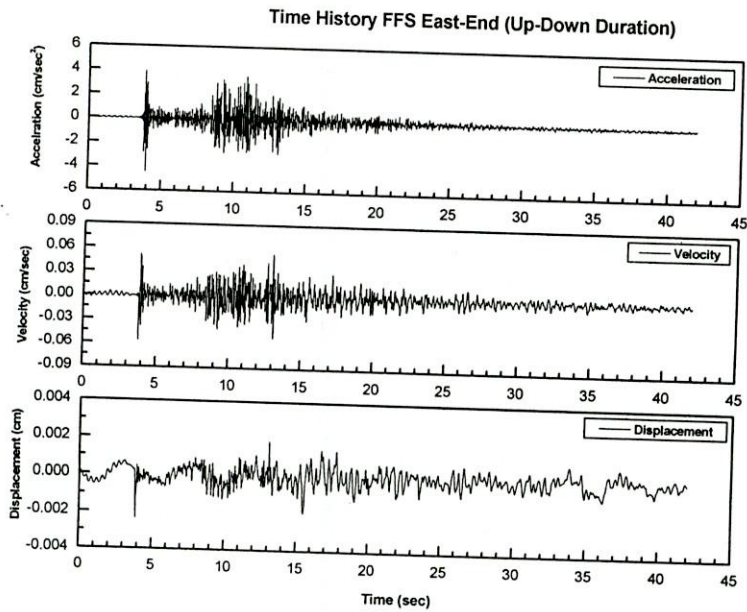


Fig. 7.6 Time History of East-End Source (Up-Down Direction)

Table 7.1 Summary of ground motion in free-field stations June 16, 2004 earthquake

Station ID#	Channel	Date	Time (GMT)	Latitude & Longitude	Derived Max. Peak Ground Acceleration (cm/sec ²)	Derived Max. Peak Ground Velocity (cm/sec)	Derived Max. Peak Ground Displacement (cm)
Bridge West-End	X	16.06.04	23:36:53	24.398°N 89.753°E	-16.674593	0.517800	-0.031480
	Y				-42.208819	1.037485	0.046156
	Z				-8.905226	0.152260	-0.003576
Bridge East-End	X	16.06.04	23:36:53	24.393°N 89.805°E	-11.45854	-0.241417	-0.017279
	Y				12.614964	0.267912	0.027178
	Z				-4.44861	-0.056746	-0.002342
	Z				3.738474	0.076052	0.002150

7.4 EARTHQUAKE RESPONSE OF THE BRIDGE

Fifteen out of sixteen sensors on the bridge recorded the motion of the bridge. The peak values of all accelerometers are given in Table 7.2. The West-End free-field station is nearest to the instrumented bridge module (7-span module next to West-end module). The ground acceleration at the West-End free-field station had a maximum value of 42.2 cm/sec² in the NS direction. From table 7.2 it is shown that the maximum value of acceleration 13.89 cm/sec² is found BR-1X at pile cap of the pier 10 and its corresponding displacement is 0.52 cm. At BR-5X in side of the deck of the same pier 10, the acceleration and displacement values are 7.73 cm/sec² and 0.026cm respectively. 100 meters apart from BR-5X the acceleration and displacement values are found 3.97 cm/sec² and -0.037cm respectively at BR-10X. -0.032cm and 0.028 cm of transverse displacement is observed at deck of mid span.

Table 7.2 Summary of Earthquake Data in Bridge, June 16, 2004 Earthquake

Channel ID	Sensor Location	Derived Max. Peak Acceleration (cm/sec ²)	Derived Max. Peak Velocity (cm/sec)	Derived Max. Peak Displacement (cm)
BR-1X	Pile Cap at Pier P10	13.886711	0.517741	0.517741
BR-2Y		-5.977106	0.200606	0.018816
BR-3Z		-2.826680	0.078672	0.003982
BR-4Z		-2.901607	-0.069071	-0.002830
BR-5X	Deck at Pier P10	7.726918	0.262712	0.026098
BR-6Y		4.608948	0.306314	-0.033408
BR-7Z		-0.033408	-0.092368	-0.004267
BR-8Z		3.386794	0.111028	0.004573
BR-9Z	Pile Cap at Pier P9	11.220399	0.317303	-0.023982
BR-10X	Deck at Pier P9	3.968054	0.274578	-0.036614
BR-11Y		-3.133283	-0.072303	0.002786
BR-12X	Deck at Mid Span	-7.738449	0.303828	-0.031692
BR-13X		-10.535200	-0.346522	0.027877

Note: X means orientation across the bridge (transverse direction)
 Y means orientation parallel to the bridge (longitudinal direction)
 Z means vertical direction

7.5 RESPONSE UNDER VARIOUS DYNAMIC LOADING

Two triaxial, one biaxial, five uniaxial accelerometer sensors and three Displacement sensors are installed in various parts of a seven-span bridge module. Ambient vibration was measured on the bridge during a Hartal when no vehicle was running. The word 'traffic' is used in this study to represent cars, buses, and trucks running on the bridge but excluding train. The train data is recorded while other traffic also moved on the bridge. The comparison of bridge response at various locations of the bridge structure without traffic, with traffic, only train and with traffic and train is given in Table 7.3. It is obvious that the response of bridge under traffic with train loading is higher than that for ambient and only traffic loading. Response of the bridge recorded at BR-5X located at Deck upon pier 10 is discussed here. From table 7.3 it is observed that acceleration of recorded data under train and other traffic loading is 7.676 cm/sec², and that for the recorded

earthquake is 7.726 cm/sec^2 which are very close. FFT of dynamic loads under various traffic conditions are also shown in figures 7.7a to 7.7j. From figure 7.7d 0.426Hz , 0.492Hz , 0.709Hz , 0.781Hz , and 1.056Hz frequencies are found for corresponding picks of FFT of ambient vibration records at BR-5X. 0.44Hz , 0.576Hz , 0.682Hz , 0.8381Hz , 0.926Hz and 1.044Hz frequencies are found for corresponding picks of FFT of Traffic vibration records at BR-5X. Similarly, 0.372Hz , 0.598Hz , 0.772Hz , and 1.013Hz are found for Train vibration and 0.43Hz , 0.627Hz , 0.85Hz and 1.013Hz are found for earthquake at BR-5X. One of the common pick is found at around 1.013Hz in various loading condition which almost mach with the predominant frequency in transverse vibration as obtained from Finite Element Model(1.00174Hz) and Transfer Ratio (1.0098Hz)

Table 7.3 Comparison of Earthquake data and Various dynamic loads on Bridge for Various Traffic Conditions

Channel ID	Sensor Location	Ambient (cm/sec ²)	Traffic Data (cm/sec ²)	Train and other Traffic Data (cm/sec ²)	Earthquake Data (cm/sec ²)
BR-1X	Pile Cap at Pier P10	0.015	1.555	4.875	13.886711
BR-2Y		0.014	0.4733	1.482	-5.977106
BR-3Z		0.01	0.4167	3.638	-2.826680
BR-4Z		0.016	0.7812	1.105	-2.901607
BR-5X	Deck at Pier P10	0.025	1.25	7.676	7.726918
BR-6Y		0.023	0.5755	2.526	4.608948
BR-7Z		0.021	0.5871	8.05	-0.033408
BR-8Z		--	--	10.52	3.386794
BR-9Z	Pile Cap at Pier P9	0.013	0.504	4.354	11.220399
BR-10X	Deck at Pier P9	0.025	1.212	3.025	3.968054
BR-11Y		0.027	0.7537	11.298	-3.133283
BR-12X	Deck at Mid Span	0.032	1.296	17.01	-7.738449
BR-13X		--	--	17.758	-10.535200

BR-1X

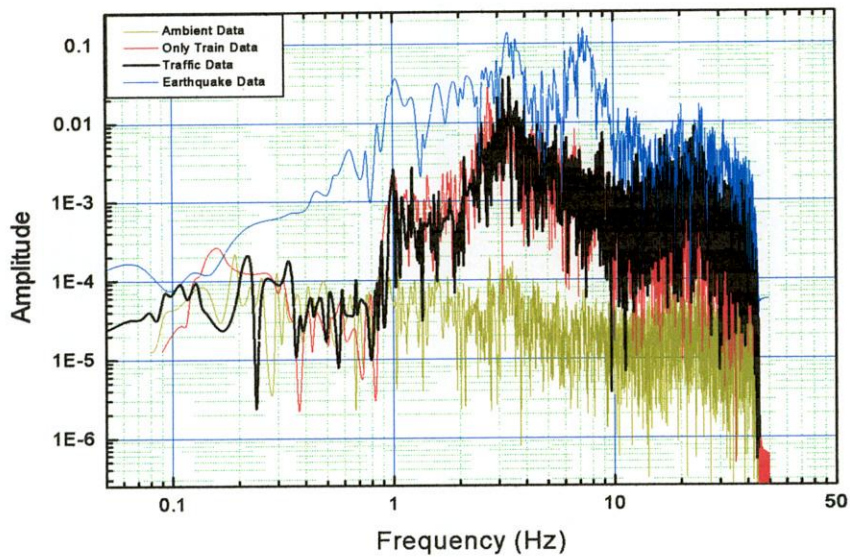


Fig. 7.7-a FFT of BR-1X

BR-3Z

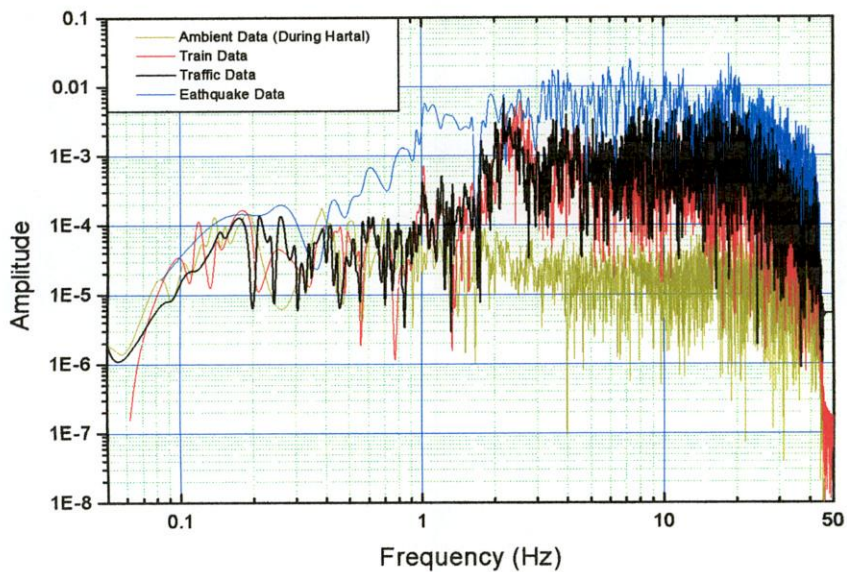


Fig. 7.7-b FFT of BR-3Z

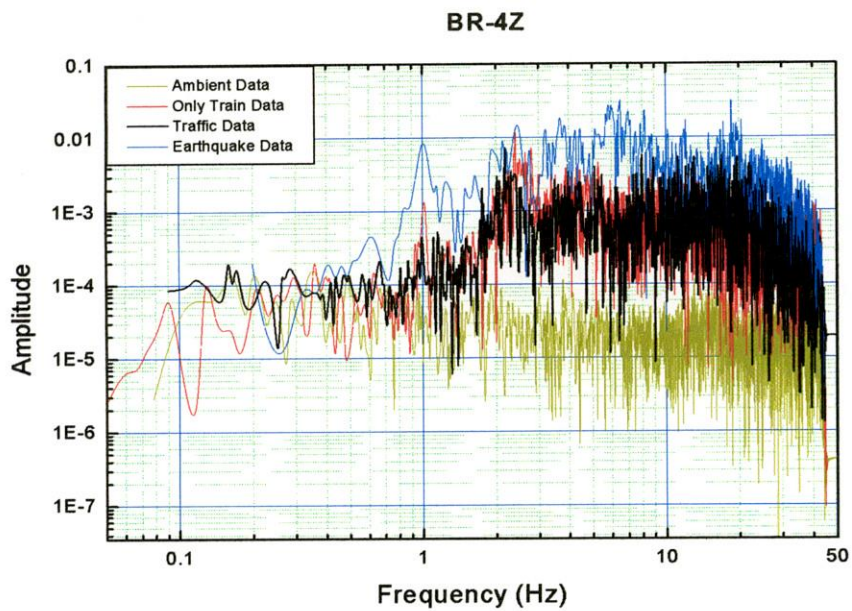


Fig. 7.7-c FFT of BR-4Z

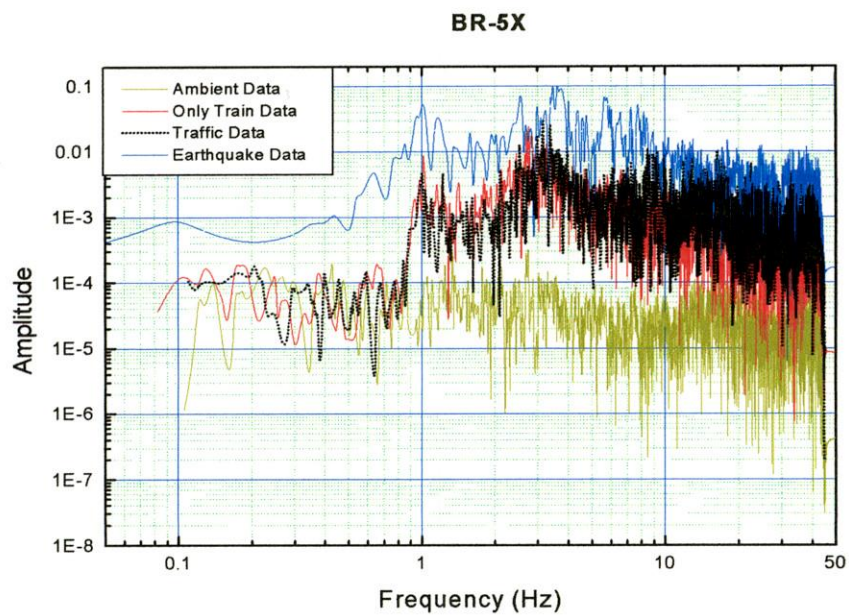


Fig. 7.7-d FFT of BR-5X

BR-7Z

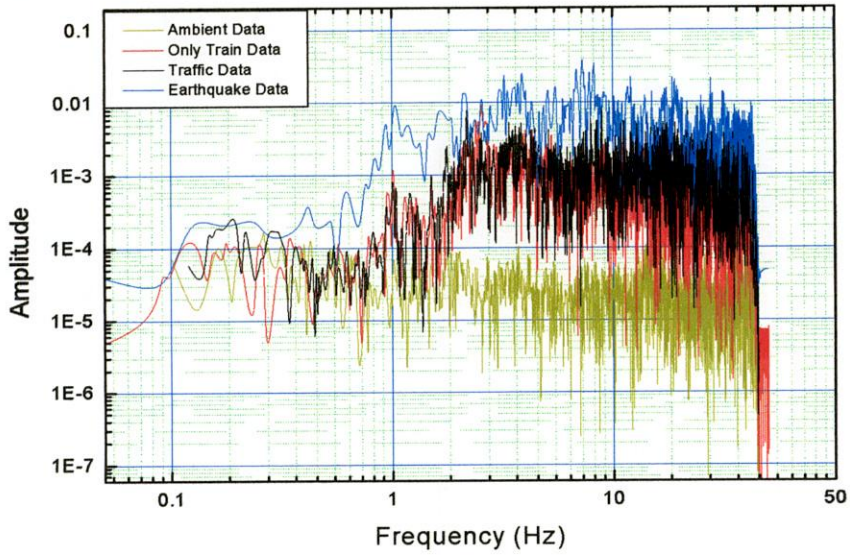


Fig. 7.7-e FFT of BR-7Z

BR-8Z

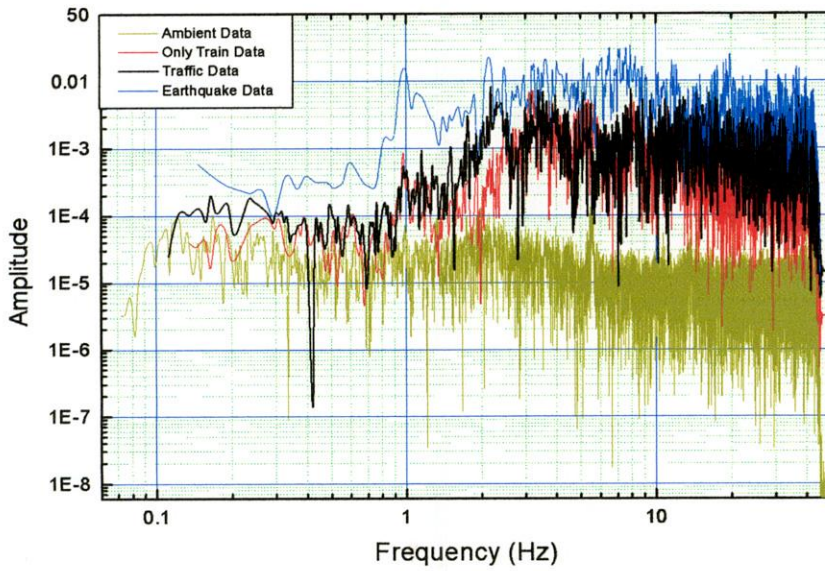


Fig. 7.7-f FFT of BR-8Z

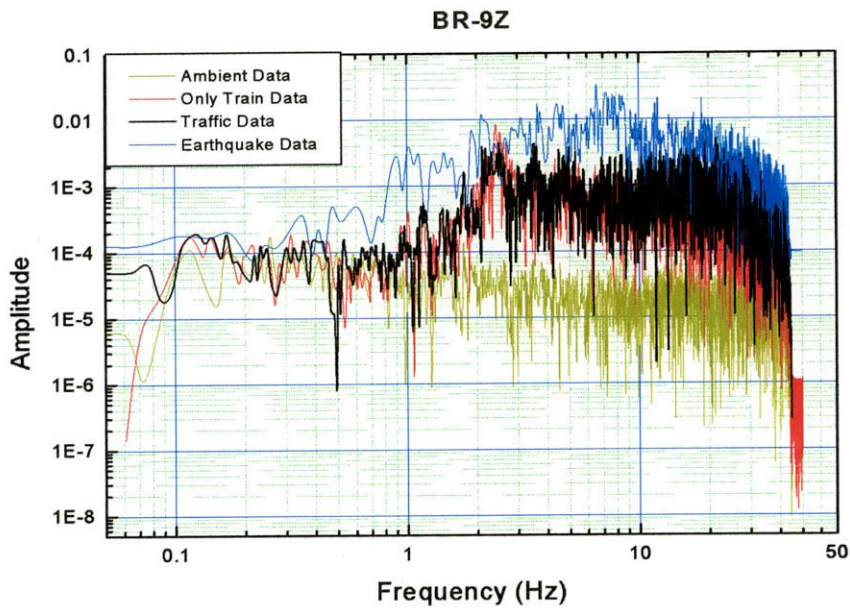


Fig. 7.7-g FFT of BR-9Z

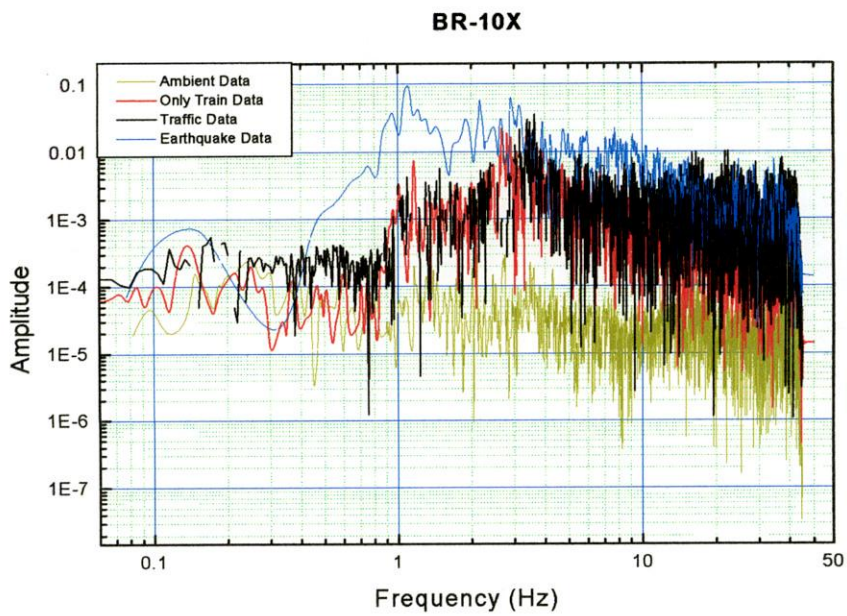


Fig. 7.7-h FFT of BR-10X

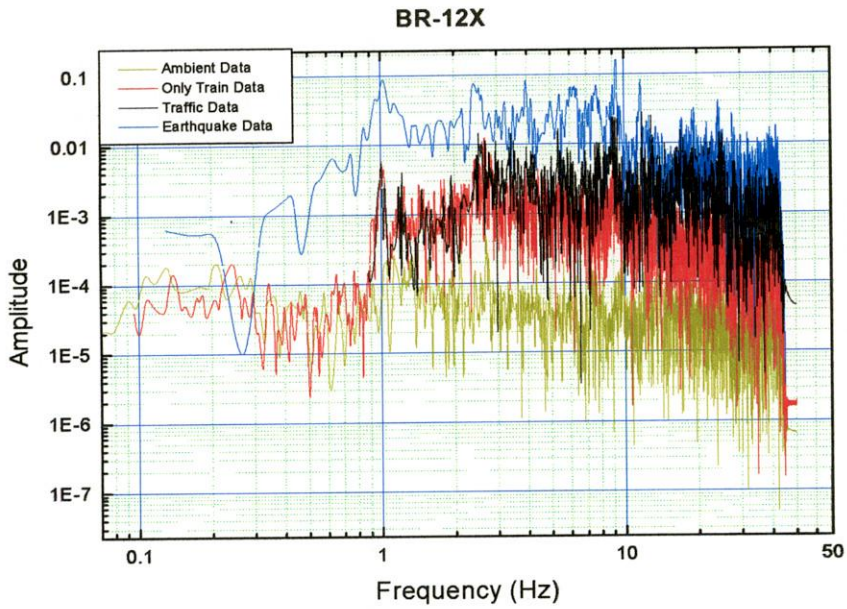


Fig. 7.7-i FFT of BR-12X

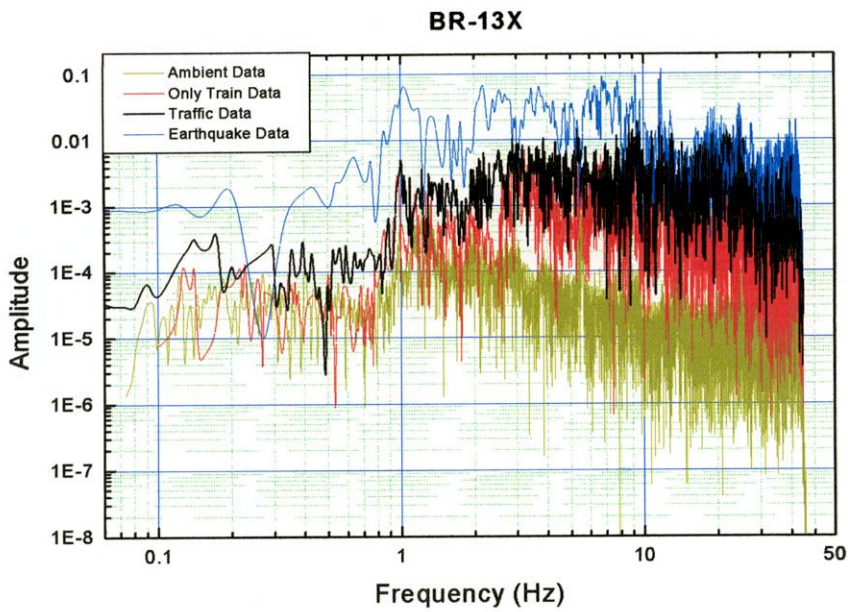


Fig. 7.7-j FFT of BR-13X

CHAPTER 8

CONCLUSIONS AND RECOMMENDATIONS

8.1 GENERAL

Behavior of bridges under the influence of seismic load has been a major point of interest for engineers over a long period of time. Jamuna Multipurpose Bridge is located in a seismically active region. The bridge has been instrumented in order to monitor the dynamic behavior. In the present study the earthquake data recorded by sensors are used to analyze the response of the bridge. For this purpose, firstly, a multi degrees of freedom system has been formulated to determine a Transfer Ratio function. The Transfer Ratio has been used to find out the predominant frequency of the Jamuna Bridge. Secondly, finite element models have also been developed considering all features of the bridge geometry and modal analyses of the generated models have also been carried out. Finally, the effects of dynamic response under various models are also observed in this study.

A summary of the whole research work is given below:

- A literature survey on system identification of the bridges has been performed.
- A multi degree of freedom system has been formulated and the transfer ratio of the system has been derived.
- The transfer ratio function was graphically represented using the first earthquake recorded at the west-end free-field station and BR-5X located at the deck at the top of the pier.
- The earthquake data of the west-end free-field station has been used as it gave maximum horizontal ground motion during the earthquake and displacement record of the BR-5X has been used as it recorded maximum displacement due to the earthquake.
- To study the seismic response of the bridge earthquake of different magnitudes have been applied to the TR function.
- A finite element model of Jamuna Multipurpose Bridge has been developed considering horizontal and vertical curvature of the bridge, parabolic variation in

the depth and width of the deck, almost actual geometry of the piers, support condition and also lateral prestressing.

- Eight more simplified finite element models have been developed to compare the results of modal analyses of these models.
- Finally a comparison of earthquake data, traffic data, train data and ambient data is made in this research work.

8.2 FINDINGS IN BRIEF

The findings of the study presented in the previous chapters are summarized below:

- ◆ A Transfer Ratio function has been established for Multi-degree of Freedom system (MDOF). From the TR function three peak values 0.0976Hz, 0.2441Hz and 1.0009Hz have been found. First two frequencies are very low due to effect of soil structure interaction. Each pier of the bridge is constructed with an average of 83 meter piles. So soil structure interaction is governed in this case.
- ◆ The TR function is also verified by Inverse Fast Fourier Transform (IFFT) of BR-5X data. The result of IFFT gives exact values of displacement at BR-5X.
- ◆ The Transfer Ratio has been used for the earthquakes of February 14 and August 5, 2006 recorded West End Free field station near the Jamuna Bridge. The TR function yields the maximum displacements of deck at pier 10 of 0.15855 cm and 0.01204 cm for the two earthquakes respectively. These displacement are lower than the trigger level set for starting the device to record earthquake data in bridge sensors. Thus no earthquake data was recorded by the sensors in the bridge
- ◆ The El Centro Earthquake, Imperial Valley, California, USA, 1940 was applied on the TR plot to study the response. The maximum acceleration of the earthquake is found to be 340.2 cm/sec^2 . Due to the application of this earthquake maximum displacement of the Jamuna Multipurpose Bridge is found to be 20.33 cm.
- ◆ The calculated values of the TR are applied to the data of the earthquake of Mexico City, Station I, September 19, 1995 to study the response of the Jamuna Multipurpose Bridge due to this earthquake. The maximum acceleration of the

applied earthquake is 167.92 cm/sec^2 . The maximum displacement due to earthquake of this magnitude is estimated to be 37.36 cm.

- ◆ From the results of the analysis it can be concluded that the TR function derived gives ample opportunity to study the response of the bridge. Performance evaluation of the bridge system will suggest necessary action to be taken to protect the bridge against earthquakes.
- ◆ A finite element model of the bridge is generated considering lateral prestressing, Pier system is considered as solid element and the hollow sections at top of the piers have also been taken into account., Internal diaphragm and Exterior rail girder is modeled with shell element. From the modal analysis of finite element model it can be concluded that the prestressing has no effect on the modal analyses.
- ◆ For simplicity Pier can be modeled with shell elements instead of solid elements which give similar results. The hollow section at the top of the pier may be ignored.
- ◆ To make the model simpler the exterior girder and bridge diaphragm can be modeled using frame elements as the effect of doing this is not so significant.
- ◆ To model any bridge especially like this type, one should be careful about modeling the restraint conditions at piers because it has a large effect on the analysis.
- ◆ From the modal analysis of the bridge it is found that the modal frequencies 0.735Hz, 0.846Hz, 1.0017Hz and 1.175Hz for mode 1, mode 2, mode 3, and mode 4 respectively.
- ◆ The modal frequency 1.0017Hz under mode 3 the first transverse mode almost mach with 1.00976Hz of FFT of BR-5X and 1.00098Hz of Transfer Ratio function.
- ◆ A detail comparative study of dynamic loads under various traffic conditions has been performed. From this study, it is shown that one of the common peak is found at 1.013Hz in transverse direction under various loading conditions which almost mach with the frequency obtained from the Finite element model (1.00174Hz) and the Transfer Ratio function(1.00098Hz).

8.3 FUTURE RECOMMENDATIONS

The present study is the preliminary investigation of Jamuna Bridge under dynamic loading .It is believed that due to the limitations of the study as is mentioned in section 1.2, the complete dynamic parameters of bridge could not be developed here. The present study may be regarded as a preliminary work for an extensive research work on dynamic parameters of the Jamuna Bridge. Therefore, some guidelines for future study on this topic may be recommended. The recommendations are:

- ◆ In the present study only transverse predominant mode was determined. The other modes of Bridge parameters may be evaluated.
- ◆ In future Time history and response spectrum analyses may be done.
- ◆ Nonlinear behavior of the structure should be considered for future study.
- ◆ Longitudinal prestressing has not been incorporated in this model it can be incorporated in a future study.
- ◆ In future study superimposed dead load and moving load for vehicle may be applied and static analysis can be done for staged construction for this with this model.
- ◆ Longitudinal and transverse vibrations have been treated separately in this study. Simultaneous application of horizontal motions in two directions may be studied.
- ◆ More detailed analysis of deck may be performed.
- ◆ The effect of soil structure interaction may be considered.
- ◆ Energy dissipating device was not considered in Transfer Ratio function. Energy dissipating device should be considered in further studies.

REFERENCES

- Ahsan, R., Al-Hussaini, T.M., Ansary, M.A and Rahman, M.M. (2005). Identification of dynamic parameters of the Jamuna Multipurpose Bridge in ambient transverse vibration. *Japan-Bangladesh Joint Seminar on Advances in Bridge Engg.*
- Ali, M.H. and Chaudhury, J.R. (1994). Assessment of Seismic Hazards in Bangladesh. *Proc. of workshop on implementation of global seismic hazard assessment program in Central and Southern Asia.* Beijing, China, 43-58.
- Bolt, B.A. (1987). Site Specific Seismicity Study of Seismic Intensity and Ground Motion Parameters for Proposed Jamuna Bridge, Bangladesh. Report prepared for seismic design of Jamuna bridge.
- Calvert, S. and Mooney, J. (2002). Bridge structural health monitoring system using fiber grating sensors: development and preparation for a permanent installation. Blue Road Research, Gresham, USA.
- Caravani, P., Watson, M.L. and Thomson, W.T. (1977). Recursive least-squares time domain identification of structural parameters. *J. Appl. Mech.* 44(3), 135-140.
- Carmichael, D.G. (1979). The state estimation problem in experimental structural mechanics. *Proc. 3rd Int. Conf. on Application of Statistics and Probability in Soil and Struct. Engrg.* Sydney, Australia, 802-815.
- Chang, C.C., Chang, T.Y.P. and Zhang, Q.W. (1999). Ambient vibration of long-span cable-stayed bridge. *J. Bridge Engrg.* 6 (1), 46-53.
- Chaudhary, M.T.A., Abe, M., Fujino, Y. and Yoshida, J. (1999). System identification of two base-isolated bridges using seismic records. *J. Struct. Engrg.* 126 (10), 1187-1195.
- Chaudhary, M.T.A., Abe, M., Fujino, Y. and Yoshida, J. (2002). Investigation of atypical seismic response of a base isolated bridge. *Engrg. Struct.* 24 (7), 945-953.

- Chen, J.H., and Lee, A.C. (1997). Identification of linearized dynamic characteristics of rolling element bearings. *J. Vibration and Acoustics*. 119, 60-69.
- Clough, R.W. and Penzien, J. (1975). *Dynamics of structures*. McGraw-Hill, London. 15-20.
- Cobb, R.G. and Liebst, B.S. (1997). Structural damage identification using assigned partial eigenstructure. *AIAA J.* 35 (1), 152-158.
- Highway Bridge Damage caused by the Hyogo-ken Nanbu Earthquake. (1996). Report on Highway Bridge Damage caused by the Hyogo-ken Nanbu Earthquake, Ministry of Construction, Tokyo, 1-140.
- Earthquake Engineering Research Institute (EERI). (1986). The Chile earthquake of March 3, 1985. *Earthquake Spectra* 2 (2), 1-513.
- Earthquake Engineering Research Institute (EERI). (1990). Loma Prieta earthquake reconnaissance report. *Earthquake Spectra* 6 (Suppl), 1-448.
- Earthquake Engineering Research Institute (EERI). (1995). Northridge earthquake reconnaissance report. *Earthquake Spectra* 11 (Suppl), 1-116.
- Feng, M.Q., Kim, D.K., Yi, J.H. and Chen, Y. (2002). Baseline models for bridge performance monitoring. *J. Engrg. Mech.* 130 (5), 562-569.
- FIP Industriale. (1996). Bearings and Seismic Devices for Jamuna Multipurpose Bridge, Test report on pin dissipating device, Padova, Italy.
- Ghanem, R. and Shinozuka, M. (1995). Structural system identification I: Theory. *J. Engrg. Mech.* 121 (2), 255-264.
- He, X., Moaveni, B., Conte, J.P., Masri, S. and Elgamal, A. (2004). System identification of Vincent Thomas Bridge using simulated wind response data. *Proc. of the Second International Conf. on Bridge Maintenance, Safety and Management (IABMAS'04)*, Kyoto, Japan.
- Herrmann, T. and Pradlwarter, H.J. (1998). Two-step identification approach for damped finite element models. *J. Engrg. Mech.* 124 (6), 639-647.

- Hoshiya, M., and Maruyama, O. (1987). Identification of non-linear structural systems. *Proc. ICAP 5*, 182-189.
- Hoshiya, M. and Satio, E. (1984). Structural identification by extended Kalman filter. *J. Engrg. Mech.* 110 (12), 1757-1770.
- Koh, C.G., Hong, B. and Liaw, C.Y. (1999). Parameter identification of large structural systems in time domain. *J. Struct. Engrg.* 126 (8), 957-963.
- Lus, H. (2000). Investigation of system identification methodology in the context of ASCE benchmark problem. *J. Engrg. Mech.* 130 (1), 71-84.
- Maeck, J., Peters, B. and Roeck, G.D. (2001). Damage identification on the Z24 Bridge using vibration monitoring. *Smart Mater. Struct.* 10 (3), 512-517.
- Nelson, L.C., Chui, J.M. and Maciejowski. (1998). Subspace Identification- A Markov Parameter Approach. *Technical report CUED/F-INFENG/TR. 337* submitted to IEEE Automatic Control.
- Paulter, P., Proulx, J. and Talbot, M. (1992). Dynamic testing procedure for highway bridges using traffic bridges using traffic loads. *J. Struct. Engrg.* 121 (2), 362-376.
- Peterson, S.T., McLean, D.I. and Pollock, D.G. (2003). Application of dynamic identification to timber bridges. *J. Struct. Engrg.* 129 (1), 116-124.
- Quek, S.T., Wang, W.P., and Koh, C.G. (1999). System identification on linear MDOF structures under ambient excitation. *Earthquake Engrg. and Struct. Dynamics* 28, 61-77.
- Sato, T. and Qi, K. (1998). Adaptive H -infinity filter: its application to structural identification. *J. Engrg. Mech.* 124 (11), 1233-1240.
- Schulz, W.L., Conte, J.P. and Seim, J.M. (2000). Static and dynamic testing of bridges and highways using long-gage fiber Bragg grating based strain sensors. Research report of Blue Road Research, Gresham and Department of Civil & Environmental Engineering, University of California, Los Angeles, USA.
- Shen, J., Tsai, M., Chang, K. and Lee, G.C. (2001). Performance of a seismically isolated bridge under near-fault earthquake ground motion. *J. Struct. Engrg.* 130 (6), 861-868.

- Shi, T., Jones, N.P. and Ellis, J.H. (2000). Simultaneous estimation of system and input parameters from output measurements. *J. Engrg. Mech.* 126 (7), 746-753.
- Shinozuka, M. and Ghanem, R. (1995). Structural-system identification II: Experimental verification. *J. Engrg. Mech.* 121 (2), 265-273.
- Street, R.L., Gua, M., Graves, R.C., Harison, J. and Gawry, M.J. (1994). Free and ambient vibration of Brent-Spence Bridge. *J. Struct. Engrg.* 123 (9), 1262-1268.
- Tang, R.Y. and Huang, M.C. (1999). System identification of a bridge with lead-rubber bearings. *Computers and Structures* 74(3), 267-280.
- Wang, D. and Haldar, A. (1994). Element-level system identification with unknown input. *J. Engrg. Mech.* 120 (1), 159-176.
- Wang, D. and Halder, A. (1995). System identification with limited observations and without input. *J. Engrg. Mech.* 123 (5), 504-511.
- Yun, C.B., Kim, W.J., and Ang, A.H.S. (1988). Damage assessment of bridge structures by system identification. *Proc. Korea-Japan Joint Seminar on Emerging Technol.* 2179-2186
- Yun, C.B., and Shinozuka, M. (1980). Identification of nonlinear structural dynamic system. *J. Struct. Mech.* 8 (2), 187-203.

APPENDIX

A mathematical representation of a multiple degree of freedom system is shown in Figure 1

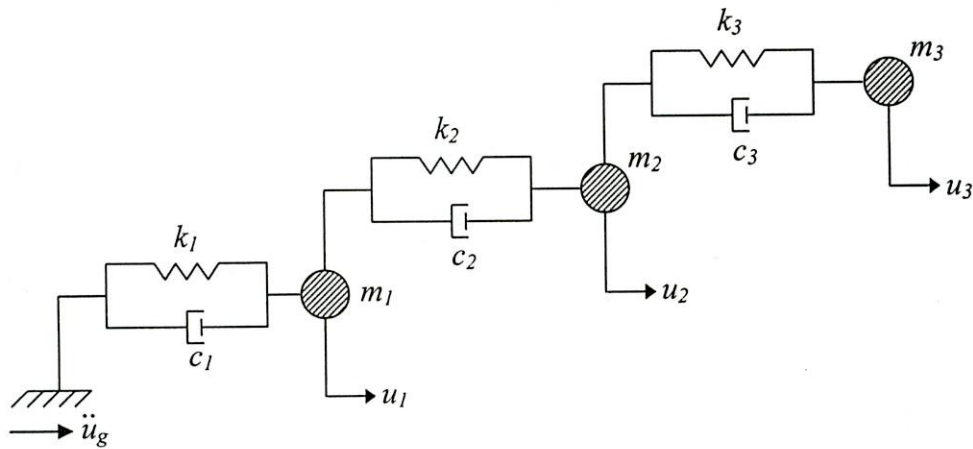


Fig.1 Ideal multiple degree of freedom system.

Where,

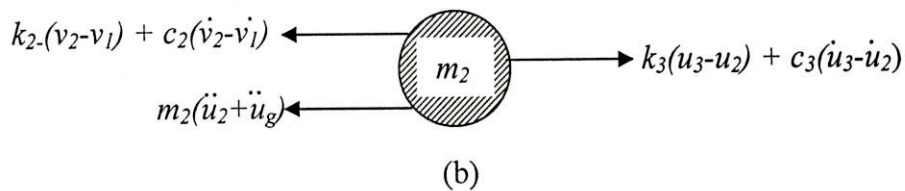
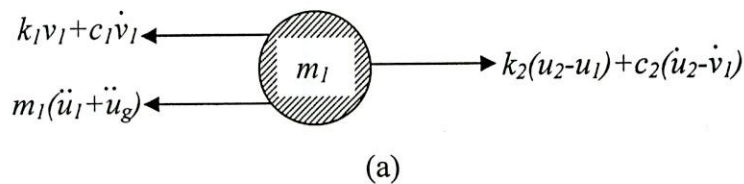
m_1, m_2 and m_3 = concentrated masses of the system

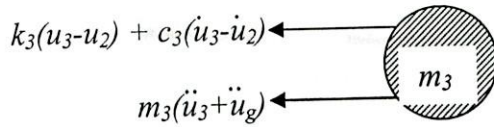
c_1, c_2 and c_3 = damper of the masses m_1, m_2 and m_3 respectively

k_1, k_2 and k_3 = stiffness of the masses m_1, m_2 and m_3 respectively

u_1, u_2 and u_3 = displacements of the masses m_1, m_2 and m_3 respectively

\ddot{u}_g = ground acceleration due to external source of excitation





(c)

Fig. 2 (a) Free body diagram of masses, (b) Free body diagram of mass m_2 ,

(c) Free body diagram of mass m_3 .

Considering equilibrium of mass m_1 (Fig. 1) the equation of motion is

$$m_1(\ddot{u}_1 + \ddot{u}_g) + k_1 u_1 + c_1 \dot{u}_1 - k_2(u_2 - u_1) - c_2(\dot{u}_2 - \dot{u}_1) = 0$$

$$\Rightarrow -\omega^2 m_1 \hat{u}_1 + m_1 \hat{u}_g + k_1 u_1 - i\omega c_1 \hat{u}_1 - k_2 \hat{u}_2 + k_2 \hat{u}_1 + i\omega c_2 \hat{u}_2 - i\omega c_2 \hat{u}_1 = 0$$

by Fourier Transformation

$$\Rightarrow \hat{u}_1 [-\omega^2 m_1 + (k_1 + k_2) - i\omega(c_1 + c_2)] + (i\omega c_2 - k_2) \hat{u}_2 + m_1 \hat{u}_g = 0 \dots\dots\dots (1)$$

Considering equilibrium of mass m_2 (Fig. 1) the equation of motion is

$$m_2(\ddot{u}_2 + \ddot{u}_g) + k_2(u_2 - u_1) + c_2(\dot{u}_2 - \dot{u}_1) - k_3(u_3 - u_2) - c_3(\dot{u}_3 - \dot{u}_2) = 0$$

$$\Rightarrow -\omega^2 m_2 \hat{u}_2 + m_2 \hat{u}_g + k_2 \hat{u}_2 - k_2 u_1 - i\omega c_2 \hat{u}_2 + i\omega c_1 \hat{u}_1 - k_3 \hat{u}_3 + k_3 \hat{u}_2 + i\omega c_3 \hat{u}_3 - i\omega c_3 \hat{u}_2 = 0$$

(by Fourier Transformation)

$$\Rightarrow \hat{u}_3 (i\omega c_3 - k_3) + \hat{u}_2 [-\omega^2 m_2 + (k_2 + k_3) - i\omega(c_2 + c_3)] \dots\dots\dots (2)$$

$$+ \hat{u}_1 (i\omega c_2 - k_2) + m_2 \hat{u}_g = 0$$

Considering equilibrium of mass m_3 (Fig. 2) the equation of motion is

$$m_3(\ddot{u}_3 + \ddot{u}_g) + k_3(u_3 - u_2) + c_3(\dot{u}_3 - \dot{u}_2) = 0$$

$$\Rightarrow -\omega^2 m_3 \hat{u}_3 + m_3 \hat{u}_g + k_3 \hat{u}_3 - k_3 \hat{u}_2 - i\omega c_3 \hat{u}_3 + i\omega c_3 \hat{u}_2 = 0 \quad \text{(by Fourier Transformation)}$$

$$\Rightarrow \hat{u}_3 (-\omega^2 m_3 + k_3 - i\omega c_3) + \hat{u}_2 (i\omega c_3 - k_3) + m_3 \hat{u}_g = 0$$

$$\Rightarrow \hat{u}_3 = \frac{-m_3 \hat{u}_g - \hat{u}_2 (i\omega c_3 - k_3)}{-\omega^2 m_3 + k_3 - i\omega c_3} \dots\dots\dots (3)$$

Where,

\hat{u}_1 = FFT of the displacement of mass m_1

\hat{u}_2 = FFT of the displacement of mass m_2

\hat{u}_3 = FFT of the displacement of mass m_3

ω = Angular frequency = $2\pi\nu$

ν = Oscillating frequency

\hat{u}_g = FFT of the ground acceleration

From Equations (2) & (3),

$$\frac{-m_3\hat{u}_g - \hat{u}_2(i\omega c_3 - k_3)}{-\omega^2 m_3 + k_3 - i\omega c_3} \times (i\omega c_3 - k_3) + \hat{u}_2[-\omega^2 m_2 + (k_2 + k_3) - i\omega(c_2 + c_3)] + \hat{u}_1(i\omega c_2 - k_2) + m_2\hat{u}_g = 0$$

$$\Rightarrow [-m_3\hat{u}_g - \hat{u}_2(i\omega c_3 - k_3)] \times (i\omega c_3 - k_3) + \hat{u}_2[-\omega^2 m_2 + (k_2 + k_3) - i\omega(c_2 + c_3)] \times (-\omega^2 m_3 + k_3 - i\omega c_3)$$

$$+ \hat{u}_1(i\omega c_2 - k_2) \times (-\omega^2 m_3 + k_3 - i\omega c_3) + m_2\hat{u}_g \times (-\omega^2 m_3 + k_3 - i\omega c_3) = 0$$

$$\Rightarrow (-m_3\hat{u}_g - \hat{u}_2 i\omega c_3 + \hat{u}_2 k_3) \times (i\omega c_3 - k_3) + \hat{u}_2(-\omega^2 m_2 + k_2 + k_3 - i\omega c_2 - i\omega c_3) \times (-\omega^2 m_3 + k_3 - i\omega c_3)$$

$$+ \hat{u}_1(i\omega c_2 - k_2) \times (-\omega^2 m_3 + k_3 - i\omega c_3) + \hat{u}_g(-\omega^2 m_2 m_3 + k_3 m_2 - i\omega m_2 c_3) = 0$$

$$\Rightarrow i\omega c_3(-m_3\hat{u}_g - \hat{u}_2 i\omega c_3 + \hat{u}_2 k_3) - k_3(-m_3\hat{u}_g - \hat{u}_2 i\omega c_3 + \hat{u}_2 k_3)$$

$$\hat{u}_2 \left[\begin{array}{l} -\omega^2 m_3(-\omega^2 m_2 + k_2 + k_3 - i\omega c_2 - i\omega c_3) + k_3(-\omega^2 m_2 + k_2 + k_3 - i\omega c_2 - i\omega c_3) \\ -i\omega c_3(-\omega^2 m_2 + k_2 + k_3 - i\omega c_2 - i\omega c_3) \end{array} \right]$$

$$+ \hat{u}_1 [i\omega c_2(-\omega^2 m_3 + k_3 - i\omega c_3) - k_2(-\omega^2 m_3 + k_3 - i\omega c_3)]$$

$$+ \hat{u}_g(-\omega^2 m_2 m_3 + k_3 m_2 - i\omega m_2 c_3) = 0$$

$$\Rightarrow -i\omega c_3 m_3 \hat{u}_g + \hat{u}_2 \omega^2 c^2_3 + \hat{u}_2 i\omega c_3 k_3 + \hat{u}_g m_3 k_3 + \hat{u}_2 i\omega c_3 k_3 - \hat{u}_2 k^2_3$$

$$+ \hat{u}_2 \left[\begin{array}{l} \omega^4 m_2 m_3 - k_2 \omega^2 m_3 - k_3 \omega^2 m_3 + i\omega^3 c_2 m_3 + i\omega^3 c_3 m_3 - k_3 \omega^2 m_2 + k_2 k_3 \\ + k^2_3 - i\omega c_2 k_3 - i\omega c_3 k_3 + i\omega^3 m_2 c_3 - i\omega c_3 k_2 - i\omega c_3 k_3 - \omega^2 c_2 c_3 - \omega^2 c^2_3 \end{array} \right]$$

$$+ \hat{u}_1 [-i c_2 \omega^3 m_3 + i\omega c_2 k_3 + \omega^2 c_2 c_3 + k_2 \omega^2 m_3 - k_2 k_3 + i\omega k_2 c_3]$$

$$\begin{aligned}
& +\hat{u}_g \left(-\omega^2 m_2 m_3 + k_3 m_2 - i\omega m_2 c_3 \right) = 0 \\
\Rightarrow & \hat{u}_1 \left[-ic_2 \omega^3 m_3 + i\omega c_2 k_3 + \omega^2 (c_2 c_3 + k_2 m_3) + i\omega (c_2 k_3 + k_2 c_3) - k_2 k_3 \right] \\
& +\hat{u}_2 \left[\omega^4 m_2 m_3 + \omega^2 (c_3^2 - k_2 m_3 - k_3 m_3 - k_3 m_2 - c_2 c_3 - c_3^2) \right. \\
& \left. + i\omega (2c_3 k_3 - c_2 k_3 - c_3 k_3 - c_3 k_2 - c_3 k_3) + i\omega^3 (c_2 m_3 + c_3 m_3 + m_2 c_3) + (-k_3^2 + k_2 k_3 + k_3^2) \right] \\
& +\hat{u}_g \left(-i\omega c_3 m_3 + m_3 k_3 - \omega^2 m_2 m_3 + k_3 m_2 - i\omega m_2 c_3 \right) = 0 \\
\Rightarrow & \hat{u}_1 \left[-ic_2 \omega^3 m_3 + \omega^2 (c_2 c_3 + k_2 m_3) + i\omega (c_2 k_3 + k_2 c_3) - k_2 k_3 \right] + \\
& \hat{u}_2 \left[\omega^4 m_2 m_3 + \omega^2 (-k_2 m_3 - k_3 m_3 - k_3 m_2 - c_2 c_3) + i\omega (-c_2 k_3 - c_3 k_2) \right. \\
& \left. + i\omega^3 (c_2 m_3 + c_3 m_3 + m_2 c_3) + k_2 k_3 \right] \\
& +\hat{u}_g \left(-i\omega c_3 m_3 + m_3 k_3 - \omega^2 m_2 m_3 + k_3 m_2 - i\omega m_2 c_3 \right) = 0 \dots\dots\dots(4)
\end{aligned}$$

From Equations (1) & (4),

$$\begin{aligned}
& \frac{\hat{u}_1}{m_1 \left[\omega^4 m_2 m_3 + \omega^2 (-k_2 m_3 - k_3 m_3 - k_3 m_2 - c_2 c_3) + i\omega (-c_2 k_3 - c_3 k_2) \right.} \\
& \left. + i\omega^3 (c_2 m_3 + c_3 m_3 + m_2 c_3) + k_2 k_3 \right]}{- \left[i\omega c_2 (-i\omega c_3 m_3 + m_3 k_3 - \omega^2 m_2 m_3 + k_3 m_2 - i\omega m_2 c_3) - \right.} \\
& \left. k_2 (-i\omega c_3 m_3 + m_3 k_3 - \omega^2 m_2 m_3 + k_3 m_2 - i\omega m_2 c_3) \right]} \\
& = \frac{\hat{u}_2}{(-i\omega c_3 m_3 + m_3 k_3 - \omega^2 m_2 m_3 + k_3 m_2 - i\omega m_2 c_3) \times (-\omega^2 m_1 + k_1 + k_2 - i\omega c_1 - i\omega c_2)} \\
& - m_1 \left[-ic_2 \omega^3 m_3 + i\omega c_2 k_3 + \omega^2 (c_2 c_3 + k_2 m_3) + i\omega (c_2 k_3 + k_2 c_3) - k_2 k_3 \right] \\
& = \frac{\hat{u}_g}{(i\omega c_2 - k_2) \times \left[-ic_2 \omega^3 m_3 + i\omega c_2 k_3 + \omega^2 (c_2 c_3 + k_2 m_3) + i\omega (c_2 k_3 + k_2 c_3) - k_2 k_3 \right]} \\
& - (-\omega^2 m_1 + k_1 + k_2 - i\omega c_1 - i\omega c_2) \times \left[\omega^4 m_2 m_3 + \omega^2 (-k_2 m_3 - k_3 m_3 - k_3 m_2 - c_2 c_3) \right. \\
& \left. + i\omega (-c_2 k_3 - c_3 k_2) + i\omega^3 (c_2 m_3 + c_3 m_3 + m_2 c_3) + k_2 k_3 \right]
\end{aligned}$$

Now,

$$\begin{aligned}
 & \frac{\hat{u}_1}{\left[\begin{array}{l} \omega^4 m_1 m_2 m_3 + \omega^2 (-k_2 m_1 m_3 - k_3 m_1 m_2 - m_1 c_2 c_3) \\ + i\omega (-m_1 c_2 k_3 - m_1 c_3 k_2) + i\omega^3 (c_2 m_1 m_3 + c_3 m_1 m_2 + m_1 m_2 c_3) + m_1 k_2 k_3 \\ - \left[\begin{array}{l} \omega^2 c_2 c_3 m_3 + i\omega c_2 m_3 k_3 - i\omega^3 c_2 m_2 m_3 + i\omega c_2 k_3 m_2 + \omega^2 c_2 m_2 c_3 + i\omega c_3 m_3 k_2 \\ - m_3 k_2 k_3 + \omega^2 m_2 m_3 k_2 - k_2 k_3 m_2 + i\omega m_2 c_3 k_2 \end{array} \right] \end{array} \right]} \\
 &= \frac{\hat{u}_1}{\omega^4 m_1 m_2 m_3 + i\omega^3 (c_2 m_1 m_3 + c_3 m_1 m_2 + m_1 m_2 c_3 + c_2 m_2 m_3) \\
 & \quad + \omega^2 (-k_2 m_1 m_3 - k_3 m_1 m_2 - m_1 c_2 c_3 - c_2 c_3 m_3 - c_2 m_2 c_3 - m_2 m_3 k_2) \\
 & \quad + i\omega (-m_1 c_2 k_3 - m_1 c_3 k_2 - c_2 m_3 k_3 - c_2 k_3 m_2 - c_3 m_3 k_2 - m_2 c_3 k_2) \\
 & \quad + m_1 k_2 k_3 + m_3 k_2 k_3 + k_2 k_3 m_2} \\
 &= \frac{\hat{u}_1}{\omega^4 m_1 m_2 m_3 + i\omega^3 [c_2 (m_1 m_3 + m_2 m_3) + c_3 (m_1 m_3 + m_1 m_2)] \\
 & \quad + \omega^2 [-k_2 (m_1 m_3 + m_2 m_3) - k_3 (m_1 m_3 + m_1 m_2) - c_2 c_3 (m_1 + m_2 + m_3)] \\
 & \quad + i\omega [-m_1 (c_2 k_3 + c_3 k_2) - m_2 (c_2 k_3 + c_3 k_2) - m_3 (c_2 k_3 + c_3 k_2)] \\
 & \quad + k_2 k_3 (m_1 + m_3 + m_2)} \\
 &= \frac{\hat{u}_1}{\omega^4 + i\omega^3 \left[c_2 \left(\frac{1}{m_2} + \frac{1}{m_1} \right) + c_3 \left(\frac{1}{m_3} + \frac{1}{m_2} \right) \right] \\
 & \quad + \omega^2 \left[-k_2 \left(\frac{1}{m_2} + \frac{1}{m_1} \right) - k_3 \left(\frac{1}{m_2} + \frac{1}{m_3} \right) - c_2 c_3 \left(\frac{m_1 + m_2 + m_3}{m_1 m_2 m_3} \right) \right] \\
 & \quad + i\omega \left[-(c_2 k_3 + c_3 k_2) \frac{(m_1 + m_2 + m_3)}{m_1 m_2 m_3} \right] + k_2 k_3 \frac{(m_1 + m_2 + m_3)}{m_1 m_2 m_3}} \\
 &= \frac{\hat{u}_1}{\omega^4 + i\omega^3 A + \omega^2 B + i\omega C + D} \dots\dots\dots(5)
 \end{aligned}$$

Where,

$$A = \left[c_2 \left(\frac{1}{m_2} + \frac{1}{m_1} \right) + c_3 \left(\frac{1}{m_3} + \frac{1}{m_2} \right) \right] + \omega^2 \left[-k_2 \left(\frac{1}{m_2} + \frac{1}{m_1} \right) - k_3 \left(\frac{1}{m_2} + \frac{1}{m_3} \right) - c_2 c_3 \left(\frac{m_1 + m_2 + m_3}{m_1 m_2 m_3} \right) \right]$$

$$B = \left[-k_2 \left(\frac{1}{m_2} + \frac{1}{m_1} \right) - k_3 \left(\frac{1}{m_2} + \frac{1}{m_3} \right) - c_2 c_3 \left(\frac{m_1 + m_2 + m_3}{m_1 m_2 m_3} \right) \right]$$

$$C = \left[-(c_2 k_3 + c_3 k_2) \frac{(m_1 + m_2 + m_3)}{m_1 m_2 m_3} \right]$$

$$D = k_2 k_3 \frac{(m_1 + m_2 + m_3)}{m_1 m_2 m_3}$$

Again,

$$\frac{\hat{u}_2}{\left[\begin{array}{l} -\omega^2 m_1 (-i\omega c_3 m_3 + m_3 k_3 - \omega^2 m_2 m_3 + k_3 m_2 - i\omega m_2 c_3) \\ +k_1 (-i\omega c_3 m_3 + m_3 k_3 - \omega^2 m_2 m_3 + k_3 m_2 - i\omega m_2 c_3) \\ +k_2 (-i\omega c_3 m_3 + m_3 k_3 - \omega^2 m_2 m_3 + k_3 m_2 - i\omega m_2 c_3) \\ -i\omega c_1 (-i\omega c_3 m_3 + m_3 k_3 - \omega^2 m_2 m_3 + k_3 m_2 - i\omega m_2 c_3) \\ -i\omega c_2 (-i\omega c_3 m_3 + m_3 k_3 - \omega^2 m_2 m_3 + k_3 m_2 - i\omega m_2 c_3) \end{array} \right]}$$

$$- \left[-i\omega^3 c_2 m_1 m_3 + \omega^2 (m_1 c_2 c_3 + k_2 m_1 m_3) + i\omega m_1 (c_2 k_3 + k_2 c_3) - m_1 k_2 k_3 \right]$$

$$= \frac{\hat{u}_2}{\begin{array}{l} i\omega^3 c_3 m_1 m_3 - \omega^2 m_1 m_3 k_3 + \omega^4 m_1 m_2 m_3 - \omega^2 m_1 m_2 k_3 + i\omega^3 m_1 m_2 c_3 - i\omega c_3 m_3 k_1 \\ + m_3 k_1 k_3 - \omega^2 m_2 m_3 k_1 + k_1 k_3 m_2 - i\omega m_2 c_3 k_1 - i\omega c_3 m_3 k_2 + m_3 k_2 k_3 - \omega^2 m_2 m_3 k_2 \\ + k_2 k_3 m_2 - i\omega m_2 c_3 k_2 - \omega^2 c_1 c_3 m_3 - i\omega c_1 m_3 k_3 + i\omega^3 c_1 m_2 m_3 - i\omega c_1 k_3 m_2 \\ - \omega^2 c_1 m_2 c_3 - \omega^2 c_2 c_3 m_3 - i\omega c_2 m_3 k_3 + i\omega^3 c_2 m_2 m_3 - i\omega c_2 k_3 m_2 - \omega^2 c_2 m_2 c_3 \\ + i\omega^3 c_2 m_1 m_3 - \omega^2 m_1 c_2 c_3 - \omega^2 k_2 m_1 m_3 - i\omega m_1 c_2 k_3 - i\omega m_1 k_2 c_3 + m_1 k_2 k_3 \end{array}}$$

$$= \frac{\hat{u}_2}{\begin{array}{l} \omega^4 m_1 m_2 m_3 + i\omega^3 (c_3 m_1 m_3 + m_1 m_2 c_3 + c_1 m_2 m_3 + c_2 m_2 m_3 + c_2 m_1 m_3) \\ + \omega^2 \left(\begin{array}{l} -m_1 m_3 k_3 - m_1 m_2 k_3 - m_2 m_3 k_1 - m_2 m_3 k_2 - c_1 c_3 m_3 \\ -c_1 m_2 c_3 - c_2 c_3 m_3 - c_2 m_2 c_3 - m_1 c_2 c_3 - k_2 m_1 m_3 \end{array} \right) \\ + i\omega \left(\begin{array}{l} -c_3 m_3 k_1 - m_2 c_3 k_1 - c_3 m_3 k_2 - m_2 c_3 k_2 - c_1 m_3 k_3 \\ -c_1 k_3 m_2 - c_2 m_3 k_3 - c_2 k_3 m_2 - m_1 c_2 k_3 - m_1 k_2 c_3 \end{array} \right) \\ + m_3 k_1 k_3 + k_1 k_3 m_2 + m_3 k_2 k_3 + k_2 k_3 m_2 + m_1 k_2 k_3 \end{array}}$$

$$\begin{aligned}
&= \frac{\hat{u}_2}{\omega^4 m_1 m_2 m_3 + i\omega^3 [c_3 (m_1 m_3 + m_1 m_2) + m_2 m_3 (c_1 + c_2) + c_2 m_1 m_3]} \\
&\quad + \omega^2 \left[k_3 (-m_1 m_3 - m_1 m_2) - m_2 m_3 (k_1 + k_2) - m_3 (c_1 c_3 + c_2 c_3) \right. \\
&\quad \left. - m_2 (c_1 c_3 + c_2 c_3) - m_1 c_2 c_3 - c_1 c_3 m_1 + c_1 c_3 m_1 - k_2 m_1 m_3 \right] \\
&\quad + i\omega \left[-c_3 m_3 (k_1 + k_2) - m_2 c_3 (k_1 + k_2) - m_3 (c_1 k_3 + c_2 k_3) \right. \\
&\quad \left. - m_2 (c_1 k_3 + c_2 k_3) - m_1 (c_2 k_3 + k_2 c_3) + m_1 c_1 k_3 - m_1 k_2 c_3 \right] \\
&\quad + k_1 k_3 (m_3 + m_2) + k_2 k_3 (m_3 + m_2 + m_1) \\
&= \frac{\hat{u}_2}{\omega^4 m_1 m_2 m_3 + i\omega^3 [c_3 (m_1 m_3 + m_1 m_2) + m_2 m_3 (c_1 + c_2) + c_2 m_1 m_3]} \\
&\quad + \omega^2 \left[-k_3 (m_1 m_3 + m_1 m_2) - m_2 m_3 (k_1 + k_2) - m_3 (c_1 c_3 + c_2 c_3) \right. \\
&\quad \left. - m_2 (c_1 c_3 + c_2 c_3) - m_1 (c_2 c_3 + c_1 c_3) + m_1 (c_1 c_3 - k_2 m_3) \right] \\
&\quad + i\omega \left[-c_3 m_3 (k_1 + k_2) - m_2 c_3 (k_1 + k_2) - m_3 (c_1 k_3 + c_2 k_3) - m_2 (c_1 k_3 + c_2 k_3) \right. \\
&\quad \left. - m_1 (c_1 k_3 + k_3 c_2) - m_1 c_3 (k_1 + k_2) + m_1 (c_1 k_3 + k_1 c_3) \right] \\
&\quad + k_1 k_3 (m_3 + m_2) + k_2 k_3 (m_3 + m_2 + m_1) \\
&= \frac{\hat{u}_2}{\omega^4 m_1 m_2 m_3 + i\omega^3 [c_3 (m_1 m_3 + m_1 m_2) + m_2 m_3 (c_1 + c_2) + c_2 m_1 m_3]} \\
&\quad + \omega^2 \left[-k_3 (m_1 m_3 + m_1 m_2) - m_2 m_3 (k_1 + k_2) - (c_1 c_3 + c_2 c_3) (m_1 + m_2 + m_3) + m_1 (c_1 c_3 - k_2 m_3) \right] \\
&\quad + i\omega \left[-c_3 (m_3 + m_2 + m_1) (k_1 + k_2) - (c_1 k_3 + c_2 k_3) (m_1 + m_2 + m_3) + m_1 (c_1 k_3 + k_1 c_3) \right] \\
&\quad + k_1 k_3 (m_3 + m_2) + k_2 k_3 (m_3 + m_2 + m_1) \\
&= \frac{\hat{u}_2}{\omega^4 + i\omega^3 \left[c_3 \left(\frac{1}{m_2} + \frac{1}{m_3} \right) + \frac{1}{m_1} (c_1 + c_2) + c_2 \frac{1}{m_2} \right]} \\
&\quad + \omega^2 \left[-k_3 \left(\frac{1}{m_2} + \frac{1}{m_3} \right) - \frac{1}{m_1} (k_1 + k_2) - (c_1 c_3 + c_2 c_3) \frac{(m_1 + m_2 + m_3)}{m_1 m_2 m_3} + \frac{1}{m_2 m_3} (c_1 c_3 - k_2 m_3) \right] \\
&\quad + i\omega \left[-c_3 \frac{(m_3 + m_2 + m_1)}{m_1 m_2 m_3} (k_1 + k_2) - (c_1 k_3 + c_2 k_3) \frac{(m_1 + m_2 + m_3)}{m_1 m_2 m_3} + \frac{1}{m_2 m_3} (c_1 k_3 + k_1 c_3) \right] \\
&\quad + k_1 k_3 \frac{(m_3 + m_2)}{m_1 m_2 m_3} + k_2 k_3 \frac{(m_3 + m_2 + m_1)}{m_1 m_2 m_3} \\
&= \frac{\hat{u}_2}{\omega^4 + i\omega^3 P + \omega^2 Q + i\omega R + S} \dots\dots\dots (6)
\end{aligned}$$

Where,

$$P = \left[c_3 \left(\frac{1}{m_2} + \frac{1}{m_3} \right) + \frac{1}{m_1} (c_1 + c_2) + c_2 \frac{1}{m_2} \right]$$

$$Q = \left[-k_3 \left(\frac{1}{m_2} + \frac{1}{m_3} \right) - \frac{1}{m_1} (k_1 + k_2) - (c_1 c_3 + c_2 c_3) \frac{(m_1 + m_2 + m_3)}{m_1 m_2 m_3} + \frac{1}{m_2 m_3} (c_1 c_3 - k_2 m_3) \right]$$

$$R = \left[-c_3 \frac{(m_3 + m_2 + m_1)}{m_1 m_2 m_3} (k_1 + k_2) - (c_1 k_3 + c_2 k_3) \frac{(m_1 + m_2 + m_3)}{m_1 m_2 m_3} + \frac{1}{m_2 m_3} (c_1 k_3 + k_1 c_3) \right]$$

$$S = k_1 k_3 \frac{(m_3 + m_2)}{m_1 m_2 m_3} + k_2 k_3 \frac{(m_3 + m_2 + m_1)}{m_1 m_2 m_3}$$

Again,

$$\frac{\hat{u}_g}{(i\omega c_2 - k_2) \times \left[-ic_2 \omega^3 m_3 + i\omega c_2 k_3 + \omega^2 (c_2 c_3 + k_2 m_3) + i\omega (c_2 k_3 + k_2 c_3) - k_2 k_3 \right]} - \left(-\omega^2 m_1 + k_1 + k_2 - i\omega c_1 - i\omega c_2 \right) \times \left[\begin{array}{l} \omega^4 m_2 m_3 + \omega^2 (-k_2 m_3 - k_3 m_3 - k_3 m_2 - c_2 c_3) \\ + i\omega (-c_2 k_3 - c_3 k_2) + i\omega^3 (c_2 m_3 + c_3 m_3 + m_2 c_3) + k_2 k_3 \end{array} \right]$$

$$= \frac{\hat{u}_g}{i\omega c_2 \left[-ic_2 \omega^3 m_3 + \omega^2 c_2 c_3 + \omega^2 k_2 m_3 + i\omega c_2 k_3 + i\omega k_2 c_3 - k_2 k_3 \right]} - k_2 \left[-ic_2 \omega^3 m_3 + \omega^2 c_2 c_3 + \omega^2 k_2 m_3 + i\omega c_2 k_3 + i\omega k_2 c_3 - k_2 k_3 \right] - \left(-\omega^2 m_1 \right) \left[\begin{array}{l} \omega^4 m_2 m_3 - \omega^2 k_2 m_3 - \omega^2 k_3 m_3 - \omega^2 k_3 m_2 - \omega^2 c_2 c_3 \\ -i\omega c_2 k_3 - i\omega c_3 k_2 + i\omega^3 c_2 m_3 + i\omega^3 c_3 m_3 + i\omega^3 m_2 c_3 + k_2 k_3 \end{array} \right] + k_1 \left[\begin{array}{l} \omega^4 m_2 m_3 - \omega^2 k_2 m_3 - \omega^2 k_3 m_3 - \omega^2 k_3 m_2 - \omega^2 c_2 c_3 - i\omega c_2 k_3 \\ -i\omega c_3 k_2 + i\omega^3 c_2 m_3 + i\omega^3 c_3 m_3 + i\omega^3 m_2 c_3 + k_2 k_3 \end{array} \right] + k_2 \left[\begin{array}{l} \omega^4 m_2 m_3 - \omega^2 k_2 m_3 - \omega^2 k_3 m_3 - \omega^2 k_3 m_2 - \omega^2 c_2 c_3 - i\omega c_2 k_3 \\ -i\omega c_3 k_2 + i\omega^3 c_2 m_3 + i\omega^3 c_3 m_3 + i\omega^3 m_2 c_3 + k_2 k_3 \end{array} \right] - i\omega c_1 \left[\begin{array}{l} \omega^4 m_2 m_3 - \omega^2 k_2 m_3 - \omega^2 k_3 m_3 - \omega^2 k_3 m_2 - \omega^2 c_2 c_3 - i\omega c_2 k_3 \\ -i\omega c_3 k_2 + i\omega^3 c_2 m_3 + i\omega^3 c_3 m_3 + i\omega^3 m_2 c_3 + k_2 k_3 \end{array} \right] - i\omega c_2 \left[\begin{array}{l} \omega^4 m_2 m_3 - \omega^2 k_2 m_3 - \omega^2 k_3 m_3 - \omega^2 k_3 m_2 - \omega^2 c_2 c_3 - i\omega c_2 k_3 \\ -i\omega c_3 k_2 + i\omega^3 c_2 m_3 + i\omega^3 c_3 m_3 + i\omega^3 m_2 c_3 + k_2 k_3 \end{array} \right]$$

\hat{u}_g

$$\begin{aligned}
& \frac{c_2^2 \omega^4 m_3 + i \omega^3 c_2^2 c_3 + i c_2 \omega^3 k_2 m_3 - \omega^2 c_2^2 k_3 - \omega^2 c_2 k_2 c_3 - i \omega c_2 k_2 k_3 + i c_2 \omega^3 m_3 k_2}{=} \\
& - \omega^2 c_2 c_3 k_2 - \omega^2 k_2^2 m_3 - i \omega c_2 k_2 k_3 - i \omega k_2^2 c_3 + k_2^2 k_3 - \\
& \left[\begin{aligned}
& - \omega^6 m_1 m_2 m_3 + \omega^4 k_2 m_1 m_3 + \omega^4 k_3 m_1 m_2 + \omega^4 k_3 m_1 m_2 + \omega^4 m_1 c_2 c_3 + i \omega^3 m_1 c_2 k_3 \\
& + i \omega^3 m_1 c_3 k_2 - i \omega^5 m_1 c_2 m_3 - i \omega^5 c_3 m_1 m_3 - i \omega^5 m_1 m_2 c_3 - \omega^2 m_1 k_2 k_3 + \omega^4 m_2 m_3 k_1 \\
& - \omega^2 k_2 m_3 k_1 - \omega^2 k_3 m_3 k_1 - \omega^2 k_3 m_2 k_1 - \omega^2 c_2 c_3 k_1 - i \omega c_2 k_3 k_1 - i \omega c_3 k_1 k_2 \\
& + i \omega^3 c_2 m_3 k_1 + i \omega^3 c_3 m_3 k_1 + i \omega^3 m_2 c_3 k_1 + k_1 k_2 k_3 + \omega^4 m_2 m_3 k_2 - \omega^2 k^2 m_3 \\
& - \omega^2 k_2 k_3 m_3 - \omega^2 k_2 k_3 m_2 - \omega^2 c_2 c_3 k_2 - i \omega c_2 k_2 k_3 - i \omega c_3 k_2^2 + i \omega^3 c_2 m_3 k_2 \\
& + i \omega^3 c_3 m_3 k_2 + i \omega^3 m_2 c_3 k_2 + k_2^2 k_3 - i \omega^5 c_1 m_2 m_3 + i \omega^3 c_1 k_2 m_3 + i \omega^3 c_1 k_3 m_3 \\
& + i \omega^3 c_1 k_3 m_2 + i \omega^3 c_1 c_2 c_3 - \omega^2 c_1 c_2 k_3 - \omega^2 c_1 c_3 k_2 + \omega^4 c_1 c_2 m_3 + \omega^4 c_1 c_3 m_3 \\
& + \omega^4 c_1 m_2 c_3 - i \omega c_1 k_2 k_3 - i \omega^5 c_2 m_2 m_3 + i \omega^3 c_2 k_2 m_3 + i \omega^3 c_2 k_3 m_3 + i \omega^3 c_2 k_3 m_2 \\
& + i \omega^3 c_2^2 c_3 - \omega^2 c_2^2 k_3 - \omega^2 c_2 c_3 k_2 + \omega^4 c_2^2 m_3 + \omega^4 c_2 c_3 m_3 + \omega^4 m_2 c_2 c_3 - i \omega c_2 k_2 k_3
\end{aligned} \right]
\end{aligned}$$

 \hat{u}_g

$$\begin{aligned}
& \frac{\omega^4 c_2^2 m_3 + i \omega^3 c_2^2 c_3 + i \omega^3 c_2 k_2 m_3 - \omega^2 c_2^2 k_3 - \omega^2 c_2 k_2 c_3 - i \omega c_2 k_2 k_3 + i \omega^3 c_2 m_3 k_2}{=} \\
& - \omega^2 c_2 c_3 k_2 - \omega^2 k_2^2 m_3 - i \omega c_2 k_2 k_3 - i \omega k_2^2 c_3 + k_2^2 k_3 + \omega^6 m_1 m_2 m_3 - \omega^4 k_2 m_1 m_3 \\
& - \omega^4 k_3 m_1 m_2 - \omega^4 k_3 m_1 m_2 - \omega^4 m_1 c_2 c_3 - i \omega^3 m_1 c_2 k_3 - i \omega^3 m_1 c_3 k_2 + i \omega^5 m_1 c_2 m_3 \\
& + i \omega^5 c_3 m_1 m_3 + i \omega^5 m_1 m_2 c_3 + \omega^2 m_1 k_2 k_3 - \omega^4 m_2 m_3 k_1 + \omega^2 k_2 m_3 k_1 + \omega^2 k_3 m_3 k_1 \\
& + \omega^2 k_3 m_2 k_1 + \omega^2 c_2 c_3 k_1 + i \omega c_2 k_3 k_1 + i \omega c_3 k_1 k_2 - i \omega^3 c_2 m_3 k_1 - i \omega^3 c_3 m_3 k_1 \\
& - i \omega^3 m_2 c_3 k_1 - k_1 k_2 k_3 - \omega^4 m_2 m_3 k_2 + \omega^2 k^2 m_3 + \omega^2 k_2 k_3 m_3 + \omega^2 k_2 k_3 m_2 + \omega^2 c_2 c_3 k_2 \\
& + i \omega c_2 k_2 k_3 + i \omega c_3 k_2^2 - i \omega^3 c_2 m_3 k_2 - i \omega^3 c_3 m_3 k_2 - i \omega^3 m_2 c_3 k_2 - k_2^2 k_3 + i \omega^5 c_1 m_2 m_3 \\
& - i \omega^3 c_1 k_2 m_3 - i \omega^3 c_1 k_3 m_3 - i \omega^3 c_1 k_3 m_2 - i \omega^3 c_1 c_2 c_3 + \omega^2 c_1 c_2 k_3 + \omega^2 c_1 c_3 k_2 - \omega^4 c_1 c_2 m_3 \\
& - \omega^4 c_1 c_3 m_3 - \omega^4 c_1 m_2 c_3 + i \omega c_1 k_2 k_3 + i \omega^5 c_2 m_2 m_3 - i \omega^3 c_2 k_2 m_3 - i \omega^3 c_2 k_3 m_3 - i \omega^3 c_2 k_3 m_2 \\
& - i \omega^3 c_2^2 c_3 + \omega^2 c_2^2 k_3 + \omega^2 c_2 c_3 k_2 - \omega^4 c_2^2 m_3 - \omega^4 c_2 c_3 m_3 - \omega^4 m_2 c_2 c_3 + i \omega c_2 k_2 k_3
\end{aligned}$$

$$\begin{aligned}
&= \frac{\hat{u}_g}{\omega^6 m_1 m_2 m_3 + i\omega^5 (c_2 m_1 m_3 + c_3 m_1 m_2 + m_1 m_2 c_3 + c_1 m_2 m_3 + c_2 m_2 m_3)} \\
&+ \omega^4 \left(\begin{aligned} &c_2^2 m_3 - k_2 m_1 m_3 - k_3 m_1 m_3 - k_3 m_1 m_2 - m_1 c_2 c_3 - m_2 m_3 k_1 - m_2 m_3 k_2 \\ &-c_1 c_2 m_3 - c_1 c_3 m_3 - c_1 m_2 c_3 - c_2^2 m_3 - c_2 c_3 m_3 - m_2 c_2 c_3 \end{aligned} \right) \\
&+ i\omega^3 \left(\begin{aligned} &c_2^2 c_3 + c_2 k_2 m_3 + c_2 m_3 k_2 - m_1 c_2 k_3 - m_1 c_3 k_2 - c_2 m_3 k_1 - c_3 m_3 k_1 \\ &-m_2 c_3 k_1 - c_2 m_3 k_2 - c_3 m_3 k_2 - m_2 c_3 k_2 - c_1 k_2 m_3 - c_1 k_3 m_3 \\ &-c_1 k_3 m_2 - c_1 c_2 c_3 - c_2 k_2 m_3 - c_2 k_3 m_3 - c_2 k_3 m_2 - c_2^2 c_3 \end{aligned} \right) \\
&+ \omega^2 \left(\begin{aligned} &-c_2^2 k_3 - c_2 k_2 c_3 - c_2 c_3 k_2 - k_2^2 m_3 + m_1 k_2 k_3 + k_2 m_3 k_1 \\ &+k_3 m_3 k_1 + k_3 m_2 k_1 + c_2 c_3 k_1 + k^2 m_3 + k_2 k_3 m_3 + k_2 k_3 m_2 \\ &+c_2 c_3 k_2 + c_1 c_2 k_3 + c_1 c_3 k_2 + c_2^2 k_3 + c_2 c_3 k_2 \end{aligned} \right) \\
&+ i\omega \left(\begin{aligned} &-c_2 k_2 k_3 - c_2 k_2 k_3 - k_2^2 c_3 + c_2 k_3 k_1 + c_3 k_1 k_2 \\ &+c_2 k_2 k_3 + c_3 k_2^2 + c_1 k_2 k_3 + c_2 k_2 k_3 \end{aligned} \right) \\
&+ k_2^2 k_3 - k_1 k_2 k_3 - k_2^2 k_3
\end{aligned}$$

$$\begin{aligned}
&= \frac{\hat{u}_g}{\omega^6 m_1 m_2 m_3 + i\omega^5 [c_2 (m_1 m_3 + m_2 m_3) + c_3 (m_1 m_3 + m_1 m_2) + c_1 m_2 m_3]} \\
&+ \omega^4 \left[\begin{aligned} &-k_2 (m_1 m_3 + m_2 m_3) - k_3 (m_1 m_3 + m_1 m_2) - c_1 c_2 m_3 \\ &-c_2 c_3 (m_1 + m_2 + m_3) - m_2 m_3 k_1 - c_1 c_3 (m_3 + m_2) \end{aligned} \right] \\
&+ i\omega^3 \left[\begin{aligned} &-c_2 k_3 (m_1 + m_2 + m_3) - c_3 k_2 (m_1 + m_2 + m_3) - c_1 c_2 c_3 \\ &-m_3 (c_2 k_1 + c_3 k_1 + c_1 k_2 + c_1 k_3) - m_2 (c_3 k_1 + c_1 k_3) \end{aligned} \right] \\
&+ \omega^2 \left[\begin{aligned} &k_2 k_3 (m_1 + m_2 + m_3) + k_3 k_1 (m_3 + m_2) \\ &+k_2 k_1 m_3 + c_2 c_3 k_1 + c_1 c_3 k_2 + c_1 c_2 k_3 \end{aligned} \right] \\
&+ i\omega (c_2 k_3 k_1 + c_3 k_1 k_2 + c_1 k_2 k_3) - k_1 k_2 k_3
\end{aligned}$$

$$\begin{aligned}
&= \frac{\hat{u}_g}{\omega^6 + i\omega^5 \left[c_3 \left(\frac{1}{m_3} + \frac{1}{m_2} \right) + c_2 \left(\frac{1}{m_2} + \frac{1}{m_1} \right) + \frac{c_1}{m_1} \right]} \\
&\quad + \omega^4 \left[-k_3 \left(\frac{1}{m_3} + \frac{1}{m_2} \right) - k_2 \left(\frac{1}{m_2} + \frac{1}{m_1} \right) - \frac{c_1 c_2}{m_1 m_2} \right. \\
&\quad \left. - c_2 c_3 \left(\frac{m_1 + m_2 + m_3}{m_1 m_2 m_3} \right) - \frac{k_1}{m_1} - c_1 c_3 \left(\frac{m_3 + m_2}{m_1 m_2 m_3} \right) \right] \\
&\quad + i\omega^3 \left[-(c_2 k_3 + c_3 k_2) \left(\frac{m_1 + m_2 + m_3}{m_1 m_2 m_3} \right) - \frac{c_1 c_2 c_3}{m_1 m_2 m_3} \right. \\
&\quad \left. - m_3 (c_2 k_1 + c_3 k_1 + c_1 k_2 + c_1 k_3) - m_2 (c_3 k_1 + c_1 k_3) \right] \\
&\quad + \omega^2 \left[k_2 k_3 \left(\frac{m_1 + m_2 + m_3}{m_1 m_2 m_3} \right) + k_3 k_1 \left(\frac{m_3 + m_2}{m_1 m_2 m_3} \right) \right. \\
&\quad \left. + \frac{k_2 k_1}{m_1 m_2} + \left(\frac{c_2 c_3 k_1 + c_1 c_3 k_2 + c_1 c_2 k_3}{m_1 m_2 m_3} \right) \right] \\
&\quad + i\omega \left(\frac{c_2 k_3 k_1 + c_3 k_1 k_2 + c_1 k_2 k_3}{m_1 m_2 m_3} \right) - \frac{k_1 k_2 k_3}{m_1 m_2 m_3} \\
&= \frac{\hat{u}_g}{\omega^6 + i\omega^5 K + \omega^4 L + i\omega^3 M + \omega^2 N + i\omega U + V} \dots\dots\dots (7)
\end{aligned}$$

Where,

$$\begin{aligned}
K &= \left[c_3 \left(\frac{1}{m_3} + \frac{1}{m_2} \right) + c_2 \left(\frac{1}{m_2} + \frac{1}{m_1} \right) + \frac{c_1}{m_1} \right] \\
L &= \left[-k_3 \left(\frac{1}{m_3} + \frac{1}{m_2} \right) - k_2 \left(\frac{1}{m_2} + \frac{1}{m_1} \right) - \frac{c_1 c_2}{m_1 m_2} - c_2 c_3 \left(\frac{m_1 + m_2 + m_3}{m_1 m_2 m_3} \right) - \frac{k_1}{m_1} - c_1 c_3 \left(\frac{m_3 + m_2}{m_1 m_2 m_3} \right) \right] \\
M &= \left[-(c_2 k_3 + c_3 k_2) \left(\frac{m_1 + m_2 + m_3}{m_1 m_2 m_3} \right) - \frac{c_1 c_2 c_3}{m_1 m_2 m_3} - m_3 (c_2 k_1 + c_3 k_1 + c_1 k_2 + c_1 k_3) - m_2 (c_3 k_1 + c_1 k_3) \right] \\
N &= \left[k_2 k_3 \left(\frac{m_1 + m_2 + m_3}{m_1 m_2 m_3} \right) + k_3 k_1 \left(\frac{m_3 + m_2}{m_1 m_2 m_3} \right) + \frac{k_2 k_1}{m_1 m_2} + \left(\frac{c_2 c_3 k_1 + c_1 c_3 k_2 + c_1 c_2 k_3}{m_1 m_2 m_3} \right) \right] \\
U &= \left(\frac{c_2 k_3 k_1 + c_3 k_1 k_2 + c_1 k_2 k_3}{m_1 m_2 m_3} \right) \\
V &= -\frac{k_1 k_2 k_3}{m_1 m_2 m_3}
\end{aligned}$$

Now, from Equations (5), (6) and (7) we get

$$\frac{\hat{u}_1}{\hat{u}_g} = \frac{\omega^4 + i\omega^3 A + \omega^2 B + i\omega C + D}{\omega^6 + i\omega^5 K + \omega^4 L + i\omega^3 M + \omega^2 N + i\omega U + V} \dots\dots\dots (8)$$

and

$$\frac{\hat{u}_2}{\hat{u}_g} = \frac{\omega^4 + i\omega^3 P + \omega^2 Q + i\omega R + S}{\omega^6 + i\omega^5 K + \omega^4 L + i\omega^3 M + \omega^2 N + i\omega U + V} \dots\dots\dots (9)$$

Where,

$\frac{\hat{u}_1}{\hat{u}_g}$ or $\frac{\hat{u}_2}{\hat{u}_g}$ are Transfer ratio (TR) for degrees of freedom u_1 and u_2 respectively.

